

QCD-Scale $f(R)$ Theories: Local and Cosmological Constraints

Zur Erlangung des akademischen Grades

DOKTORS DER NATURWISSENSCHAFTEN

von der Fakultät für Physik des
Karlsruher Instituts für Technologie (KIT)

genehmigte

DISSERTATION

von

M.Sc. Hamzeh Alavirad
aus Kerman, Iran

Karlsruher Institut für Technologie
Fakultät für Physik
Institut für Theoretische Physik

Tag der mündlichen Prüfung: 14.02.2014

Referent: Prof. Dr. F. R. Klinkhamer (Institut für Theoretische Physik, KIT)

Korreferent: Prof. Dr. D. Giulini (Institut für Theoretische Physik, U. Hannover)

To my best friend,
Parinaz

Acknowledgements

I would like to begin my acknowledgments by thanking Prof. Frans R. Klinkhamer, my supervisor, for the continuous support of my Ph.D studies and research and for his immense knowledge. I would also like to thank Prof. Dr. Domenico Giulini for co-supervising this Thesis.

I would like to thank other faculty members of the ITP—Prof. D. Zeppenfeld and Prof. M. Mülleitner— for their helpful advice during my study. Besides my advisor, I would like to thank Dr. Joel M. Weller for his guidance and advice throughout the research project, as well as his pain-staking effort in proofreading the drafts, which are greatly appreciated.

I would like to thank other members of ITP (former and present) — Hanno, Elisabeth, Markus, Marco, Eva, Slava, Bastian, Christoph, Sabine, Lu — for their friendly guidance during my stay here. I would like to thank my parents for their support over the years and for above all giving birth to me. Finally, I would like to thank my best friend, my wife, for her endless love, kindness, encouragement and support she has shown during the past four years it has taken me to finalize this thesis.

Abstract

In this Thesis we investigate the phenomenology of two QCD-scale modified gravity models. The first $f(R)$ modified gravity model is the square-root QCD-scale modified-gravity model (MG1), which is motivated by q-theory, a phenomenological approach to solve the cosmological constant problem. By applying a Markov Chain Monte Carlo (MCMC) simulation using cosmological data we find that this model can describe the large-scale structure of the universe very well and can be considered as a viable candidate for dark energy (DE). In addition, we obtain a best fit value of the gluon condensate compatible with previous theoretical estimates. We also solve the cosmological perturbation equations numerically in the framework of this model and analyze the behavior of the effective gravitational coupling constant and the gravity estimator E_G . The consequences of this model are also considered on local scales using the chameleon mechanism. We find that the model cannot satisfy local tests of gravity as its scalar degree of freedom does not exhibit the chameleon effect. However, a local version of this model, involving an additional free parameter is shown to satisfy all local tests of gravity with appropriate choices for the model free parameters.

The second $f(R)$ model which is investigated in this Thesis is a modified gravity model that is relevant in the high-curvature regime. We consider the effect of a logarithmic $f(R)$ theory (MG2), motivated by the form of the one-loop effective action arising from gluons in curved spacetime, on the structure of relativistic stars. In addition to analyzing the consistency constraints on the potential of the scalar degree of freedom, we discuss the possibility of observational features arising from a fifth force in the vicinity of the neutron star surface. We find that the model exhibits a chameleon effect that completely suppresses the effect of the modification on scales exceeding

a few radii, but close to the surface of the neutron star, the deviation from General Relativity can significantly affect the surface redshift that determines the shift in absorption (or emission) lines. We also use the method of perturbative constraints to solve the modified Tolman-Oppenheimer-Volkov equations for normal and self-bound neutron stars (quark stars).

Contents

List of Figures	xiii
List of Tables	xv
1 Introduction	1
1.1 Conventions	2
1.2 Homogeneous universe	3
1.3 Cosmological constant problem	7
1.3.1 Description of the problem	7
1.3.2 q -theory	9
1.4 Cosmological perturbations	12
1.5 Yang-Mills theory and QCD	15
1.6 Overview	20
2 $f(R)$ theories and the chameleon mechanism	21
2.1 $f(R)$ theories	22
2.2 Chameleon mechanism	24
2.2.1 Effective gravitational coupling constant	28
2.2.2 Fifth force searches	29
3 $R ^{1/2}$ QCD-scale modified-gravity (MG1)	31
3.1 $ R ^{1/2}$ QCD-scale modified-gravity model	32
3.1.1 Gluon condensate and q -theory	32
3.1.2 The MG1 model	34
3.2 Cosmological perturbations in the MG1 model	37
3.2.1 Parametrization of perturbations in modified gravity	38

3.2.2	Effective gravitational coupling constant	41
3.2.3	Gravity estimator E_G	43
3.2.4	Late integrated Sachs-Wolfe effect	48
3.2.5	Discussion	49
3.3	Cosmological parameter estimation	50
3.4	Chameleon behavior of the MG1 model	52
3.4.1	Local tests	53
3.4.2	Large-scale model	55
3.4.3	Local-scale model	59
3.4.4	Discussion	61
3.5	Summary	64
4	Logarithmic $f(R)$ theory (MG2) and relativistic stars	67
4.1	Motivations for the MG2 model	68
4.2	Constraints on the MG2 model	72
4.2.1	Consistency constraints	73
4.2.2	Observational constraints	78
4.3	Relativistic stars in the MG2 model	81
4.3.1	Field equations	81
4.3.2	Modified Tolman-Oppenheimer-Volkov equations	82
4.3.3	Neutron stars	84
4.3.3.1	Polytropic EoS	84
4.3.3.2	SLy EoS	85
4.3.4	Binding energy	87
4.3.5	Quark stars	89
4.3.6	Perturbative regime	92
4.4	Summary	92
5	Concluding remarks	97
	Appendices	101

A Data fitting method	103
A.1 Cosmic microwave background	103
A.2 Type Ia supernovae data	105
A.3 Baryon acoustic oscillation	106
A.4 X-Ray gas mass fraction	106
B Chameleon-field solutions	109
Bibliography	113

List of Figures

2.1	A typical runaway potential.	26
3.1	Evolution of the perturbation potentials Φ and Ψ in the MG1 model. . .	40
3.2	Φ/Ψ in the MG1 model.	41
3.3	G_{eff}/G in the MG1 model.	43
3.4	Comparison of observational constraints with predictions from General Relativity and viable modified theories of gravity for E_G	44
3.5	The gravity estimator E_G in the MG1 model.	46
3.6	Evolution of the logarithmic density perturbation growth rate in the MG1 model.	47
3.7	Matter power spectrum in the MG1 model.	48
3.8	The temperature anisotropy power spectrum in the MG1 and the Λ CDM model.	50
3.9	2-D constraint contours of the cosmological parameters with 1σ and 2σ regions in the MG1 model.	53
3.10	Chameleon field of the $f(R) = R - \frac{1}{L_0} R ^{\frac{1}{2}}$ (MG1) model.	57
3.11	The chameleon field and acceleration in the $f(R) = R - \frac{ R ^{1/2}/L_0}{1+\zeta L_0 R ^{1/2}}$ model with $\zeta = 1$	60
3.12	The chameleon field and acceleration in the $f(R) = R - \frac{ R ^{1/2}/L_0}{1+\zeta L_0 R ^{1/2}}$ model with $\zeta = 100$	62
4.1	The potential of the MG2 model in the Jordan frame.	75
4.2	Effective gravitational coupling constant for the MG2 model against the distance from the surface of a neutron star.	79

4.3	The gravitational redshift parameter z_s against the distance from the surface of a neutron star in the MG2 model.	80
4.4	The mass-radius diagram for neutron stars in GR and the MG2 model using a simplified polytropic equation of state	86
4.5	The mass-radius diagram for neutron stars in GR and the MG2 model using the realistic SLy equation of state.	88
4.6	The gravitational binding energy BE_G as a function of the total mass M for the polytropic and SLy equations of state in the MG2 model. . .	90
4.7	The mass-radius diagram for the quark star case in GR and the MG2 model using a linear equation of state	91
4.8	The parameter $ \Delta_{\max} = A_{MG}(r)/A_{GR}(r) - 1 _{\max}$ as a function of $\alpha_5 = \alpha/10^5$ in the MG2 model.	93

List of Tables

3.1	Cosmological parameters resulting from the MG1 model.	38
3.2	The best fit values of the model parameter with 1σ and 2σ regions for the MG1 model.	54
3.3	The behavior of the chameleon field for the $f(R) = R - R ^{\frac{1}{2}}/L_0$ (MG1) model.	56
3.4	The behavior of the chameleon field for the $f(R) = R - \frac{ R ^{1/2}/L_0}{1+\zeta L_0 R ^{1/2}}$ model for $\zeta = 1$	61
3.5	The behavior of the chameleon field for the $f(R) = R - \frac{ R ^{1/2}/L_0}{1+\zeta L_0 R ^{1/2}}$ model for $\zeta = 100$	63
4.1	The unitarity and positive-squared-mass constraints for the MG2 model.	77
4.2	Parameters of the SLy EoS model	85

1

Introduction

Modification of the Einstein-Hilbert action (EH) to include higher order curvature invariants has a distinguished history, beginning just a few years after the introduction of General Relativity (GR) [1, 2]. However, it was the realisation that renormalization at one-loop order demands that the EH action be supplemented with higher order terms that stimulated interest in modifications in the strong gravity regime, such as Starobinsky's well-known curvature driven inflationary scenario [3]. The possibility that such corrections could affect gravitational phenomenology at low energies was not seriously considered until the discovery of the acceleration of the expansion of the universe [4, 5], whereupon $f(R)$ models in particular, in which the EH action is replaced with a more general function of the Ricci scalar, have been intensely studied by many authors (see [6, 7] for comprehensive reviews).

Modifications of gravity that lead to deviations in the low energy regime, corresponding to the late universe, must, in addition to compatibility with cosmological observations and internal consistency requirements, stand up to a host of constraints arising from equivalence principle tests and solar system measurements on local scales [8]. Since $f(R)$ theories can be reformulated as a scalar-tensor theory with a fixed coupling to matter, these tests are sufficient to rule out the models, unless the fifth force generated by the scalar degree of freedom is effectively screened, as in the chameleon mechanism [9–11]. By comparison, the strong gravity regime is poorly constrained by observations [12].

The most natural candidate for a model of the strong force is a non-Abelian gauge theory with gauge group $SU(N_c)$ ($N_c = 3$) where it is coupled to fermions (quarks) in

the fundamental representation. This theory is known as Quantum Chromodynamics (QCD) (see [13] and references therein). The perturbative content of this theory is given by N_f flavors of quarks and $N_c^2 - 1 = 8$ gluons. This theory has two interesting properties: confinement and the asymptotic freedom [14, 15]. By confinement it is meant that the force between quarks does not diminish as they are separated. Therefore, one needs an infinite amount of energy to separate two quarks and therefore they are bounded forever into hadrons like protons and neutrons. In the low-energy limit, calculations in QCD require a nonperturbative approach. On the other hand, asymptotic freedom means the color force get weaker at increasing energy or decreasing length scales, so that it is possible to do perturbative calculations in QCD in high energies. In addition, the ground state in QCD, which is an example of a nonperturbative vacuum, is typically characterized by the presence of non-vanishing condensates, including the gluon condensate and quark condensates [16].

In the remainder of this chapter we introduce the basic concepts that will be used throughout this Thesis. First, in section 1.2, we will briefly describe the treatment of the homogeneous universe in General Relativity. Then in section 1.3 we will discuss the cosmological constant problem and a possible solution: q -theory. Cosmological perturbation theory is discussed in section 1.4, followed by an introduction to Yang-Mills theory and QCD in section 1.5. Section 1.6 contains an overview of this Thesis.

1.1 Conventions

Throughout this Thesis (except where explicitly stated) we work in units with $\hbar = c = 1$, where \hbar is the reduced Planck constant and c is the speed of light in vacuum. In addition, we use the metric signature $(-, +, +, +)$ so that the Minkowski metric is $\eta_{\mu\nu} = \text{diag}(-1, +1, +1, +1)$. Greek indices $\alpha, \beta, \mu, \nu, \dots$ indicate spacetime coordinates $0, 1, 2, 3$ and the Einstein sum rule is adopted unless otherwise indicated. Latin indices i, j, k run over the three spatial coordinates $1, 2, 3$ and latin indices a, b, c, \dots for an $SU(N)$ group run over $1 \dots N^2 - 1$.

The metric covariant derivative is defined as $\nabla_\mu A_\nu = \partial_\mu A_\nu - \Gamma_{\mu\nu}^\delta A_\delta$ where ∂_μ represents a partial derivative with respect to the spacetime coordinates and $\Gamma_{\alpha\beta}^\mu$ is the Christoffel symbol defined by $\Gamma_{\alpha\beta}^\mu = \frac{1}{2}g^{\mu\nu} \{g_{\alpha\nu,\beta} + g_{\beta\nu,\alpha} - g_{\alpha\beta,\nu}\}$ with $g_{\alpha\beta,\delta} \equiv \partial g_{\alpha\beta} / \partial x_\delta$. A derivative with respect to a scalar field ϕ will be indicated by $\partial V / \partial \phi = V_{,\phi}$.

The Riemann-Christoffel curvature tensor is $R^\lambda_{\mu\nu\kappa} = \partial_\kappa \Gamma^\lambda_{\mu\nu} - \partial_\nu \Gamma^\lambda_{\mu\kappa} + \Gamma^\eta_{\mu\nu} \Gamma^\lambda_{\kappa\eta} - \Gamma^\eta_{\mu\kappa} \Gamma^\lambda_{\nu\eta}$. The Ricci tensor and Ricci scalar are defined as $R_{\mu\nu} = R^\lambda_{\mu\lambda\nu}$ and $R = g^{\mu\nu} R_{\mu\nu}$ respectively.

1.2 Homogeneous universe

The cornerstone of modern cosmology is Einstein’s General Theory of Relativity (GR). This theory relates the geometry of spacetime with its matter content via the Einstein field equations. This theory is a generalization of Newtonian gravity and the Special Theory of Relativity. General relativity is based on the Equivalence Principle, which in its strong form is stated as [17]:

“at every spacetime point in an arbitrary gravitational field it is possible to choose a locally inertial coordinate system such that, within a sufficient small region of the point in question, the laws of nature take the same form as in unaccelerated Cartesian coordinate systems in the absence of gravitation.”

In its weak form, the Weak Equivalence Principle (WEP), we should replace *the laws of nature* by the *laws of motion of freely falling particles*. Violation of the WEP is described by the parameter η , which is identically zero in any metric theory of gravity, including General Relativity [18]. It is defined by

$$\eta = 2 \frac{a_A - a_B}{a_A + a_B}, \quad (1.1)$$

where a_A and a_B are the acceleration of two bodies A and B towards each other, when there is no other source of acceleration. The parameter η has been constrained by WEP violation tests as: $|\eta| < (0.3 \pm 1.8) \times 10^{-13}$ [19], $|\eta| < 5 \times 10^{-14}$ [20]. In addition, future experiments will further tighten these constraints. For example, the MICROSCOPE project is capable of achieving the precision $|\eta| < 10^{-16}$ [21] and the Reasenbergs/SR-POEM project should reach $2 \times |\eta| < 10^{-17}$ [22].

Let us take a brief look at the Einstein field equations. One starting point is the standard Einstein-Hilbert action

$$S_{\text{EH}} = \frac{1}{16\pi G} \int \sqrt{-g} d^4x (R - 2\Lambda) + S^{\text{matter}}[g_{\mu\nu}, \psi_m], \quad (1.2)$$

where Λ is the cosmological constant term and G is the gravitational coupling constant. The last term in the Einstein-Hilbert action is the action of the matter fields ψ_m . The

Einstein field equations

$$R_{\mu\nu} - \frac{1}{2}Rg_{\mu\nu} + \Lambda g_{\mu\nu} = 8\pi GT_{\mu\nu}^{\text{matter}}, \quad (1.3)$$

are obtained by varying the action (1.2) with respect to the metric $g_{\mu\nu}$, where the energy-momentum tensor of the matter $T_{\mu\nu}^{\text{matter}}$ is defined as

$$T_{\mu\nu}^{\text{matter}} = -\frac{2}{\sqrt{-g}} \frac{\delta S^{\text{matter}}}{\delta g^{\mu\nu}}. \quad (1.4)$$

The energy-momentum tensor contains information about the matter content of the physical model under consideration. The Einstein field equations satisfy the Equivalence Principle. For example, as the gravitational coupling constant G is constant throughout spacetime in the framework of GR, the Strong Equivalence Principle is respected in this theory. By specifying the energy content of the problem in question and applying symmetries, one can solve the Einstein field equations to obtain the metric coefficients and the evolution of the matter and energy content, as we will do in this section for the case of a homogeneous and isotropic universe.

To describe the universe on cosmological scales it is necessary to apply the Cosmological Principle to the Einstein field equations. The Cosmological Principle can be stated as [17]: the universe is homogeneous and isotropic when it is looked on enough large scales. It can be rephrased as: the position of us on the Earth is not an specific privileged location within the universe as a whole.

The twin requirements of homogeneity and isotropy are satisfied by the Friedmann-Robertson-Walker (FRW) metric [17]. For a flat universe, the FRW metric can be expressed as

$$g_{\mu\nu} = \begin{pmatrix} -1 & 0 & 0 & 0 \\ 0 & a^2(t) & 0 & 0 \\ 0 & 0 & a^2(t) & 0 \\ 0 & 0 & 0 & a^2(t) \end{pmatrix}, \quad (1.5)$$

where the time dependent function $a(t)$ is called the scale factor. The evolution of the scale factor, which depends on the matter and energy content of the universe, will be given shortly.

With this metric, the components of the Ricci tensor and the Ricci scalar are calculated to be

$$R_{00} = -3\frac{\ddot{a}}{a}, \quad (1.6a)$$

$$R_{ij} = \delta_{ij} [2\dot{a}^2 + a\ddot{a}], \quad (1.6b)$$

$$R = 6 \left[\frac{\ddot{a}}{a} + \left(\frac{\dot{a}}{a} \right)^2 \right], \quad (1.6c)$$

where an overdot indicates differentiation with respect to cosmological time t . In addition, the symmetries imposed by the Cosmological Principle also require that the energy-momentum tensor be in the form of a perfect fluid

$$T_{\nu}^{\text{matter}\mu} = \begin{pmatrix} -\rho(t) & 0 & 0 & 0 \\ 0 & P(t) & 0 & 0 \\ 0 & 0 & P(t) & 0 \\ 0 & 0 & 0 & P(t) \end{pmatrix}, \quad (1.7)$$

where $\rho(t)$ and $P(t)$ are the energy density and pressure of the fluid respectively. To get the evolution of the scale factor, one needs only the time-time component of the Einstein field equations

$$R_{00} - \frac{1}{2}g_{00}R = 8\pi GT_{00}, \quad (1.8)$$

which gives

$$H^2 = \frac{\dot{a}^2}{a^2} = \frac{8\pi G\rho}{3}, \quad (1.9)$$

where $H(t) \equiv \frac{\dot{a}}{a}$ is the Hubble parameter. The ii components also give

$$\dot{H} + H^2 = \frac{\ddot{a}}{a} = -\frac{4\pi G}{3}(\rho + 3p). \quad (1.10)$$

The density parameter is defined as

$$\Omega_i = \frac{\rho_i}{\rho_{cr}}, \quad (1.11)$$

where the index i refers to the type of content, such as matter (m), radiation (r) or the cosmological constant (Λ). The critical density ρ_{cr} is defined as

$$\rho_{cr} = \frac{3H^2}{8\pi G}. \quad (1.12)$$

The first Friedmann equation (1.9) can then be rewritten as

$$\frac{H^2}{H_0^2} = \Omega_r^0 a^{-4} + \Omega_m^0 a^{-3} + \Omega_\Lambda^0, \quad (1.13)$$

where the 0 index indicates value of the relevant quantity at the present time.

The Friedmann equations have an exact solution in the presence of a single perfect fluid with the equation of state (EoS) w

$$P(t) = w\rho(t) , \tag{1.14}$$

In a spatially flat universe, the solution for the scale factor is

$$a(t) = a_0 t^{\frac{2}{3(w+1)}} , \tag{1.15}$$

where a_0 is an integration constant which here can be taken as 1. Different types of matter have different equations of state that give rise to different behavior.

- Matter dominated universe ($w = 0$) $a(t) \propto t^{2/3}$.
- Radiation dominated universe ($w = 1/3$) $a(t) \propto t^{1/2}$.
- Cosmological constant dominated universe ($w = -1$) where the scale factor grows exponentially.

1.3 Cosmological constant problem

1.3.1 Description of the problem

The cosmological constant problem is almost as old as quantum field theory. The Heisenberg uncertainty principle asserts that the ground state energy of quantum oscillators cannot be zero as the kinetic and potential energy cannot vanish simultaneously. Since a quantum field can be considered as a superposition of an infinite number of harmonic oscillators, the result is an infinite ground state energy. This infinite energy can be ignored as long as gravity is absent. It can be neglected by definition (normal ordering), as only energy differences are important in quantum field theory in flat spacetime.

But when gravity comes to the scene, the problem returns. Gravity is sensitive to the total amount of energy, not only the differences, so a difficult question arises: does the ground state energy of quantum fields gravitate? If the answer to this question is positive, then we encounter a big problem. Observations indicate that the vacuum energy density that gravitates (which plays the role of the cosmological constant), should be at least 41 orders of magnitude smaller than the vacuum energy of the quantum fields.

To see this in more detail, we include the vacuum energy of quantum fields into the action (1.2). Lorentz invariance requires that the vacuum energy-momentum tensor should be of the form [23]

$$\langle 0|T_{\mu\nu}|0\rangle = -\rho_{\text{vac}}g_{\mu\nu}, \quad (1.16)$$

where ρ_{vac} is the quantum vacuum energy density. By assuming that the vacuum energy of the quantum fields gravitates, the field equations (1.3) should be rewritten as

$$R_{\mu\nu} - \frac{1}{2}Rg_{\mu\nu} + \Lambda g_{\mu\nu} = 8\pi GT_{\mu\nu}^{\text{matter}} + 8\pi G \langle 0|T_{\mu\nu}|0\rangle, \quad (1.17)$$

or by replacing Λ with Λ_{eff}

$$\Lambda_{\text{eff}} = \Lambda + 8\pi G\rho_{\text{vac}}, \quad (1.18)$$

one obtains

$$R_{\mu\nu} - \frac{1}{2}Rg_{\mu\nu} + \Lambda_{\text{eff}}g_{\mu\nu} = 8\pi GT_{\mu\nu}^{\text{matter}}. \quad (1.19)$$

The effective cosmological constant Λ_{eff} is the observable value that should be obtained from observations. However, as mentioned above, the value of the observed cosmological

constant ρ_{obs} is much less than the theoretical expectation. Observations indicate that [4]

$$\rho_{\text{obs}} \equiv \rho_{\text{vac}} + \Lambda/8\pi G \simeq 10^{-47} \text{GeV}^4. \quad (1.20)$$

On the other hand, the energy of the ground state in quantum field theory (QFT), taking for example a scalar field, is obtained naively as

$$\rho_{\text{vac}} = \int_0^{\Lambda_{\text{cutoff}}} \frac{d^3k}{(2\pi)^3} \frac{1}{2} \sqrt{k^2 + m^2} \simeq \frac{\Lambda_{\text{cutoff}}^4}{16\pi^2}. \quad (1.21)$$

If General Relativity is valid up to the Planck scale, then we can take $\Lambda_{\text{cutoff}} = M_{\text{Pl}} = 1/\sqrt{8\pi G}$, which would give

$$\rho_{\text{vac}} \simeq 2^{-10} \pi^{-4} G^{-2} = 2 \times 10^{71} \text{GeV}^4. \quad (1.22)$$

However, from eq. (1.20) we have $\rho_{\text{vac}} + \Lambda/8\pi G \simeq 10^{-47} \text{GeV}^4$, so the two terms should cancel to 118 decimal places [4]. This is what is called the main cosmological constant problem (CCP1). If we assume $\Lambda_{\text{cutoff}} = E_{\text{QCD}}$ where $E_{\text{QCD}} \simeq 0.3 \text{ GeV}$ is the QCD cutoff, the two terms should cancel out to 41 decimal places.

The main cosmological constant problem exposes a mismatch between General Relativity and QFT. However, after the discovery of the accelerated expansion of the universe, cosmologists were forced to address two other related problems. The first (which we refer to it as CCP2a) is that in order to explain the data, one needs a value of the cosmological constant that is not exactly zero, but is fantastically small compared to the typical scales of quantum field theories, implying a high degree of fine-tuning. The second (CCP2b) is that the observed value of the dark energy density is within an order of magnitude of the present matter density (and to a lesser extent, the radiation density) despite having differed by many orders of magnitude in the history of the universe. These can be summarized as [24]:

- **CCP1.** why $\Lambda_{\text{obs}} \ll (E_{\text{Pl}})^4$?
- **CCP2a.** why $\Lambda \neq 0$?
- **CCP2b.** why $\Lambda \sim \rho_{\text{matter}} \Big|_{\text{present}} \sim +10^{-11} (\text{eV})^4$?

Several directions to solve the cosmological constant problem such as supersymmetry [25], supergravity [26], string theory [27–30], the anthropic principle [31, 32], and the q -theory [33, 34] have been considered. In section 1.3.2 we will consider the q -theory approach to the cosmological constant problem.

1.3.2 q -theory

q -theory describes the gravitational effect of the vacuum energy density [33–40]. The basic idea of q -theory can be stated as follows: the energy density of the quantum vacuum ϵ_{micro} , which could be of order of $\mathcal{O}(E_{\text{UV}}^4)$ where E_{UV} is a UV cutoff, does not appear in the low-energy field equations. The quantum vacuum is assumed to be a self-sustained Lorentz-invariant medium that should be characterized by some conserved charge q i.e. $\epsilon_{\text{micro}} \equiv \epsilon_{\text{micro}}(q)$. It is the macroscopic vacuum energy density $\epsilon_{\text{macro}}(q)$ that appears in low-energy effective theories such as GR. For an equilibrium value of the parameter q , say \tilde{q}_0 , the macroscopic energy density is nullified $\epsilon_{\text{macro}}(\tilde{q}_0) = 0$; therefore the main cosmological constant problem is in principle solved, as we will see in following.

By considering a variable $q(x)$, the effective action for the gravitational and matter sectors can be written

$$S_{\text{eff}}[g] = \int \sqrt{-g} d^4x \left(\frac{R}{16\pi G(q)} + \epsilon(q) \right) + S^{\text{matter}} , \quad (1.23)$$

where the vacuum energy density $\epsilon(q)$ can be a generic function

$$\epsilon(q) = \Lambda_{\text{bare}} + \epsilon_{\text{var}}(q) , \quad (1.24)$$

where Λ_{bare} is a constant term from the ground state energies of the Standard Model (SM) fields and $\epsilon_{\text{var}}(q)$ is the dynamical part of $\epsilon(q)$. Then by using the Gibbs-Duhem relation¹ and Lorentz invariance we obtain [33]

$$P_V = - \left(\epsilon - q \frac{d\epsilon}{dq} \right) = -\rho_V . \quad (1.25)$$

In equation (1.25), each term could be of order $(E_{\text{Pl}})^4$, but they can cancel exactly for an appropriate value of the vacuum variable \tilde{q}_0

$$\rho_V(\tilde{q}_0) = \left[\epsilon(q) - q \frac{d\epsilon(q)}{dq} \right]_{q=\tilde{q}_0} = 0 , \quad (1.26)$$

therefore the main cosmological constant problem CCP1 is in principle solved.

¹ From the Gibbs-Duhem relation $Nd\mu = VdP - SdT$ (which follows from the first law of thermodynamics) for $dT = 0$ one can write $dP = \frac{N}{V}d\mu$. Then by identifying the chemical potential $\mu = d\epsilon/dq$ and integrating, one obtains the first equality in (1.25).

The preceding analysis is valid for an equilibrium situation; in an expanding universe, one would expect perturbations in the variable \tilde{q}_0 , giving rise to a new value $q = q_0$ that can result in a tiny non-zero vacuum energy (cosmological constant) $\rho_V(q_0) = \rho_{\text{obs}} \neq 0$. We will discuss this situation in more detail in section 3.1.

Some concrete candidates for the variable q that have been considered in the literature are as follows.

1. The vacuum variable q could arise from a three-form gauge field A [34, 41, 42]

$$q \equiv -\frac{1}{24\sqrt{-g}}\epsilon^{\alpha\beta\gamma\delta}\nabla_\alpha A_{\beta\gamma\delta}, \quad (1.27)$$

where q is obtained from the four-form field strength $F = dA$ and $\epsilon^{\alpha\beta\gamma\delta}$ is the Levi-Civita symbol. The modified Einstein and Maxwell equations are obtained by applying the variational principle to the action (1.23)

$$2K(q)(R_{\mu\nu} - \frac{1}{2}Rg_{\mu\nu}) = -2(\nabla_\mu\nabla_\nu - g_{\mu\nu}\square)K(q) + \rho_V g_{\mu\nu} - T_{\mu\nu}^{\text{matter}}, \quad (1.28a)$$

$$\frac{d\rho_V(q)}{dq} + R\frac{d}{dq}K(q) = 0, \quad (1.28b)$$

where $k(q) \equiv 1/8\pi G(q)$ with a vacuum energy density

$$\begin{aligned} \rho_V &= \epsilon - q \left(\frac{d\epsilon}{dq} + R\frac{d}{dq}K(q) \right) \\ &= \epsilon - q\mu, \end{aligned} \quad (1.29)$$

where μ is an integration constant corresponding to the chemical potential.

2. Another candidate can be realized by a pseudoscalar [33]

$$q \propto F_{\mu\nu}\tilde{F}^{\mu\nu}, \quad (1.30)$$

where $F_{\mu\nu} \equiv \nabla_\mu A_\nu - \nabla_\nu A_\mu$ is the field strength and $\tilde{F}_{\mu\nu}$ is a dual tensor. For a gauge vector field A that belongs to the $SU(N)$ group, one has

$$q \propto \text{tr}(F_{\mu\nu}\tilde{F}^{\mu\nu}), \quad (1.31)$$

where $F_{\mu\nu} \propto [D_\mu, D_\nu]$ and D_μ is the covariant derivative associated with the local $SU(N)$ group. One example related to this type has q proportional to the gluon condensate [37, 42, 43]. This will be discussed in more detail in section 3.1.

3. The last possibility which we discuss here is a vector-field realization such as an aether-type velocity field u_μ [33]. In this case one assumes that the action does not depend on u_μ but instead depend on its covariant derivative $u^\mu_{;\nu} \equiv \nabla_\nu u^\mu$. In a flat FRW universe with cosmic time t , the asymptotic solution $u_\mu = (u_0, u_i)$ is

$$u_0(t) \rightarrow q_0 t, \quad u_i = 0, \quad (1.32a)$$

$$u^\nu_\mu = q_0 \delta^\nu_\mu. \quad (1.32b)$$

and $H(t) \rightarrow 1/t$. Starting from a de-Sitter universe with $\Lambda > 0$, for a unique value of $\tilde{q}_0 \equiv q_0/(E_{\text{Pl}})^2$, one ends up with a static Minkowski spacetime $\tilde{q}_0 = \sqrt{\Lambda/(2E_{\text{Pl}}^2)}$. However, in this case there is the danger of ruining the standard Newtonian physics for a small self-gravitating system [44]. This problem can be avoided in a special model with two massless vector fields [45–49].

There are other dynamical cancellation and adjustment approaches to the cosmological constant problem. For example, Dolgov [50] and Ford [51] have used a massless scalar field, non-minimally coupled to gravity, to cancel the cosmological constant dynamically. In addition, it is also possible that quantum effects restore conformal invariance on length scales comparable to the cosmological horizon size, so as to cancel the cosmological constant [52–54]. Another possibility is to cancel the cosmological constant by quantum particle production in de Sitter spacetime [55–57]. In this scenario, the effective energy-momentum tensor of the produced particles can act to cancel out the cosmological constant. There are also another approaches such as a step-wise relaxation of the vacuum energy density [58] and vacuum-energy decay from particle production [59].

1.4 Cosmological perturbations

It is possible to produce any cosmic history $H = H(a)$ using the extra degree of freedom in $f(R)$ models [60, 61]. Therefore the background (zero-order) cosmology is not enough to distinguish the $f(R)$ models from other theories of gravity. To find some observables to distinguish $f(R)$ theories one can use the perturbation (first-order) cosmology [62].

The first relativistic consideration of the linear cosmological perturbations in a FRW universe was first done by Lifshitz [63], and subsequently refined by many authors [62, 64] (see [65] for a textbook treatment). An initial fluctuation in the gravitational potential with amplitude $\simeq 10^{-5}$ can grow to reproduce the current structure of our universe [62]. This initial fluctuation can be produced by inflation [66–69].

To understand the structure of the Universe we should go beyond the simple homogeneous FRW model. This can be done perturbatively, i.e. splitting the physical quantities in two parts. The homogeneous background part depends only on the cosmic time t and is described by the FRW equations. The perturbative part depends on time and scale. This means we can write the metric as (in this subsection a quantity with a bar indicates the corresponding background quantity)

$$g_{\mu\nu} = \bar{g}_{\mu\nu}(t) + \delta g_{\mu\nu}(t, \mathbf{x}), \quad (1.33)$$

where t is the cosmic time and \mathbf{x} indicates the spatial coordinates. These perturbations in the metric can lead to perturbations in the Einstein and energy-momentum tensor

$$G_{\mu\nu} = \bar{G}_{\mu\nu}(t) + \delta G_{\mu\nu}(t, \mathbf{x}), \quad (1.34a)$$

$$T_{\mu\nu} = \bar{T}_{\mu\nu}(t) + \delta T_{\mu\nu}(t, \mathbf{x}), \quad (1.34b)$$

where the homogeneous part is satisfied separately by the FRW equations

$$\bar{G}_{\mu\nu} = 8\pi G \bar{T}_{\mu\nu}. \quad (1.35)$$

However, we are interested in the inhomogeneous part

$$\delta G_{\mu\nu} = 8\pi G \delta T_{\mu\nu}. \quad (1.36)$$

In section 1.2 we considered the FRW homogeneous solutions of (1.35); in following we consider the perturbed equations that stem from (1.36).

The treatment of the perturbations is made simpler by the fact that the scalar, vector and tensor modes are decoupled at linear order, so the resulting Einstein equations can be solved separately. The tensor modes correspond to gravitational waves, and the vector modes decay in an expanding universe, so the scalar modes are most important for structure formation. The most general form of the metric for the scalar perturbations (1.33) can be written

$$\begin{aligned} g_{00} &= -(1 + 2\psi) , \\ g_{0i} &= -aB_{,i} , \\ g_{ij} &= a^2 (\delta_{ij}(1 - 2\phi) - 2E_{,ij}) . \end{aligned} \tag{1.37}$$

However, the four variables ψ , B , ϕ and E represent too many degrees of freedom so we must impose a gauge. In this Thesis we make use of the Newtonian gauge ($B = E = 0$, $\psi = \Psi$ and $\phi = \Phi$) in which the scalar degrees of Freedom Ψ and Φ can be identified with the Newtonian and spatial curvature potentials respectively. Changing coordinates to conformal time τ , where $dt = a(\tau)d\tau$, so the metric takes a simpler form, the perturbations to the homogeneous FRW metric (1.5) in the Newtonian gauge can be written as [65]

$$ds^2 = a(\tau)^2 [-(1 + 2\Psi(\mathbf{x}, \tau))d\tau^2 + (1 - 2\Phi(\mathbf{x}, \tau))d\mathbf{x}^2] . \tag{1.38}$$

In GR, in the absence of anisotropic stress, $\Psi = \Phi$.

One can write the perturbed energy-momentum tensor as

$$T_0^0 = \bar{T}_0^0 + \delta T_0^0 = -\rho(1 + \delta) , \tag{1.39a}$$

$$T_i^0 = \bar{T}_i^0 + \delta T_i^0 = -(\rho + P)v_i , \tag{1.39b}$$

$$T_j^i = \bar{T}_j^i + \delta T_j^i = (P + \delta P)\delta_j^i + \pi_j^i , \tag{1.39c}$$

where $\delta\rho(t, \mathbf{x}) = \rho(t, \mathbf{x}) - \bar{\rho}(t)$ and $\delta P(t, \mathbf{x}) = P(t, \mathbf{x}) - \bar{P}(t)$ are the energy density and pressure perturbations. In addition $\delta \equiv \delta\rho/\rho$ is the density contrast, v_i is the velocity field and π_j^i is the traceless component of the energy-momentum tensor perturbations. It is easier to analyze the linear evolution equations of the perturbations in Fourier space. Let $f = \{\Psi, \dots, \delta\rho\}$ denote the set of all metric and matter perturbations. Then we can relate the real space perturbations to the corresponding Fourier components as

$$f(\tau, \mathbf{x}) = \int \frac{d^3k}{(2\pi)^{3/2}} f_{\mathbf{k}}(\tau) e^{i\mathbf{k}\cdot\mathbf{x}} , \tag{1.40}$$

where $\mathbf{k} = k\hat{k}$ is the comoving wave number vector. Then the partial differential equations for $f(\tau, \mathbf{x})$ become ordinary differential equations for each Fourier mode $f_{\mathbf{k}}(\tau)$. Individual Fourier modes are decoupled.

The energy-momentum conservation equations ($\nabla_{\mu}T^{\mu\nu} = 0$) gives two equations which relate the metric potentials and matter perturbations [70]

$$\dot{\delta} = -(1+w)(\theta - 3\dot{\Phi}) - 3\frac{\dot{a}}{a}\left(\frac{\delta P}{\delta\rho} - w\right)\delta, \quad (1.41)$$

$$\dot{\theta} = -\frac{\dot{a}}{a}(1-3w)\theta - \frac{\dot{w}}{1+w} + \frac{\delta P/\delta\rho}{1+w}k^2\delta - k^2\sigma + k^2\Psi, \quad (1.42)$$

where an overdot represents the derivative with respect to the conformal time τ and $w \equiv P/\rho$ is the equation of state of matter. The parameters σ and θ are anisotropic stress and momentum perturbations respectively which are defined by the relations

$$(\rho + P)\sigma \equiv -(\hat{k}^i\hat{k}_j - \frac{1}{3}\delta_j^i)\pi_i^j, \quad (1.43a)$$

$$(\rho + P)\theta \equiv -ik^j\delta T_j^0. \quad (1.43b)$$

The anisotropic stress σ vanishes for baryons and CDM.

We need two more equations which are obtained from field equations for the metric. In GR, by inserting the perturbed metric (1.38) and the perturbed energy-momentum tensor (1.39) into the field equations ($G_{\mu\nu} = 8\pi GT_{\mu\nu}$) one obtains the Poisson and anisotropy equations respectively

$$k^2\Phi = -4\pi Ga^2\rho\Delta, \quad (1.44a)$$

$$k^2(\Phi - \Psi) = 12\pi Ga^2(\rho + P)\sigma, \quad (1.44b)$$

where Δ is the comoving density perturbation

$$\rho\Delta = \rho\delta + \frac{\mathcal{H}}{k}(\rho + P)\sigma, \quad (1.45)$$

in which $\mathcal{H} \equiv \frac{1}{a}\frac{da}{d\tau}$. In chapter 3 we will discuss perturbation theory for the QCD-scale modified-gravity model.

1.5 Yang-Mills theory and QCD

In 1954, Chen Ning Yang and Robert Mills [71] extended gauge theory for Abelian groups to include non-Abelian groups to describe the strong interaction. A non-Abelian gauge theory was used to unify the electromagnetic and weak forces by Glashow [72] and Goldstone, Salam and Weinberg [73]. In addition, the strong force, which describe the interaction between gluons and quarks is a Yang-Mills theory [74]. So, all forces in nature except gravity can be described by Yang-Mills theories. Electromagnetism is invariant under the gauge group $U(1)$ and the other forces are invariant under the gauge groups $SU(2)$ and $SU(3)$. In this section we review briefly Yang-Mills theory with special attention to QCD.

A central object in field theory in d-dimensional spacetime is the action which is a functional of the fields

$$S = \int d^d x \mathcal{L}(x) . \quad (1.46)$$

A field theory is established when the fields $\psi(x)$ and the Lagrangian $\mathcal{L}(x)$ are defined. Then the fundamental equations of motion of the classical field theory are obtained by the least action principle

$$\frac{\delta S}{\delta \psi(x)} = 0 . \quad (1.47)$$

Suppose the field $\psi(x)$ describes fermions (in the case of QCD, quarks) with mass m and Lagrangian $\mathcal{L}(x)$

$$\mathcal{L}(x) = \bar{\psi}(x)(i\gamma^\mu \partial_\mu - m)\psi(x) , \quad (1.48)$$

where γ^μ s are the Dirac gamma matrices which are defined by the anticommutation relation $\{\gamma^\mu, \gamma^\nu\} = -2\eta^{\mu\nu}$ and $\bar{\psi} = \psi^\dagger \gamma^0$. The fermion field $\psi(x)$ belongs to the N-dimensional fundamental representation of the group G, which has N components $\psi_i(x)$, where $i = 1, 2, \dots, N$.

The gauge principle requires that the Lagrangian (1.48) be invariant under the local transformation (see Sec. 2.1.2 of Ref [75])

$$\psi'_i(x) = U_{ij}(x)\psi_j(x), \quad U(x) = \exp(-it^a \theta^a(x)) , \quad (1.49)$$

where the t^a s are the generators of the group G and θ^a are the transformation parameters for the $SU(N)$ group, $a = 1 \dots N^2 - 1$. If t^a satisfy

$$[t^a, t^b] = if^{abc}t^c , \quad (1.50)$$

where f^{abc} are the structure constants, then the transformation (1.50) is a non-Abelian gauge transformation. In addition, θ^a is a spacetime dependent parameter, and the transformation is a local gauge transformation.

It is clear that the Lagrangian (1.48) is not invariant under a non-Abelian local gauge transformation. The non-invariant term stems from the use of the partial derivative ∂_μ . However, it can be made invariant by replacing the ordinary derivative with the covariant derivative

$$\partial_\mu \rightarrow D_\mu = \partial_\mu - ie_g t^a A_\mu^a, \quad (1.51)$$

where e_g is a coupling constant and A_μ^a are the gauge fields which should transform under a gauge transformation as

$$t^a A_\mu^a \rightarrow t^a A_\mu^{\prime a} = U \left(t^a A_\mu^a - \frac{i}{e_g} U^{-1} \partial_\mu U \right) U^{-1}. \quad (1.52)$$

So, the Lagrangian density

$$\mathcal{L}(x) = \bar{\psi}(x)(i\gamma^\mu D_\mu - m)\psi(x) - \frac{1}{4} F_{\mu\nu}^a F^{a\mu\nu}, \quad (1.53)$$

is invariant under gauge transformations (1.49) and (1.52). The second term in eq. (1.53) is a kinetic term for the gauge fields (here gluons) with

$$F_{\mu\nu}^a = \partial_\mu A_\nu^a - \partial_\nu A_\mu^a + e_g f^{abc} A_\mu^b A_\nu^c. \quad (1.54)$$

Finally, the classical Lagrangian density of QCD can be written as

$$\mathcal{L}^{QCD}(x) = \sum_{k=1}^{N_f} \bar{\psi}^k(x)(i\gamma^\mu D_\mu - m_k)\psi^k(x) - \frac{1}{4} F_{\mu\nu}^a F^{a\mu\nu}, \quad (1.55)$$

where N_f is the number of fermions (quarks).

Before quantizing a Yang-Mills theory, first the problem of gauge freedom should be addressed. To see the importance of the gauge fixing problem, consider the QCD Lagrangian density without fermions in Eq. (1.55)

$$\mathcal{L}^{QCD}(x) = -\frac{1}{4} F_{\mu\nu}^a F^{a\mu\nu}. \quad (1.56)$$

This Lagrangian defines a classical theory of non-Abelian gauge fields which interact with each other. In order to quantize this theory by using the canonical formalism, we should first construct the canonical momenta Π_μ^a conjugate to the field A_μ^a . Then by

setting the appropriate commutation relation for these operators, one can quantize the theory. The canonical momentum conjugate to A_μ^a is defined by

$$\Pi_\mu^a = \frac{\partial \mathcal{L}}{\partial \dot{A}^{a\mu}} = -F_{0\mu}^a, \quad (1.57)$$

with $\dot{A}^{a\mu} = \partial_0 A^{a\mu}$. The canonical commutation relation can be written as

$$[A_\mu^a(x), \Pi_\nu^b(y)]_{x_0=y_0} = i\delta_{ab}g_{\mu\nu}\delta^3(\mathbf{x} - \mathbf{y}). \quad (1.58)$$

Assuming $\mu = \nu = 0$ and $a = b = 1$ in (1.58), one obtains

$$[A_0^a(x), \Pi_0^1(y)]_{x_0=y_0} = i\delta^3(\mathbf{x} - \mathbf{y}), \quad (1.59)$$

However from (1.57), we get

$$\Pi_0^a = 0. \quad (1.60)$$

So, eqs. (1.60) and (1.59) are inconsistent and the use of the canonical formalism to quantize the theory fails.

Like quantum electrodynamics, the problem is the invariance of the original Lagrangian under gauge transformations [75]

$$A_\mu^a \rightarrow A_\mu^a + f^{abc}\theta^b A_\mu^c - \frac{1}{e_g}\partial_\mu\theta^a, \quad (1.61)$$

One way to eliminate the gauge freedom is to fix the gauge, for example, by imposing the Lorentz condition

$$\partial^\mu A_\mu^a = 0. \quad (1.62)$$

One way to dealing with constrained systems is the Lagrangian multiplier method [76]. According to the Lagrangian multiplier method, the following term should be added to Lagrangian (1.56)

$$-\frac{1}{2\omega}(\partial^\mu A_\mu^a)^2, \quad (1.63)$$

where $-\frac{1}{2\omega}$ acts as a Lagrangian multiplier and the parameter ω is called the gauge fixing parameter. Then the modified Lagrangian can be written

$$\mathcal{L}^{\text{QCD}}(x) = -\frac{1}{4}F_{\mu\nu}^a F^{a\mu\nu} - \frac{1}{2\omega}(\partial^\mu A_\mu^a)^2. \quad (1.64)$$

Because of the gauge fixing term, the Lagrangian is no longer gauge invariant. However, the physical predictions of Lagrangian (1.56) are independent of the gauge fixing term.

So, the value of ω is arbitrary. Two common choices are Feynman gauge ($\omega = 1$) and Landau gauge ($\omega \rightarrow 0$).

Lagrangian (1.64) solve the problem of vanishing canonical momentum. In the case of quantum electrodynamics, we could have a consistent quantized theory with Lagrangian density (1.64). However in the case of non-Abelian gauge theory, there arises a new problem. To keep the unitarity of the theory one should introduce the Faddeev-Popov ghost term into the Lagrangian (1.64) [77] (see also section 2.2 of [75])

$$\mathcal{L}_{\text{FP}} = (\partial^\mu \bar{\eta}^a) D_\mu^{ab} \eta^b, \quad D_\mu^{ab} = \delta^{ab} \partial_\mu - e_g f^{abc} A_\mu^c, \quad (1.65)$$

where χ is the ghost field.

Finally, the total Lagrangian of quantum chromodynamics can be written as

$$\mathcal{L}_{\text{QCD}} = \mathcal{L}_{\text{G}} + \mathcal{L}_{\text{GF}} + \mathcal{L}_{\text{FP}} + \mathcal{L}_{\text{F}}, \quad (1.66a)$$

$$\mathcal{L}_{\text{G}} = -\frac{1}{4} F_{\mu\nu}^a F^{a\mu\nu}, \quad (1.66b)$$

$$\mathcal{L}_{\text{GF}} = -\frac{1}{2\omega} (\partial^\mu A_\mu^a)^2, \quad (1.66c)$$

$$\mathcal{L}_{\text{FP}} = (\partial^\mu \bar{\eta}^a) D_\mu^{ab} \eta^b, \quad (1.66d)$$

$$\mathcal{L}_{\text{F}} = \bar{\psi}(x) (i\gamma^\mu D_\mu - m) \psi(x), \quad (1.66e)$$

where \mathcal{L}_{G} is the gauge vector field (gluon) kinetic term, \mathcal{L}_{GF} is the gauge fixing term, \mathcal{L}_{FP} is the Faddeev-Popov ghost term, and \mathcal{L}_{F} is the fermion (quark) Lagrangian. A, η, ψ are vector gauge field, Faddeev-Popove ghost field, and the fermion field respectively.

Forming the generating functional

$$\begin{aligned} Z[J, \xi, \xi^*, \eta, \bar{\eta}] &= \int [dA][d\chi][d\chi^*][d\psi][d\bar{\psi}] \\ &\times \exp\left\{i \int d^4x (\mathcal{L}_{\text{QCD}} + A_\mu^a J^{a\mu} + \chi^{a*} \xi^a + \xi^{a*} \chi^a + \bar{\psi}^a \eta^a + \bar{\eta}^a \psi^a)\right\}, \quad (1.67) \end{aligned}$$

one can quantize the Lagrangian (1.66a) using the functional-integral formalism [78], where J, ξ, η are the source functions for the bosons, ghost and fermions (quarks) respectively. Using the generating functional (1.67) one can obtain the connected Green's function

$$G_n^c(x_1, \dots, x_n) = (-i)^{n-1} \frac{\delta^n W[J, \dots]}{\delta J(x_1) \dots \delta J(x_n)} \Bigg|_{J=0}, \quad (1.68)$$

where $W[J, \dots] = -i \ln Z[J, \dots]$. Using these Green's function and defining the associated Feynman rules, one can calculate the propagators and vertices using perturbation theory in QCD.

1.6 Overview

This Thesis consists of two main parts, each focused on different $f(R)$ models of gravity. Before discussing the models in detail, in chapter 2 we will describe the phenomenology of $f(R)$ theories and the chameleon mechanism. Then in chapter 3 we will consider squared-root ($|R|^{1/2}$) QCD-scale modified-gravity (MG1), a $f(R)$ theory motivated by q -theory. After introducing the MG1 model in section 3.1, in section 3.2 we investigate the behavior of the cosmological perturbations in order to distinguish the model from Λ CDM. Then, in section 3.3 we constrain the model parameters using cosmological data through a Markov Chain Monte Carlo (MCMC) simulation. Finally we will investigate the viability of this model on local scales using the chameleon mechanism in section 3.4.

In chapter 4 we investigate a $f(R)$ theory motivated by the semiclassical approach to quantum gravity and its effect on the structure of relativistic stars (MG2). In section 4.1 we propose a phenomenological $f(R)$ model of the form $R + \alpha R^2 + \frac{\beta}{2} R^2 \ln(R^2/\mu^4)$ by considering the calculation of the gauge invariant effective action for gauge fields in curved spacetime. Then in section 4.2 we investigate constraints imposed upon the model from the requirements of internal consistency and compatibility with observations, and discuss the potential observational signatures due to a change in the effective gravitational constant near the surface of the star. In section 4.3, we will solve the modified Tolman-Oppenheimer-Volkov equations and calculate the effect of the $f(R)$ theory on the mass-radius diagram of neutron stars with different equations of state. In this section we also consider the effect of the $f(R)$ model on a separate class of neutron stars, self-bound stars, consisting of strange quark matter with finite density but zero pressure at their surface.

In chapter 5, we summarize the main results and provide conclusions.

2

$f(R)$ theories and the chameleon mechanism

In modern cosmology it is assumed that the Universe has undergone two phases of cosmic acceleration. One accelerating phase occurred in the early universe shortly after the big bang, known as inflation [66–69]. This phase of acceleration is essential to solve the flatness, monopole and horizon problems [67] and in addition can give rise to the almost flat spectrum of temperature anisotropies observed in the Cosmic Microwave Background (CMB) radiation [79]. The second accelerating phase, which has started relatively recently, was discovered by two independent groups in 1998 using observations of type Ia supernovae [4, 5]. The simplest, but most natural candidate to explain this recent accelerating expansion is the cosmological constant term Λ , with the constant equation of state (EoS) $w = -1$ [80, 81]. As described in section 1.3.1, the cosmological constant confronts us with two difficulties: the fine-tuning (CCP1, CCP2a) and cosmic coincidence problems (CCP2b). In order to solve or alleviate these problems many dynamical dark energy models with time-varying EoSs have been proposed. The quintessence [82, 83], phantom [84–86], quintom [87–89], K-essence [90, 91] and ghost condensate [92, 93] scenarios are examples of dynamical models involving scalar fields. In those models, the dark energy effect comes about due to the potential energy of the fields, and the dynamics is affected by the form of the field’s kinetic term. Although many dynamical dark energy models have been suggested, the basic Λ CDM model with a cosmological constant remains an excellent description of the universe on large scales.

$f(R)$ theories modify the Einstein-Hilbert action to include a general function of

the Ricci scalar, however, any $f(R)$ theory can be transformed to the Einstein frame where the action for the gravitational sector takes the standard form. The extra scalar degree of freedom (scalaron) in $f(R)$ theories is coupled directly to the matter sector with a coupling of order unity. If we want to use this scalar field to explain the dark energy (as in quintessence models) its mass must be of order H_0 , the present Hubble parameter. However, a directly coupling to the matter sector of this scalar field of order unity causes violations of the Equivalence Principle (EP) and constraints derived from other local experiments. [8, 94]. One way to suppress the offending terms is the chameleon mechanism [9–11].

In this chapter, beginning in section 2.1 we discuss $f(R)$ theories of gravity and then in section 2.2, we will discuss the chameleon mechanism.

2.1 $f(R)$ theories

One approach to model the accelerating phases is to modify the Einstein-Hilbert action by replacing the simple Ricci scalar R term by a general function of R , i.e. $f(R)$. For example, Starobinsky in 1980 proposed a model to describe inflation using $f(R) = R + \alpha R^2$ with $\alpha > 0$ [95]. One of the first attempts to model dark energy with $f(R)$ theory was $f(R) = R - \alpha/R^n$, where the corresponding curvature becomes significant in low-curvature limits, corresponding to late-time cosmology [96–98]. It was shown that this model has an instability [99, 100] and, in addition, contradicts the local tests of gravity [101–103]. However there are a number of viable $f(R)$ gravity models that can pass cosmological and local gravity constraints [104–108]. One can list the most important conditions for viability of $f(R)$ models for $R_0 \geq 0$ as [106]

$$f_R > 0, \quad (2.1a)$$

$$f_{RR} > 0, \quad (2.1b)$$

where $f_R = df/dR$, $f_{RR} = d^2f/dR^2$ and R_0 is the Ricci scalar today. The first condition is essential to avoid problems with unitarity arising from ghost degrees of freedom. When the $f_{RR} > 0$ condition is satisfied, the squared mass of the scalaron field is positive, avoiding potential problems with instabilities.

Consider a 4-dimensional modified action

$$S = \frac{M_{\text{Pl}}^2}{2} \int d^4x \sqrt{-g} f(R) + \int d^4x \mathcal{L}_{\text{matter}}(g_{\mu\nu}, \psi_{\text{m}}), \quad (2.2)$$

where $f(R)$ is a general function of the Ricci scalar R , $M_{\text{Pl}}^2 = (8\pi G)^{-1}$, G is the bare gravitational coupling constant and $\mathcal{L}_{\text{matter}}$ is a matter Lagrangian density that depends on the metric $g_{\mu\nu}$ and the matter fields ψ_{m} . The modified Einstein equations are obtained by varying (2.2) with respect to the metric $g_{\mu\nu}$ as

$$f_R R_{\mu\nu} - \frac{1}{2}f(R)g_{\mu\nu} - \nabla_\mu \nabla_\nu f_R + g_{\mu\nu} \square f_R = 8\pi G T_{\mu\nu}^{\text{matter}}, \quad (2.3)$$

where $f_R \equiv df(R)/dR$. $T_{\mu\nu}^{\text{matter}}$ is the energy-momentum tensor of the matter fields, which is defined by the variation of $\mathcal{L}_{\text{matter}}$ with respect to $g^{\mu\nu}$ as

$$T_{\mu\nu}^{\text{matter}} = -\frac{2}{\sqrt{-g}} \frac{\delta S_{\text{matter}}}{\delta g^{\mu\nu}}. \quad (2.4)$$

One can rewrite the field equations (2.3) as

$$R_{\mu\nu} - \frac{1}{2}Rg_{\mu\nu} = 8\pi G (T_{\mu\nu}^{\text{matter}} + T_{\mu\nu}^{\text{DE}}), \quad (2.5)$$

where the dark energy stress-energy tensor $T_{\mu\nu}^{\text{DE}}$ is defined as

$$T_{\mu\nu}^{\text{DE}} = \frac{1}{8\pi G} \left((1 - f_R)R_{\mu\nu} - \frac{1}{2}(1 - f(R))g_{\mu\nu} + \nabla_\mu \nabla_\nu f_R + g_{\mu\nu} \square f_R \right). \quad (2.6)$$

Then one can reproduce the accelerating solutions by an appropriate choice of the function $f(R)$ [109, 110].

Eq. (2.3) is a set of equations that are second order in derivatives of R , which is itself second order in derivatives of $g_{\mu\nu}$, so the resulting equations are fourth order. Fortunately, metric $f(R)$ theories (i.e. $f(R)$ theories in which the metric $g_{\mu\nu}$ is the only independent variable in the gravitational sector) can be transformed to the Einstein frame (EF) in which we have second order differential equations in terms of a metric with an extra scalar degree of freedom.¹ This is achieved by applying the following conformal transformation

$$\tilde{g}_{\mu\nu} = F(\phi)g_{\mu\nu}, \quad (2.7a)$$

$$F(\phi) = f_R \equiv e^{-2Q\phi/M_{\text{Pl}}}, \quad (2.7b)$$

¹ In addition to the metric $f(R)$ theories considered in this Thesis one can also have Palantini $f(R)$ theories, in which the metric and the connection are treated as independent degrees of freedom. See [6] and references therein for details.

where $Q = 1/\sqrt{6}$. By applying above transformations to the action (2.2) we obtain

$$\tilde{S} = \int d^4x \sqrt{-\tilde{g}} \left[\frac{M_{Pl}^2}{2} \tilde{R} - \frac{1}{2} \tilde{g}^{\mu\nu} \partial_\mu \phi \partial_\nu \phi - V(\phi) \right] + \int d^4x \mathcal{L}_{\text{matter}}(F^{-1}(\phi) \tilde{g}_{\mu\nu}, \psi_m), \quad (2.8)$$

where a tilde represents quantities in the Einstein frame and

$$V(\phi) = \frac{M_{Pl}^2}{2} \frac{f_R R - f(R)}{f_R^2}. \quad (2.9)$$

Although solving the field equations arising from the action (2.8) is easier than those arising from the original action 2.2, there is a difficulty. The scalaron ϕ is coupled directly to the matter sector with a coupling of order unity through the $F^{-1}(\phi) \tilde{g}_{\mu\nu}$ term.

2.2 Chameleon mechanism

One can model dark energy as quintessence i.e. a scalar field rolling down a potential [83, 111]. For a single scalar field the dynamics of such a scalar field in the Einstein frame is given by (cf. 2.8)

$$\tilde{S} = \int d^4x \sqrt{-\tilde{g}} \left(\frac{M_{Pl}^2}{2} \tilde{R} - \frac{1}{2} (\partial\phi)^2 - V(\phi) \right) - \int d^4x \mathcal{L}_{\text{matter}}(e^{2Q\phi/M_{Pl}} \tilde{g}_{\mu\nu}, \psi_m). \quad (2.10)$$

The scalar field ϕ interacts directly with the matter through a conformal coupling of the form $e^{Q\phi/M_{Pl}}$. The matter field ψ_m couples to the Jordan frame (JF) metric $g_{\mu\nu}$ which is related to the Einstein-frame metric $\tilde{g}_{\mu\nu}$ by

$$g_{\mu\nu} = e^{2Q\phi/M_{Pl}} \tilde{g}_{\mu\nu}, \quad (2.11)$$

where Q is a dimensionless constant ($Q = 1/\sqrt{6}$ for $f(R)$ theories). Therefore the scalar field of the quintessence or $f(R)$ theory is directly coupled to the matter section with a coupling of gravitational strength. Such couplings lead to strong violations of the Equivalence Principle (EP) [8]. Therefore it is interesting to consider a mechanism that can suppress its EP violating contribution. Here we discuss one of these mechanisms, viz., chameleon gravity [9–11]. In this mechanism, the mass of the scalar field depends on the density of the environment. In a high density medium such as the solar system or inside the atmosphere, the mass of the scalar field is very large, with the result that the range of the scalar field is undetectable in local gravitational tests. Moreover, for

large bodies such as planets and stars, the thin-shell effect (see section 2.2) suppresses the fifth force due to this scalar degree of freedom and the scalar field is trapped inside the celestial object. Therefore, it is almost impossible to detect the footprint of the chameleon field for test bodies in ground based experiments or in solar system tests of gravity (with current instrumental accuracy) if the scalar field behaves like a chameleon field [112]. However, on large scales, where the matter density is much smaller than the atmospheric matter density, the mass of the scalar field is of order of the Hubble parameter H_0 and can therefore give rise to the accelerated expansion.

The chameleon potential $V(\phi)$ can be assumed to be (at least in some regions) of the runaway form (see figure 2.1). That is, the potential should be monotonically decreasing and satisfies for $\phi \rightarrow \infty$ (for other possible potentials see [11])

$$V(\phi) \rightarrow 0, \quad \frac{V_{,\phi}}{V} \rightarrow 0, \quad \frac{V_{,\phi\phi}}{V_{,\phi}} \rightarrow 0, \quad \dots, \quad (2.12)$$

and also for $\phi \rightarrow 0$

$$V(\phi) \rightarrow \infty, \quad \frac{V_{,\phi}}{V} \rightarrow \infty, \quad \frac{V_{,\phi\phi}}{V_{,\phi}} \rightarrow \infty, \quad \dots, \quad (2.13)$$

where $V_{,\phi} \equiv dV/d\phi$ and $V_{,\phi\phi} \equiv d^2V/d\phi^2$. Varying the action (2.10) with respect to ϕ , we get the following field equation for the chameleon field

$$\tilde{\square}\phi = V_{,\phi} - \frac{Q}{M_{\text{Pl}}} g^{\mu\nu} T_{\mu\nu}^{\text{matter}}, \quad (2.14)$$

where $T_{\mu\nu}^{\text{matter}} = -\frac{2}{\sqrt{-g}} \frac{\delta \mathcal{L}_{\text{matter}}}{\delta g^{\mu\nu}}$. The trace of the energy momentum tensor is given by $T \equiv g^{\mu\nu} T_{\mu\nu}^{\text{matter}} = -\rho_J$ for a nonrelativistic fluid, where ρ_J is the energy density in the Jordan frame. In the Einstein frame we have $\tilde{\rho}_E = \rho_J e^{4Q\phi/M_{\text{Pl}}}$, which is not conserved (for example in a FRW universe $\dot{\tilde{\rho}}_E + 3H\tilde{\rho}_E = \frac{Q}{M_{\text{Pl}}} \dot{\phi} \tilde{\rho}_E$), however, $\rho = e^{3Q\phi/M_{\text{Pl}}} \tilde{\rho}_E$ is conserved. Then eq. (2.14) reduces to

$$\tilde{\square}\phi = V_{,\phi} + \frac{Q}{M_{\text{Pl}}} \rho e^{Q\phi/M_{\text{Pl}}} \equiv V_{\text{eff},\phi}(\phi), \quad (2.15)$$

where the effective potential V_{eff} is defined as

$$V_{\text{eff}}(\phi) \equiv V(\phi) + \rho e^{Q\phi/M_{\text{Pl}}}. \quad (2.16)$$

The effective potential has a minimum at a field value ϕ_{min} , which is a solution of the equation

$$V_{,\phi}(\phi_{\text{min}}) + \frac{Q}{M_{\text{Pl}}} \rho e^{Q\phi_{\text{min}}/M_{\text{Pl}}} = 0, \quad (2.17)$$

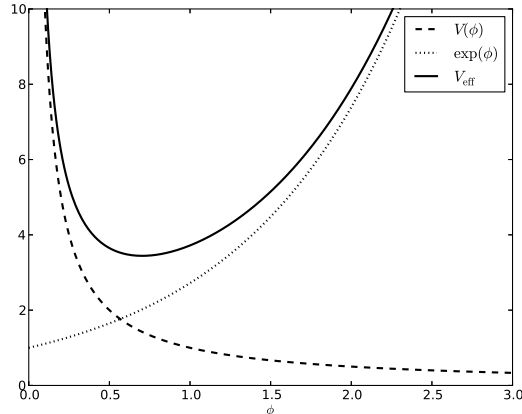


Figure 2.1: A typical runaway potential $V(\phi) = 1/\phi$ (dash-line) that can give rise to the chameleon effect and the effective potential V_{eff} (solid-line).

and the corresponding squared effective mass of the scalar field is defined

$$m_{\text{min}}^2 \equiv \left. \frac{d^2 V_{\text{eff}}}{d\phi^2} \right|_{\phi=\phi_{\text{min}}} . \quad (2.18)$$

Equation (2.17) shows that if ρ increases, then ϕ_{min} decreases, as $V_{,\phi}$ and $e^{Q\phi/M_{\text{Pl}}}$ are increasing functions of ϕ . Then we expect m_{min} to increase, because $V_{,\phi\phi}$ is a decreasing function of ϕ . This is what is called chameleon behavior.

In the case of a spherically symmetric body, eq. (2.15) yields

$$\frac{d^2 \phi}{dr^2} + \frac{2}{r} \frac{d\phi}{dr} = \frac{dV_{\text{eff}}}{d\phi} = V_{,\phi} + \frac{Q}{M_{\text{Pl}}} \rho e^{Q\phi/M_{\text{Pl}}} . \quad (2.19)$$

To solve eq. (2.19) we use the following boundary conditions [10]

$$\begin{aligned} \frac{d\phi}{dr}(r=0) &= 0 , \\ \phi(r \rightarrow \infty) &= \phi_{\text{b}} . \end{aligned} \quad (2.20)$$

The first condition asserts that the the solution is non-singular at the origin and the second condition specifies that the fifth force on test particles vanishes at infinity.

Now consider a spherically symmetric body with density ρ_c which is immersed in a medium with density ρ_b . The mass of the body is $M_c = (4\pi/3)\rho_c R_c^3$, where R_c is the radius of the body. In addition we have the following quantities

$$\begin{aligned} \phi_c &\equiv \phi_{\text{min}} \Big|_{\rho=\rho_c} , & \phi_b &\equiv \phi_{\text{min}} \Big|_{\rho=\rho_b} , \\ m_c &\equiv m_{\text{min}}(\phi_c) , & m_b &\equiv m_{\text{min}}(\phi_b) . \end{aligned} \quad (2.21)$$

In the following we discuss the solution of the field equation (2.19), following the treatment in [112] (see Appendix B for details of the derivation).

To obtain the solutions of the field equation (2.19) we assume that $V_{\text{eff},\phi}$ can be approximated with a harmonic oscillator in the region $r > R_c$ (where $\phi \simeq \phi_c$) as

$$\frac{d^2\phi}{dr^2} + \frac{2}{r} \frac{d\phi}{dr} = m_b^2(\phi - \phi_b). \quad (2.22)$$

The solution in this case is

$$\phi(r) = A \frac{e^{-m_b(r-R_c)}}{r} + B \frac{e^{m_b(r-R_c)}}{r} + \phi_b, \quad (2.23)$$

with two dimensionless constants A and B . By imposing the boundary condition $\phi \rightarrow \phi_b$ as $r \rightarrow \infty$ we get $B = 0$. Therefore the solution for the external regions of the test body can be written

$$\phi(r) = A \frac{e^{-m_b(r-R_c)}}{r} + \phi_b. \quad (2.24)$$

To investigate the interior solutions $r < R_c$, we divide the interior region into two different regions: from $r = 0$ to R_1 where ($\phi \simeq \phi_c$), and from $r = R_1$ to $r = R_c$ (where $\phi \gg \phi_c$). When $\phi \gg \phi_c$, the second term in the effective potential dominates and so

$$V_{\text{eff},\phi} \approx \frac{Q}{M_{\text{Pl}}} \rho_c. \quad (2.25)$$

We can then rewrite equation (2.19) as

$$\frac{d^2\phi}{dr^2} + \frac{2}{r} \frac{d\phi}{dr} \approx \frac{Q}{M_{\text{Pl}}} \rho_c. \quad (2.26)$$

The solution of eq. (2.26) is

$$\phi(r) = \frac{Q}{6M_{\text{Pl}}} \rho_c r^2 + \frac{C}{r} + D\phi_c \quad R_1 < r < R_c, \quad (2.27)$$

where D and C are dimensionless constants. When $\phi \simeq \phi_c$ again we can use the harmonic oscillator approximation

$$V_{\text{eff},\phi} = m_c^2(\phi - \phi_c), \quad (2.28)$$

with solution

$$\phi(r) = E \frac{e^{-m_c r}}{r} + F \frac{e^{m_c(r-R_c)}}{r} + \phi_c \quad 0 < r < R_1, \quad (2.29)$$

where E and F are dimensionless constants (and $E = -Fe^{-m_c R_c}$ to prevent singularity at $r = 0$).

Using the boundary conditions (2.20) and the continuity of solutions (2.24), (2.27) and (2.29) and their first derivatives $d\phi/dr$ at the boundaries $r = R_1$ and $r = R_c$ we can obtain the dimensionless constants A , C , D , E , and F .

Therefore, for a test body of density ρ_c mass M_c and radius R_c in a medium with density ρ_b , the chameleon field outside the body is expressed approximately [using equations B.14, B.15a (in the $m_b R_c \ll 1$), B.16 and B.21a] as [10]

$$\phi_{\text{thick}}(r) = -\frac{QM_c}{4\pi M_{\text{Pl}}} \frac{e^{-m_b(r-R_c)}}{r} + \phi_b, \quad (2.30a)$$

$$\phi_{\text{thin}}(r) = -\frac{QM_c}{4\pi M_{\text{Pl}}} 3\epsilon_{\text{th}} \frac{e^{-m_b(r-R_c)}}{r} + \phi_b, \quad (2.30b)$$

where

$$\epsilon_{\text{th}} \equiv \frac{M_{\text{Pl}}(\phi_b - \phi_c)}{Q\rho_c R_c^2}. \quad (2.31)$$

The subscripts *thin* and *thick* in eqs. (2.30a, 2.30b) define the type of solution. As we shall see in the following subsections, an $f(R)$ model can pass the local tests if it exhibits a thin shell solution. The parameter ϵ_{th} in eq. (2.31) determines whether the solution is thick- or thin-shell: a thin-shell solution corresponds to $\epsilon_{\text{th}} \ll 1$.

2.2.1 Effective gravitational coupling constant

For the chameleon force \vec{F}_{ch} (fifth-force) on a test body of mass m at distance r from a central body of mass M_c and radius R_c we have¹ [10]

$$|\vec{F}_{ch}| = m \frac{Q}{M_{\text{Pl}}} |\vec{\nabla}\phi|, \quad (2.32)$$

¹The geodesic equation in the Jordan frame has the form

$$\ddot{x}^\mu + \Gamma_{\alpha\nu}^\mu \dot{x}^\alpha \dot{x}^\nu = 0,$$

and in the Einstein frame can be written

$$\ddot{x}^\mu + \tilde{\Gamma}_{\alpha\nu}^\mu \dot{x}^\alpha \dot{x}^\nu = -\theta_{,\phi} \dot{\phi}^\mu - 2\theta_{,\phi} \dot{x}^\nu \dot{x}^\mu \phi_{,\nu},$$

where $\theta \equiv Q\phi/M_{\text{Pl}}$. In the nonrelativistic limit the last term can be neglected and the chameleon force on a test particle is given by:

$$\vec{F}_{ch} = -m\theta_{,\phi} \vec{\nabla}\phi.$$

where ϕ is described by one of the external chameleon field solutions in (2.30).

One can write for the total force (gravitational+chameleon) on a test particle with mass m at distance r from a central body with mass M_c and radius R_c in a medium with density ρ_b

$$F_{tot} \equiv F_G + F_\phi = G_{\text{eff}} \frac{mM_c}{r^2}, \quad (2.33)$$

where the effective gravitational coupling constant for the thin- thick-shell case is defined as

$$G_{\text{eff}} = \begin{cases} [1 + 6Q^2 \epsilon_{th} e^{-m_b(r-R_c)}]G & \text{thin-shell} \\ [1 + 2Q^2 e^{-m_b(r-R_c)}]G & \text{thick-shell} \end{cases} \quad (2.34)$$

where G is the bare gravitational coupling constant. One can easily see that $G_{\text{eff}} \simeq G$ for the thin-shell case, while $G_{\text{eff}} \neq G$ in the thick-shell regime. Therefore, a theory can satisfy the laboratory tests of gravity if it has the thin-shell solution on local scales [10]. We define

$$\delta^2 \equiv \frac{G_{\text{eff}}}{G}, \quad (2.35)$$

and use this parameter to check the deviation from General Relativity. In GR $\delta^2 = 1$ and $G_{\text{eff}} = G = G_N$.

2.2.2 Fifth force searches

One way to search for a fifth force due to a scalar field is to consider the potential energy associated with it. The potential energy is generally parametrized by a Yukawa potential [113]

$$U(r) = \alpha \frac{M_1 M_2}{8\pi M_{\text{Pl}}^2} \frac{e^{-r/\lambda}}{r}, \quad (2.36)$$

where M_1 and M_2 are the masses of the two test bodies with separation r . The strength of the interaction is determined by the parameter α (gravitational strength corresponds to $\alpha = \mathcal{O}(1)$) and λ is the range of the potential. Null fifth force searches constrain the (α, λ) plane (cf. figure 2.13 of ref [18]). For $\lambda \simeq 10 \text{ cm} - 1 \text{ m}$, the tightest bound on the coupling constant α is from Hoskins et al [114]. For laboratory experiments it is

$$\alpha < 10^{-3}, \quad (2.37)$$

and for $\lambda \simeq 10^{10} m$, one has $\alpha < 10^{-10}$. Now consider two identical test bodies of uniform density ρ_c and radius R_c and total mass M_c . Using the external chameleon

fields of eqs. (2.30a) and (2.30b), the chameleon potential energy is obtained as

$$U_{\text{thick}}(r) = -2Q^2 \frac{M_c^2}{8\pi M_{\text{Pl}}} \frac{e^{-m_b(r-R_c)}}{r}, \quad (2.38a)$$

$$U_{\text{thin}}(r) = -2Q^2 (9\epsilon_{th}^2) \frac{M_c^2}{8\pi M_{\text{Pl}}} \frac{e^{-m_b(r-R_c)}}{r}, \quad (2.38b)$$

where here m_b plays the role of $1/\lambda$. So, by comparing with eq. (2.36), we will obtain for the interaction strength parameter

$$\alpha_{\text{thick}} = 2Q^2, \quad \alpha_{\text{thin}} \simeq 18Q^2 \epsilon_{th}. \quad (2.39)$$

α_{thick} clearly violates the bound in eq. (2.37) for $Q \sim \mathcal{O}(1)$. We shall also see this in the case of the QCD-scale modified-gravity model in the following chapter. But one can easily check that $\alpha_{\text{thin}} < 10^{-3}$ for $Q \sim \mathcal{O}(1)$. Current experimental data give an upper bound $\lambda \leq 1$ mm for a strong ($\alpha \simeq 1$) Yukawa potential force which translates to a mass of $m_b \geq 10^{-13}$ GeV [114].

3

$|R|^{1/2}$ QCD-scale modified-gravity (MG1)

One of the recent models that has been suggested to describe the accelerating expansion of the universe is the squared-root QCD-scale modified-gravity model [43] (sometimes we refer to the model just QCD-scale modified-gravity). Starting from q -theory as an approach to solve the main cosmological constant problem (CCP1), the huge value of the quantum vacuum energy in the action is nullified. Then by identifying the parameter q in the q -theory with the gluon condensate and considering its perturbation due to the expansion of the universe [42, 43], one obtains a nonanalytical term in the effective gravitational action, which can be interpreted as an $f(R)$ gravity model. This model explains the late time expansion of the universe very well only with two fundamental energy scales, the QCD energy scale E_{QCD} and the Planck energy E_{Pl} , and a single dimensionless coupling constant η . This QCD-scale modified-gravity model (or square-root modified-gravity model) has been suggested to explain the large scale structure of the Universe. To describe gravity at local scales, another $f(R)$ model has been suggested with an extra dimensionless constant ζ [43].

In this chapter we will consider different aspects of QCD-scale modified-gravity. In section 3.1 we will discuss briefly QCD vacuum and introduce the model. In section 3.2 we will investigate the cosmological perturbations in the QCD-scale modified-gravity model. We will consider the effect of the modification on some of the perturbation theory parameters such as the effective gravitational coupling constant G_{eff} , the gravity estimator E_G [115], the late integrated Sachs-Wolf (ISW) effect [116] and the matter

power spectrum. Then in section 3.3, using a Markov Chain Monte Carlo simulation, we will constrain the cosmological and the model parameters with observational data. The constraints on the parameter $\beta_q \equiv q_0/q$ where $q_0 = (300\text{MeV})^4$ is the expectation value of gluon condensate, are especially interesting. As the QCD-scale modified-gravity provides a relation between high-energy physics and cosmology, we can therefore constrain a quantity from particle physics (i.e. the gluon condensate) by large-scale observations. If a modified theory gives rise to the observed phenomenology on large scales and could pass the local gravity tests by exhibiting a chameleon effect on the local scales, then this model would be a viable theory of gravity from largest scales to the local scales. In section 3.4 we will check the consistency of QCD-scale modified-gravity with the local experiments of gravity by using the chameleon formalism [9, 10]. In this section, we also check the consistency of the local QCD-scale modified-gravity model with the local tests as well.

3.1 $|R|^{1/2}$ QCD-scale modified-gravity model

3.1.1 Gluon condensate and q -theory

As in this chapter we investigate a version of q -theory that uses the QCD vacuum to solve the main cosmological constant problem, we begin by briefly discussing some properties of the QCD vacuum.

The ground state in QCD, which is an example of a nonperturbative vacuum, is typically characterized by non-vanishing condensates i.e., the gluon and quark condensates. For example, in the framework of the instanton liquid models [117], the topological modes of the gluon and quark condensates are given by the strong non-perturbative fluctuations of the gluons and light quarks. Such fluctuations are caused by the quantum tunneling of the gluon vacuum between topologically different classical states [118]. One of the main characteristics of the QCD vacuum is the topological instanton-type contribution ϵ_{vac} [16] which is derived from the QCD trace anomaly [119–121]

$$T_i{}^i{}_{QCD} = \frac{\alpha_s}{2} F_{\mu\nu}^a F^{a\mu\nu} + \sum_{q=u,d,s} m_q \bar{\psi}_q \psi_q, \quad (3.1)$$

where $T_i{}^i{}_{QCD}$ is the trace of the energy-momentum tensor, m_q is the quark mass, $\psi_q = u, d, s$ are the quark fields (up, down and strange respectively), $F_{\mu\nu}^a$ is the field

strength of the gluon gauge fields (see eq. (1.54)) and $\alpha_s = e_g^2/4\pi$ where e_g is the gauge coupling constant (see eq. (1.51)). On the other hand, if we assume that the QCD vacuum is Lorentz invariant, then the quantum vacuum should have the form of the cosmological constant [23, 122]

$$\langle 0|T_{\mu\nu}|0\rangle = -\epsilon_{\text{vac}}g_{\mu\nu} . \quad (3.2)$$

Using eq. (3.2), one can write for the instanton energy density from eq. (3.1) [123]

$$\begin{aligned} \epsilon_{\text{vac}} &= = \frac{9}{32} \langle 0| : \frac{\alpha_s}{\pi} F_{\mu\nu}^a(x) F^{a\mu\nu}(x) : |0\rangle + \frac{1}{4} [\langle 0| : m_u \bar{u}u : |0\rangle , \\ &\quad - \langle 0| : m_d \bar{d}d : |0\rangle - \langle 0| : m_s \bar{s}s : |0\rangle] \\ &\simeq = (5 \pm 1) \times 10^9 \text{MeV}^4 , \end{aligned} \quad (3.3)$$

where $::$ indicates normal ordering. It is clear that the magnitude of ϵ_{vac} in eq. (3.3) is much larger than the value of the observed cosmological constant $\rho_V \simeq 10^{-47} \text{GeV}^4$ [4]. Therefore, there should be a mechanism to suppress it to the observed value ρ_{obs} . We have already discussed one of these mechanism to nullify this huge vacuum energy density in the field equations in section 1.3.2 viz., q -theory.

The next step is to suggest a model to explain the current accelerated expansion of the Universe. To find such a model we will identify the variable q in q -theory as the gluon condensate from quantum chromodynamics (QCD) [37]

$$q \equiv \left\langle 0 \left| \frac{1}{4\pi^2} F_{\mu\nu}^a F^{a\mu\nu} \right| 0 \right\rangle , \quad (3.4)$$

where the field strength $F_{\mu\nu}^a$ is defined in eq. (1.54) and the numerical value is estimated to be $q \simeq (300 \text{MeV})^4$ [124]. Then we assume that there is an equilibrium value of the gluon condensate q (i.e. \tilde{q}_0) that nullifies the vacuum energy density $\rho_V(\tilde{q}_0) = 0$. However, in a nonequilibrium state such as in an expanding universe, the vacuum quantity q is perturbed to a new value $q_0 \neq \tilde{q}_0$

$$q_0 = \tilde{q}_0 + \delta q(H) \Rightarrow \rho_V(q_0) \sim \frac{d\rho_V}{dq} \delta q(H) \neq 0 . \quad (3.5)$$

Parametrizing the dynamics in terms of the Hubble parameter, one can use the ansatz

$$\begin{aligned} \rho_V(H) &\sim 0 + a_1 H^2 \Lambda_{\text{QCD}}^2 + a_2 H^4 + \dots \\ &\quad + a_3 |H| \Lambda_{\text{QCD}}^3 + a_4 |H|^3 \Lambda_{\text{QCD}}^3 + \dots , \end{aligned} \quad (3.6)$$

where $a_1 \dots a_4$ are constants of order unity. The linear term in H gives the right order of magnitude for the observed vacuum energy density $\rho_V \simeq H_0 \Lambda_{\text{QCD}}^3$ [37]. On the other hand, in a spatially flat Robertson-Walker universe the Ricci scalar has the form $R = 6(2H^2 + \dot{H})$. Recognizing that $|H| \Lambda_{\text{QCD}}^3 \sim |R|^{1/2} |q_0|^{3/4}$ ($\Lambda_{\text{QCD}} \sim q_0^{1/4}$) motivates the use of an $f(R)$ model. In the next subsection we will describe this QCD-scale modified-gravity model in more detail and in the rest of this chapter investigate its properties.

3.1.2 The MG1 model

In [42] Klinkhamer suggested the following QCD-inspired modified gravity model (MG1) as a candidate to explain the accelerating expansion of the Universe

$$S_{\text{eff}}[g, \psi_m] = \int d^4x \sqrt{-g} K(q_0) f(R, q_0) + S_{\text{matter}}(g_{\mu\nu}, \psi_m), \quad (3.7a)$$

$$f(R, q_0) = R - \frac{(R^2)^{\frac{1}{4}}}{L_0}, \quad (3.7b)$$

$$\frac{1}{L_0} = \eta q_0^{\frac{3}{4}} / K, \quad (3.7c)$$

where ψ_m represents the matter fields, $\eta > 0$ is a dimensionless coupling constant and q_0 is the equilibrium value of QCD gluon condensate [37] and $K(q_0) = (16\pi G)^{-1}$. Note that as the Ricci scalar in principle can be negative, we instead of \sqrt{R} in equation (3.7b) we have written $(R^2)^{\frac{1}{4}}$. The action (3.5) can be rewritten in the Jordan frame as a Brans-Dicke theory [8, 17, 125]

$$S_{\text{eff}}^{BD} = \int_{R^4} d^4x \sqrt{-g} [K(\chi R - U(\chi, q))] + S_{\text{matter}}(g_{\mu\nu}, \psi_m), \quad (3.8)$$

with

$$U(\chi) = \frac{\eta^2 |q_0|^{3/2}}{4K^2} \frac{1}{1 - \chi}, \quad (3.9)$$

in terms of a dimensionless scalar field $\chi < 1$.

By varying the action (3.8) with respect to $g_{\mu\nu}$, χ and the gauge field A (see eq. 1.54), we obtain the following field equations

$$\begin{aligned} R^{\mu\nu} - \frac{1}{2} R g^{\mu\nu} &= -\frac{1}{2\chi K} T_M^{\mu\nu} - \frac{1}{2\chi} U g^{\mu\nu} - \frac{1}{\chi} (\nabla^\mu \nabla^\nu - g^{\mu\nu} \square) \chi \\ R &= \frac{\partial U}{\partial \chi} \\ \frac{\partial \rho_V}{\partial q} &= K \frac{\partial U}{\partial q} \end{aligned} \quad (3.10)$$

where μ is an integration constant corresponding to the chemical potential of the conserved charge q and $\rho_V = -\mu q$.

To investigate the cosmological aspects of the model (3.7a) we consider a spatially-flat ($\Omega_k = 0$) Robertson-Walker universe $ds^2 = -dt^2 + a^2(t)dx^2$ where t is the cosmic time. We assume a one-component universe, i.e., we only consider a matter component ρ_m , which is assumed to be a perfect fluid of pressureless nonrelativistic matter (CDM) with equation of state $w_m = P_m/\rho_m = 0$. Then by taking $G = G_N$ and $q_0 = (300 \text{ MeV}^4)$ one can solve the field equations numerically [43] for the background cosmology. We consider three parameters from the background cosmology as in [43]: the present time Hubble parameter H_0 , the effective equation of state of dark energy w_{DE} and a redshift corresponding to the transition from the deceleration to acceleration era z_{inf} .

In addition to the background cosmological parameters, the value of an estimator E_G , a parameter constructed from the first order cosmological perturbations, is calculated for linear sub-horizon matter-density perturbations. The relationship between weak gravitational lensing of galaxies to their large-scale velocities has been suggested as a smoking gun for modified gravity [115]. This relationship is quantified by a measure E_G . This estimator is an observational quantity whose mean value is the ratio of the Laplacian of the perturbation potentials to the peculiar velocity. This estimator is also insensitive to the galactic bias b , a significant advantage of such a probe. In $f(R)$ theories of gravity one has [61]

$$E_G(z) = \frac{\Omega_0^m}{(1 + f_R)\beta}, \quad (3.11)$$

where Ω_0^m is the current matter density parameter, $\beta \equiv d \ln D / d \ln a = \dot{\delta} / H \delta$, D is the linear density growth factor $\delta \equiv \delta \rho / \rho$ and $f_R \equiv df/dR$. For Λ CDM, the value of the estimator E_G value is obtained as 0.418 [115]. We will discuss this gravity estimator in more detail in section 3.2.3.

To solve the equations (3.10), we introduce the following dimensionless variables

t' , $h(t')$, f , u , s and r [126]

$$t \equiv t'K/(\eta q_0^{3/4}), \quad (3.12a)$$

$$H(t) \equiv h(t')\eta q_0^{3/4}/K, \quad (3.12b)$$

$$U(t) \equiv u(t')\eta^2 q_0^{3/2}/K^2, \quad (3.12c)$$

$$\chi(t) \equiv s(t'), \quad (3.12d)$$

$$\rho_m(t) \equiv r_m(t')\eta^2 q_0^{3/2}/K, \quad (3.12e)$$

where $K \equiv 1/(16\pi G)$ and variables U and χ are defined in equation (3.9). From the action (3.8), the following closed system of four first order ordinary differential equations is obtained

$$\dot{h} = -2h^2 - \frac{1}{5} \frac{\partial u}{\partial s}, \quad (3.13a)$$

$$\dot{s} = v, \quad (3.13b)$$

$$\dot{v} = \frac{1}{6} r_m - 3hv - \frac{2}{3} u + \frac{1}{3} s \frac{\partial u}{\partial s}, \quad (3.13c)$$

$$\dot{r}_m = -3hr_m, \quad (3.13d)$$

where in the above equations the overdot stands for differentiation with respect to the dimensionless cosmic time t' and from equation (3.9)

$$u(t') = -\frac{1}{4} \frac{1}{1-s(t')}. \quad (3.14)$$

The initial conditions for (3.13) are obtained by substituting $t' = t_{\text{start}}$ in the following equations [126]

$$h_i(t') = \frac{2}{3} \frac{1}{t'} \left(1 + \frac{3\sqrt{3}}{16} t' - \frac{405}{512} t'^2 \right), \quad (3.15a)$$

$$s_i(t') = \left(1 - \frac{\sqrt{3}}{4} t' + \frac{9}{16} t'^2 \right), \quad (3.15b)$$

$$v_i(t') = \dot{s}_i(t'), \quad (3.15c)$$

$$r_{mi} = \frac{8}{3t'^2} \left(1 - \frac{3\sqrt{3}}{8} t' \right). \quad (3.15d)$$

The starting time t_{start} must be small enough but larger than the time t_{cross} , the time corresponding to the QCD crossover at temperature $T_{\text{cross}} \sim T_{\text{QCD}} \sim 300\text{MeV}$ [126]. One should take a starting time value using condition $1 \gg t_{\text{start}} \gg t_{\text{cross}} \sim$

$\eta E_{\text{QCD}}/E_{\text{Pl}} \sim 10^{-23}$ for $\eta \sim 10^{-4}$. We solve the equations (3.12) by $t_{\text{start}} = 10^{-5}$ and $G \simeq G_{\text{N}}$ realization. The results are presented in table 3.1 [43]. For comparison, we have presented in the third column the recent results from the Planck data for the Λ CDM model [127]. We can see that the results of the QCD-scale modified-gravity model (age, H_0 and E_G) are in good agreement with the Λ CDM results. However, the QCD-scale modified-gravity model prediction of -0.68 for the parameter ω_{DE} may perhaps provide as a crucial test for the model, as long as independent measurements of the present values of dH/dt , H and ρ_M can be done. The Λ CDM values of the parameters age and H_0 are obtained from the Planck data [127] and the Λ CDM value for the parameter z_{in} is obtained in [128]. We will discuss the cosmology of this model again in section 3.3, where we apply a Markov chain Monte Carlo simulation to obtain the cosmological constraints on the model and cosmological parameters. The interesting point about the result in table 3.1 is that one can obtain the first three parameters in this table without specifying q_0 and G .

For later use, we will follow [129] and parametrize $f(R)$ models by the Compton wavelength parameter

$$B_0 \equiv \left. \frac{f_{RR}}{f_R} R' \frac{H}{H'} \right|_{a=1}, \quad (3.16)$$

where $f_R = df/dR$, $f_{RR} = d^2f/dR^2$ and a prime indicates a derivative with respect to $\ln a$. Standard gravity (GR) has $B_0 = 0$ and for the QCD-scale modified-gravity $B_0 = 0.246$ [42]. Local gravity tests require $B_0 \leq 1.1 \times 10^{-3}$ at the 95 confidence level (CL) [61].

3.2 Cosmological perturbations in the MG1 model

In this section, we will investigate the cosmological perturbation in the square-root QCD-scale modified-gravity model and compare the results with the Λ CDM model. We mainly focus on two cosmological parameters of the first order perturbation cosmology, the effective gravitational coupling constant G_{eff} and a gravity estimator E_G [115]. We also discuss the late-time integrated Sachs-Wolfe (ISW) effect and the matter power spectrum in QCD-scale modified-gravity.

parameter	MG1	Λ CDM
H_0 (kms $^{-1}$ Mpc $^{-1}$)	68.1	67.30 ± 1.3 [127]
ω_{DE}	-0.662	-1.00
$z_{in}(t_i, t_0)$	0.523	$0.64_{0.07}^{0.13}$ [128]
Age (Gyr)	13.2	13.82 ± 0.048 [127]
$E_G^{th}(z = 0.25)$	0.456	0.418 [115]

Table 3.1: Cosmological parameters resulting from the MG1 model. The index 0 represents the present time value of the related parameter. The parameters of this table are as follows: H_0 is the present time Hubble parameter, ω_{DE} is the present time effective EOS parameter of the dark component and $z_{in}(t_i, t)$ is the redshift corresponds to the transition of deceleration to acceleration. E_G^{th} is gravity estimator which is introduced in [115] for searching of the deviations from standard GR. For comparison the results for the Λ CDM model is presented in the third column.

3.2.1 Parametrization of perturbations in modified gravity

In this section, we will distinguish QCD-scale modified-gravity from Λ CDM by comparing the structure formation in these two models. To accomplish this, we follow the formalism introduced in [130] to parametrize the perturbations in the modified theory by using the Compton wavelength parameter B_0 (see (3.16)) in such a way as to be able to implement them in a numerical code [130].

To obtain the perturbation equations for the modified theories of gravity, one should modify the Poisson and anisotropic equations (1.44a) and (1.44b). Here we consider the following parametrization for the deviation from GR [130]

$$k^2\Psi = -4\pi G a^2 \mu(k, a) (\rho\Delta + 3(\rho + P)\sigma) , \quad (3.17a)$$

$$k^2[\Phi - \gamma(k, a)\Psi] = \mu(k, a)12\pi G a^2(\rho + P)\sigma , \quad (3.17b)$$

where the functions $\gamma(k, a)$ and $\mu(k, a)$ include the information about the deviation from GR where both of them are unity in GR. By comparing eqs. (1.44a) and (3.17a) one sees that the spatial curvature potential Φ in eq. (1.44a) is replaced by the Newtonian potential Ψ in eq. (3.17a). This is due to the fact that non of the observable depends directly to Φ [130]. For example the clustering of matter and the peculiar velocities are directly connected to Ψ (see eq. (1.42)). In addition, with the parametrization of eq.

(3.17), the perturbation equations can be calculated for high redshifts as well, where the anisotropic stress term σ is important.

For the functions μ and γ we consider the following parametrization introduced in [131]

$$\mu(k, a) = \frac{1 + \beta_1 \lambda_1^2 k^2 a^s}{1 + \lambda_1^2 k^2 a^s}, \quad (3.18a)$$

$$\gamma(k, a) = \frac{1 + \beta_2 \lambda_2^2 k^2 a^4}{1 + \lambda_2^2 k^2 a^4}, \quad (3.18b)$$

where β s and λ s are determined by the theory. But to take into account the effects due to the modification of gravity, one should introduce a k -independent factor due to the modification of the background as well [132]. For example in $f(R)$ theory with $B_0 \lesssim 1$ one can choose $\beta_1 = 4/3$, $\beta_2 = 1/2$, $\lambda_2^2 = \beta_1 \lambda_1^2$, $\lambda_1^2 = B_0 c^2 / (2H_0^2)$ together with

$$\mu(k, a) = \frac{1}{1 - \beta_3 |\lambda_1|^2 a^3} \frac{1 + \beta_1 \lambda_1^2 k^2 a^4}{1 + \lambda_1^2 k^2 a^4}, \quad (3.19)$$

with the same $\gamma(k, a)$ as in (3.18b) and $\beta_3 = 1.4 \times 10^{-8}$. In eq. (3.19) the coefficient μ in the eq. (3.18a) is rescaled by the k -independent factor due to the modification of the gravity theory. Therefor one can see that even in the case of the $k = 0$ there could be some deviation from the GR (where $\mu = 1$). For alternative methods to parametrize the perturbations in the modified gravity see [131–134]. In the next subsection, we use the above parametrization in the MGCAMB code [130], a modified version of CAMB [135], to investigate the cosmological perturbations in the square-root QCD-scale modified-gravity. In figure 3.1, we have plotted the evolution of the potentials as a function of scale factor for Λ CDM model ($B_0 = 0$) and QCD-scale modified-gravity ($B_0 = 0.246$). We can see that the magnitude of the Newtonian potential Ψ is enhanced and the magnitude of the spatial curvature potential Φ is diminished with respect to the Λ CDM model. This behavior has been reported in [132] as well. The modes which have not entered the horizon yet ($k = 0$) are unaffected by the modification to gravity. The modes which enter the horizon earlier ($k = 0.1$ h/Mpc) are more dramatically altered in comparison to the modes which enter more recently ($k = 0.01$ h/Mpc).

We have plotted in figure 3.2 the ratio of the two potentials for different values of k . One can see that for initial times, when the $f(R)$ effects are negligible, the solutions tend to the GR solutions, i.e., $\Phi/\Psi = 1$. But when the modes enter the horizon they start to decline from one and tend to 0.5. Th effect of the recent acceleration

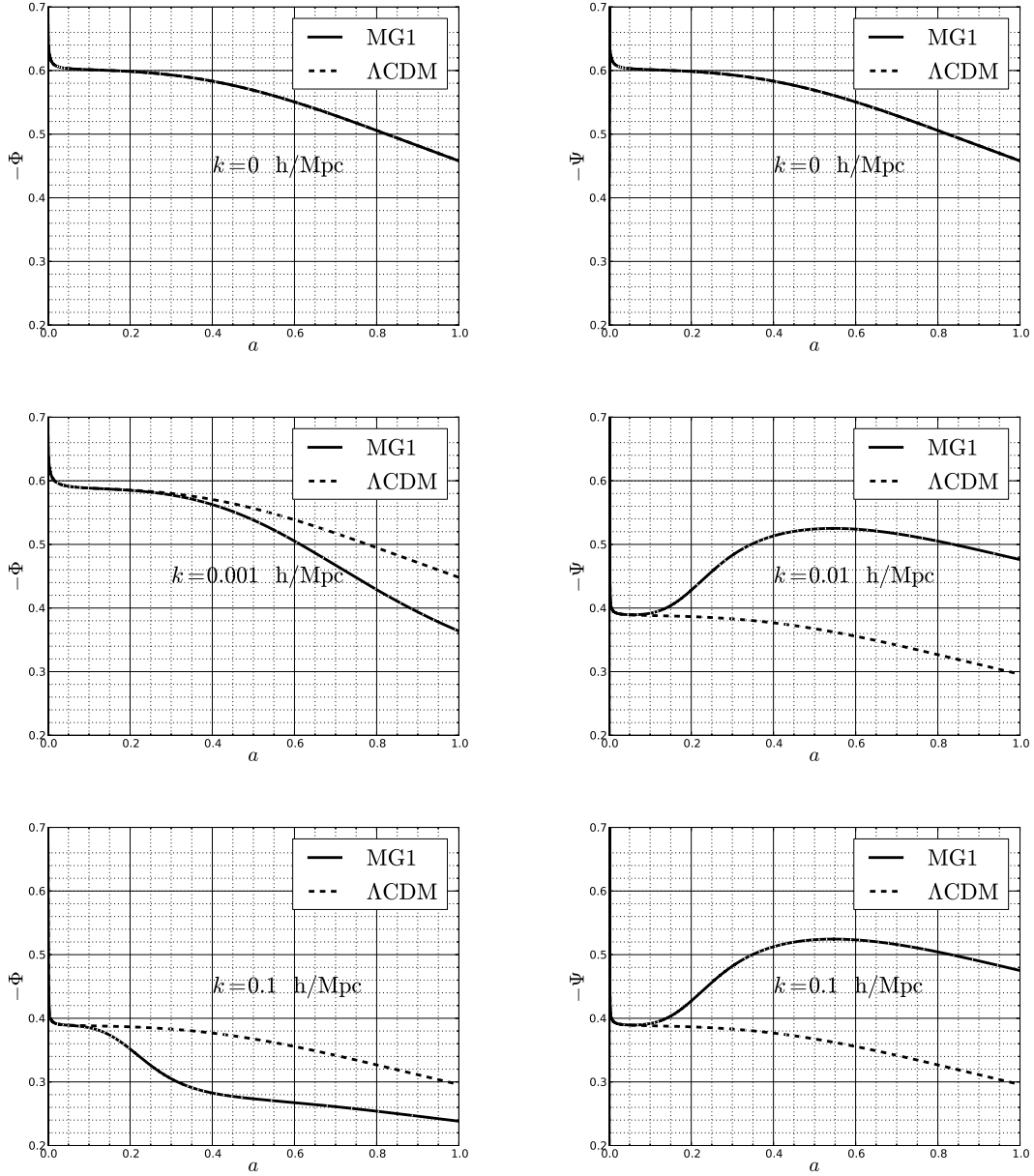


Figure 3.1: Evolution of the perturbation potentials Φ and Ψ in the long-wavelength regime in the square-root QCD-scale modified-gravity model (MG1) with $B_0 = 0.246$ (solid line) and the Λ CDM model with $B_0 = 0$ (dash line) for different values of comoving wave number k as a function of scale factor a . We can see that the magnitude of the Newtonian potential Ψ is enhanced and the magnitude of the spatial curvature potential Φ is diminished with respect to the Λ CDM model due to the modification of gravity.

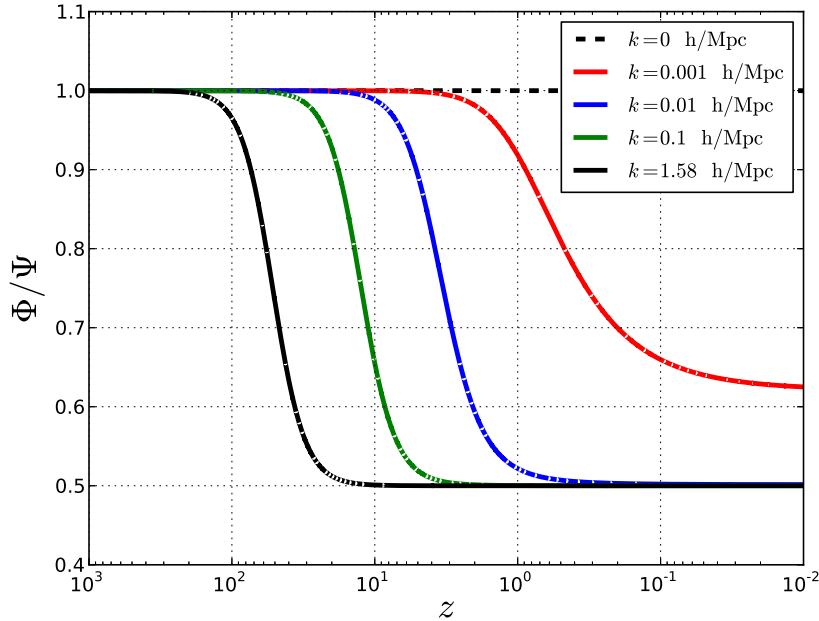


Figure 3.2: Φ/Ψ in the square-root QCD-scale modified-gravity model (MG1). In initial times ($z \gg 1$), when the $f(R)$ effects are negligible, the solutions tend to the GR solutions, i.e., $\Phi/\Psi = 1$. However, when the modes enter the horizon they start to decrease from one and tend to 0.5. The effect of the recent acceleration expansion can be seen in the different asymptotic behavior of the $k = 0.001$ h/Mpc mode which enters the horizon well after the starting of the acceleration expansion and the asymptotic behavior of larger k s (smaller scales) which enter the horizon during matter dominated era. This wavelength-dependence behavior is due to the scale-dependent transition function during the horizon crossing.

expansion can be seen in the $k = 0.001$ h/Mpc which is the mode which entered the horizon well after the start of the accelerated expansion (after the matter-dominated era). This mode behaves differently with respect to the modes which enter the horizon during the matter dominated era. This wavelength-dependent behavior is due to the scale-dependent transition function during the horizon crossing.

3.2.2 Effective gravitational coupling constant

From eq. (3.17a) one can deduce that (by ignoring σ for $z < 30$) [131]

$$\frac{G_{\text{eff}}}{G} = \mu(a, k) \quad (3.20)$$

where $\mu(k, a)$ in (3.19) contains two different terms for rescaling the bare gravitational coupling constant G , the k -independent pre-factor $1/(1 - 1.4 \times 10^{-8} |\lambda_1|^2 a^3)$ that accounts for the background rescaling due to the modifications of gravity and the k -dependent rescaling term $(1 + \beta_1 \lambda_1^2 k^2 a^4)/(1 + \lambda_1^2 k^2 a^4)$ that accounts for the first-order perturbation rescaling. We plot G_{eff}/G in figure 3.3 in the QCD-scale modified-gravity for different comoving wave numbers. We can see that as the modes enter the horizon, G_{eff}/G starts to grow. There is a difference between modes which enter the horizon during the matter dominated era and the modes which enter the horizon during the dark energy dominated era as expected. For large comoving wave numbers (small scales) the value of G_{eff}/G tends to 1.37, these modes entered the horizon before the dark energy dominated era. On the other hand, for large wavelengths, which entered the horizon well after the dark energy dominated era, the value of G_{eff}/G tends to 1.27 ($k = 0.001 \text{ h/Mpc}$). For the $k = 0$ case, the tiny deviation from G_{eff}/G comes from the $1/(1 - 1.4 \times 10^{-8} |\lambda_1|^2 a^3)$ factor starting around $z \simeq 0.8$, when the transition from the deceleration to acceleration phase happens. This behavior is not seen in figure (3.2) as the ratio Φ/Ψ is characterized by γ which does not contain any background rescaling factor like μ . This wavelength-dependence behavior is due to the scale-dependent transition functions during the horizon crossing. This results are in agreement with the previous results. For example in [136], for $f(R)$ gravity one has

$$G_{\text{eff}} = \frac{G}{8\pi F} \frac{1 + 4 \frac{k^2}{a^2 R} m}{1 + 3 \frac{k^2}{a^2 R} m}, \quad (3.21)$$

where $F \equiv f_R$ and $m \equiv R f_{RR}/f_R$. Therefore in the limiting case $\frac{k^2}{a^2 R} m \ll 1$ (small ks) one gets $G_{\text{eff}} \simeq G$ when $F \simeq 1$ as one can see for $k = 0$ in figure 3.3. On the other hand, for $\frac{k^2}{a^2 R} m \gg 1$ (large ks) one gets $G_{\text{eff}} \simeq 4G/3$ again by assuming $F \simeq 1$. In this case as k increases, the deviation from GR takes effect earlier as the relevant mode enters the horizon earlier.

ISW observational constraints gives ($z \simeq 0$, $k = 0.01 h \text{Mpc}^{-1}$) [132]:

$$1 \leq \frac{G_{\text{eff}}}{G} < 1.403, \quad 0.502 < \frac{\Phi}{\Psi} \leq 1 \quad (3.22)$$

therefore from figures 3.2 and 3.3 one can easily see that the MG1 model satisfies this constraints.

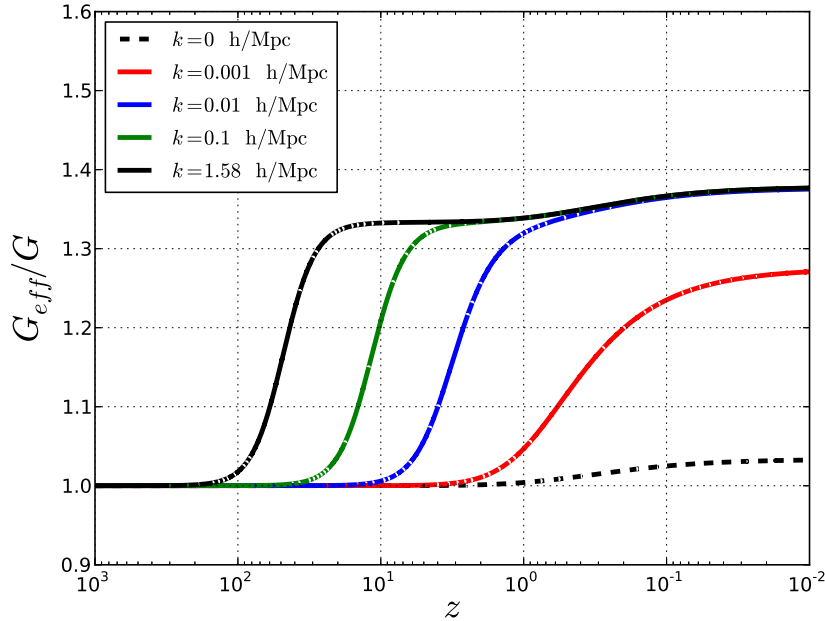


Figure 3.3: G_{eff}/G in the square-root QCD-scale modified-gravity model (MG1). For large comoving wave numbers (small scales) the value of G_{eff}/G tends to 1.37. These modes enter the horizon before the dark energy dominated era. On the other hand, for large wavelengths, that enter the horizon well after the dark energy dominated era, the value of G_{eff}/G tends to 1.27. This wavelength-dependent behavior is due to scale-dependent transition functions during the horizon crossing.

3.2.3 Gravity estimator E_G

In this section we will consider once more the gravity estimator E_G from section 3.1.2 but this time consider the perturbations parametrization (3.18). One can write this estimator as [115]

$$E_G = \frac{\nabla^2(\Phi + \Psi)}{3H_0^2 \delta \beta a^{-1}} \quad (3.23)$$

where $\beta \equiv \frac{d \ln D}{d \ln a} = \frac{\dot{\delta}}{H \delta}$ and D is the linear density growth factor. Using eq. (1.44a) for the modified gravity we can write

$$E_G = \frac{\mu(k, a)(1 + \gamma(a, k)) \Omega_{m0}}{2 \beta}, \quad (3.24)$$

where Ω_{m0} is the present time matter density parameter. In figure 3.4 one can see the observational constraints and the theoretical prediction of the parameter E_G from

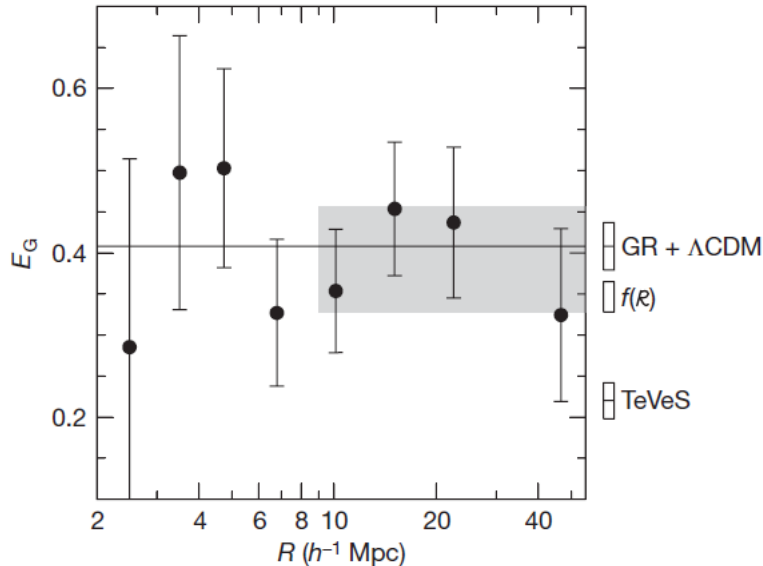


Figure 3.4: Comparison of observational constraints with predictions from general relativity and viable modified theories of gravity for E_G . The gray shaded region is the 1σ envelope of the mean E_G on scales $R = 10h^{-1}Mpc$. The horizontal line shows the mean prediction of general relativity $E_G = \Omega_{m,0}/\Omega_m(z)^{0.55}$ at the effective redshift of the measurements, $z = 0.32$. This figure has been reproduced from [139].

general relativity and viable modified theories of gravity at redshift $z = 0.32$. This plot has been obtained by analysing 70205 luminous red galaxies [137] from the SDSS data [138] by averaging over scales $R = (10 - 50)h^{-1}Mpc$.

We solved numerically the full perturbation equations for Λ CDM model ($B_0 = 0$) and QCD-scale modified-gravity ($B_0 = 0.246$) for different comoving wave numbers. The results for E_G for the squared-root QCD-scale modified-gravity and Λ CDM are plotted in figure 3.5. From this figure, we can see firstly that when the modes enter the horizon, QCD-scale modified-gravity deviates from Λ CDM. Secondly, there is again a difference between modes which enter the horizon during the matter dominated era and the modes which enter the horizon in the dark energy dominated era. The latter

case shows scale dependent behavior after entering the horizon for $z \simeq 0.8$ but for $z > 0.8$ they are scale-independent. This redshift is close to the inflection redshift in section 3.1.2 which corresponds to the redshift of the transition from the deceleration to acceleration phase. In addition the scale independent behavior of the Λ CDM model is apparent as well. Moreover we can see the inversion of the effect of the modification to gravity around $k \simeq 0.001$ h/Mpc. For the modes which have not entered the horizon yet ($k < 0.001$ h/Mpc) the effect of the modification to gravity presents itself as an enhancement in the value of E_G , as one can see in the top-left panel in figure 3.5. For the modes which have entered the horizon recently (e.g. $k = 0.001$ h/Mpc) the effect of the modification of the gravity theory on E_G almost disappears, as one can see in the top-right panel of figure 3.5. Finally for the modes which have entered the horizon during the matter dominated era $k > 0.001$ h/Mpc, the effect of the modification to gravity on the parameter E_G is reversed respect to the modes which have not entered the horizon yet. In this case, we can see that the effect of the modification to the gravitational theory causes diminishing of the parameter E_G compare to the Λ CDM model.

To compare our results with the observational results for E_G [139], from figure 3.5, we can see that for $z \simeq 0.3$ and $k = 0.1$ h/Mpc, $E_G \simeq 0.34$ which is in agreement with the observational results in figure 3 of Ref. [139] (see figure 3.4).

In addition, in figure 3.6 we have plotted the logarithmic derivative of the density perturbation growth $\beta \equiv d \ln D(a)/d \ln a = \delta/(\delta H)$ versus scale factor for QCD-scale modified-gravity and Λ CDM models. In the Λ CDM model, $d \ln D/d \ln a \simeq [\Omega_m(a)]^{6/11}$ [140]. When the universe transfers from a matter dominated era to a cosmological constant dominated universe, the growth rate is suppressed in Λ CDM. However if gravity is modified, the growth rate can be enhanced or diminished compared to Λ CDM. The reason is that the gravitational potential Ψ is enhanced (see the right column of figure 3.1) which leads to the increase of the gravitational force on the density perturbations and so the growth rate will be enhanced. One can see this from figure 3.6 for the wavelength inside the horizon as reported in [131].

In figure 3.7 we have plotted the matter power spectrum for the square-root gravity. For comparison, we have plotted the results for the Λ CDM model as well. One can see that for the large scales, the effects of the modified gravity are indistinguishable from the Λ CDM model. However, for smaller scales, due to the enhancement of the

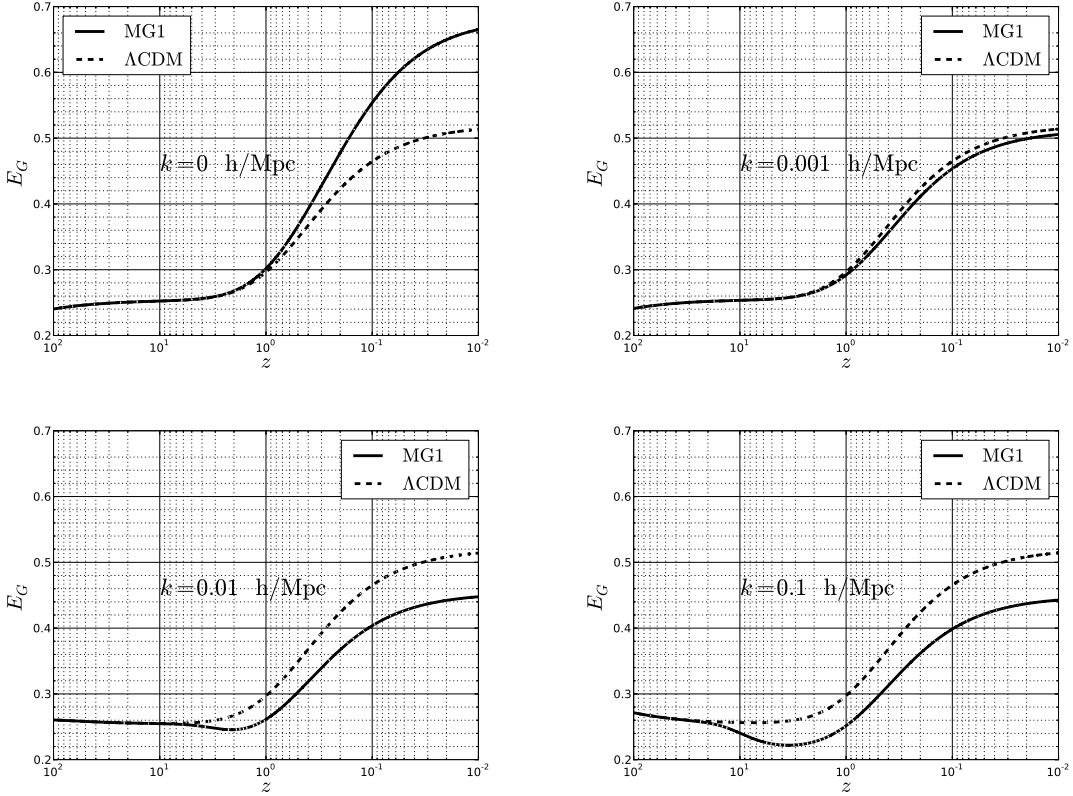


Figure 3.5: The gravity estimator E_G in the square-root QCD-scale modified-gravity model (MG1) with $B_0 = 0.246$ (solid-line) and the Λ CDM model with $B_0 = 0$ (dash-line) for different values of comoving wave number k as a function of redshift z . The subhorizon modes are diminished and the superhorizon modes (here $k = 0$) are enhanced compared to the Λ CDM model. The modes that enter the horizon during the matter dominated era ($k = 0.1$ h/Mpc, $k = 0.01$ h/Mpc) show scale dependent behavior for $z < 10$ where the modes that have not entered the horizon yet, or have entered recently ($k = 0.001$ h/Mpc), the scale dependence can be seen for $z \simeq 0.8$. The value of E_G for the modes which enter the horizon during the matter dominated era is in agreement with the observational results of Ref. [139], which report that $E_G(z = 0.32)$ from 0.328 to 0.365 in the 1σ level for $f(R)$ gravities.

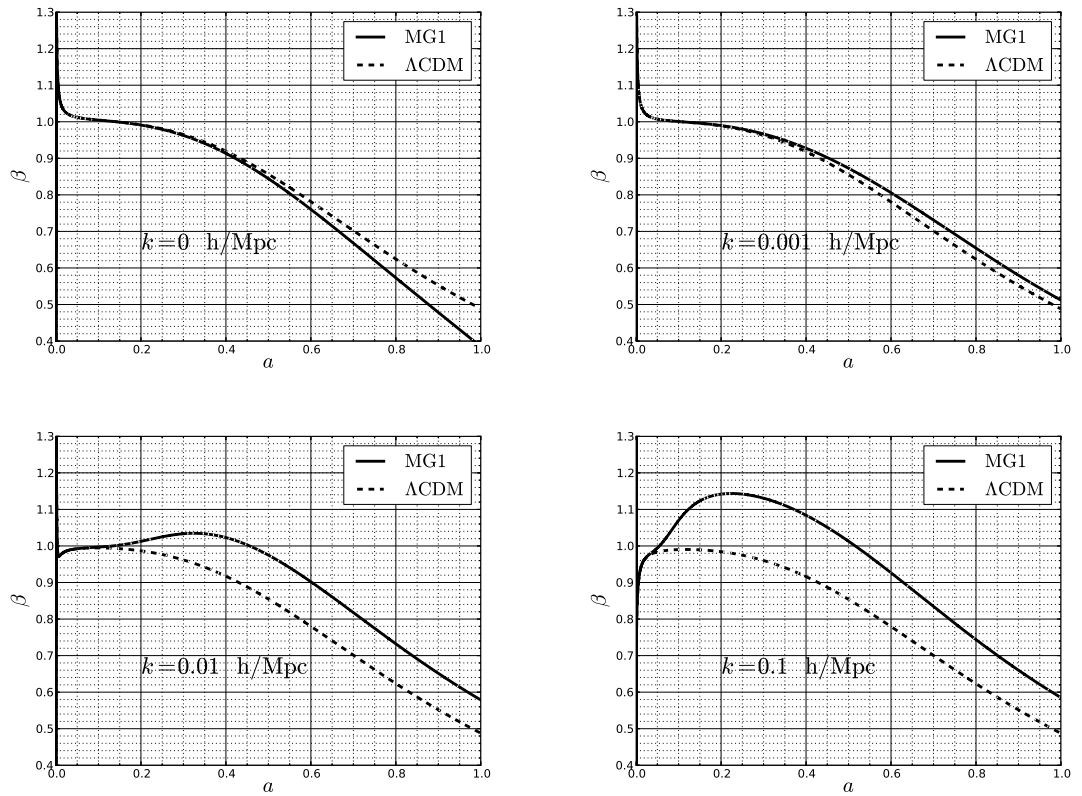


Figure 3.6: Evolution of the logarithmic density perturbation growth rate $\beta \equiv d \ln D / d \ln a$ in the square-root QCD-scale modified-gravity model (MG1) with $B_0 = 0.246$ (solid-line) and the Λ CDM model with $B_0 = 0$ (dash-line) for different values of comoving wave number k as a function of scale factor a . Models which enter the horizon during the matter dominated era are enhanced relative to the Λ CDM model because the gravitational potential Ψ is enhanced. This increases the gravitational force on density perturbations and so the growth rate will be enhanced.

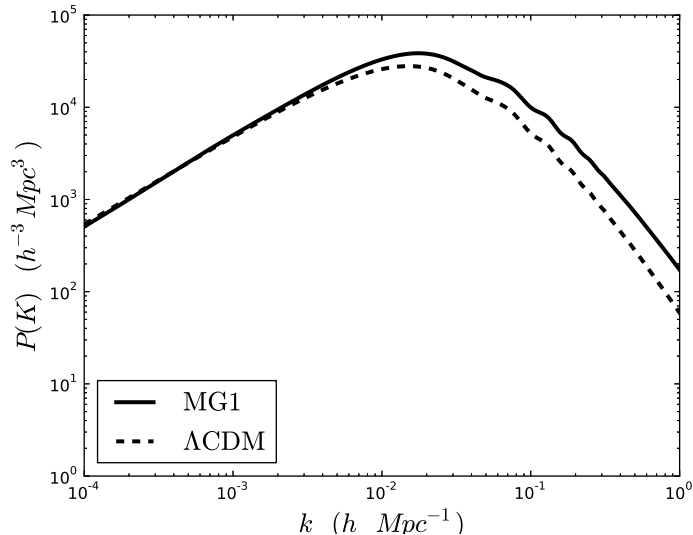


Figure 3.7: Matter power spectrum in the MG1 (solid-line) and in the Λ CDM model (dash-line).

density perturbations in the square-root modified-gravity, the matter perturbations are amplified compared to the Λ CDM model as discussed in [136].

3.2.4 Late integrated Sachs-Wolfe effect

The evolution of the gravitational potentials affect the CMB spectrum, an effect which was described for the first time by R. K. Sachs and A. M. Wolfe [141] and is known as the Sachs-Wolfe effect. There are two types of Sachs-Wolfe effect. The non-integrated Sachs-Wolfe effect [141] is caused by gravitational redshift occurring at the surface of the last scattering. In this type, the frequency of the photons shifts when the photons climb out of the potential wells at the surface of last scattering. These wells are created by the energy density at that time and also by the matter perturbations.

On the other hand, the integrated Sachs-Wolfe effect (ISW) [116, 142] is caused by the variation of the gravitational potentials between the last scattering surface and the observation point and so is not a part of the primordial CMB spectrum. There are two main contributions to the ISW. The early-time ISW occurred shortly after the surface of last scattering due to the effect on the matter perturbations of the non-negligible radiation density and the late-time ISW occurred much more recently when the universe

entered the dark-energy dominated era. When a photon enters a cosmic well (say, that of a supercluster) it gets a kick of energy and it keeps a little of that energy when it climbs out of the well, as the well is stretched out and becomes shallower due to the expansion of the Universe. Similarly, when a photon loses energy by climbing up a potential hill (such as that of a supervoid) it will not get all of that energy back as the potential hill becomes slightly squashed. The ISW effect can be expressed as

$$\frac{\Delta T}{T}(\hat{n}) = \int (\dot{\Phi} + \dot{\Psi}) d\chi, \quad (3.25)$$

where χ is the comoving distance and \hat{n} is the photon propagation direction. As this is a late time effect (important for $z < 2$), we can observe it only for large angles or equivalently at larger angular scales. The temperature anisotropy power spectrum for the square-root QCD-scale modified-gravity and the Λ CDM model is depicted in figure 3.8. We can see that only low- l 's (large angles) are affected with respect to the Λ CDM as it is expected. Therefore there is a possibility to remove the degeneracy between GR and modified theories by CMB observations. However, as this part of the spectrum is related to the low- l 's and therefore large angular scales, this degeneracy may survive due to the cosmic variance [143] even with improvement in the related data.

3.2.5 Discussion

To summarize this section, we have investigated the behavior of the square-root QCD-scale modified gravity through the first order perturbation cosmology. We parametrized this modified gravity by the value of B_0 , the Compton wavelength parameter and then investigated the first order perturbation theory in this model numerically by modifying the open source MGCAMB code [130].

First we considered the gravitational potentials Ψ and Φ . The magnitude of the Newtonian potential Ψ is enhanced and the magnitude of the spatial curvature potential Φ is diminished compared to the Λ CDM model. In addition, the modes which enter the horizon during the matter dominated era have been more enhanced or diminished with respect to the modes which enter during the dark energy dominated era. This wavelength-dependent behavior is due to the scale-dependent transition function during horizon crossing. The enhancement of the potential Ψ causes the amplification of the growth of matter density perturbations as one can see in figure 3.6.

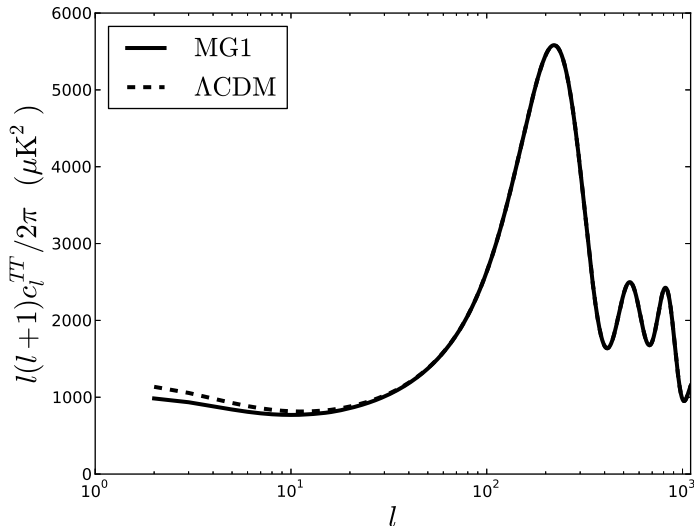


Figure 3.8: The temperature anisotropy power spectrum in the square-root QCD-scale modified-gravity (MG1) (solid-line) and the Λ CDM model (dash-line). Only low l 's (large angles) are affected with respect to the Λ CDM model as expected due to the late ISW effect.

The ratio of the effective gravitational constant to the bare gravitational constant G_{eff}/G was obtained as $G_{\text{eff}}/G \simeq 1.37$ for modes which enter the horizon during the matter-dominated era and $G_{\text{eff}}/G \simeq 1.27$ for modes which enter the horizon recently after the domination of the dark energy. This effective gravitational coupling constant is not observable directly.

Then we investigate the gravity estimator E_G for different values of the comoving wave numbers k . We found that value of E_G for the square-root QCD-scaled modified-gravity is in agreement with the results of the observations in [139], i.e. between 0.328 to 0.365 at the 1σ level. In addition for $z = z_{\text{inf}} \simeq 0.8$ (see section 3.1.2) we can see the effect of the dark energy domination on the super-horizon modes.

3.3 Cosmological parameter estimation

As discussed in section 3.1.1, the non-perturbative QCD vacuum is characterized by the presence of gluon and quark condensates. So, constraining the values of these condensates is very important to shed some light on the QCD vacuum. In this section, we will

constrain the value of the gluon condensate q through q -theory using the cosmological data. Therefore, as q -theory relates QCD vacuum to cosmology, one can constrain a quantity from the microscopic physics (QCD) by data from macroscopic (cosmological) observations.

We use the publically available CosmoMC package [135] together with modifications to MGCAMB [130]. To implement the q -theory model, we use the parametrization of the modified gravity introduced in subsection 3.2.1. Using the numerical method described in section 3.1.2, we rewrite B_0 , the Compton Wavelength parameter, as

$$B_0 = \frac{1.3091}{7.5844\beta_q^{3/4} - 2}, \quad (3.26a)$$

$$\beta_q \equiv \frac{q_0}{q}, \quad (3.26b)$$

where $q_0 = (300 \text{ MeV})^4$ as in [43].

To get the best fit values of the cosmological parameters, the maximum likelihood method is used where the total likelihood function $\mathcal{L}_{\text{total}} = e^{-\chi_{\text{total}}^2/2}$ is the product of the separate likelihood functions with

$$\chi_{\text{tot}}^2 = \chi_{\text{SNIa}}^2 + \chi_{\text{CMB}}^2 + \chi_{\text{BAO}}^2 + \chi_{\text{gas}}^2. \quad (3.27)$$

In relation (3.27) SNIa stands for type Ia supernovae, CMB for cosmic microwave background radiation, BAO for baryon acoustic oscillations and gas stands for the X-ray gas mass fraction data. The best-fitting values of the cosmological and model parameters are obtained by maximizing $\mathcal{L}_{\text{total}}$ or equivalently minimizing χ_{tot}^2 . In appendix A we have explained in detail the methods for calculating each χ^2 from the observational data.

The data we have used to fit the model in this section are as follows: cosmic microwave background radiation (CMB) data from seven-year WMAP [144], 557 Union2 data of type Ia supernova [145], baryon acoustic oscillation (BAO) data from SDSS DR7 [146], and the cluster X-ray gas mass fraction data from the Chandra X-ray observations [147].

The basic parameter set for the MCMC analysis is $P = \{\Omega_b h^2, \Omega_{DM} h^2\}$ with the following flat priors: $\Omega_b h^2 \in (0.005, 0.1)$, $\Omega_{DM} h^2 \in (0.01, 0.99)$. In addition, for the parameter $\beta_q = q_0/q$ we take the flat prior $\beta_q \in (0.1, 10)$. Figure 3.9 shows 2-D cosmological constraint contours with 1σ and 2σ confidence levels. Best fit and mean

values of the cosmological and model parameters are listed in table. 3.2 with 1σ and 2σ confidence levels. From table. 3.2 we can see that the best fit results are given as: dark energy density $\Omega_{\text{DE}} = 0.7245_{-0.0445-0.0578}^{+0.0353+0.0446}$, dark matter physical density $\Omega_c h^2 = 0.1152_{-0.0113-0.0141}^{+0.0122+0.0151}$, the baryon matter physical density $\Omega_b h^2 = 0.0223_{-0.0013-0.0017}^{+0.0016+0.0020}$ and $\beta_q \equiv q_0/q = 1.0288_{-0.7411-0.7510}^{+0.9989+0.9989}$ where $q_0 = (300 \text{ MeV})^4$. The age of the universe in this model is given by $13.7741_{-0.3013-0.3803}^{+0.2928+0.3716}$ Gyr. All cosmological values are in a good agreement with the results of the Λ CDM model [127] as predicted in [43] as one can see in the last column of table 3.2. In addition, one can see that these results are in agreement with the latest cosmological constraints on modified-gravity theories [148].

An interesting result of this section is the bounds on the parameter $\beta_q = (300\text{MeV})^4/q$. From table 3.2, one can see that the best fit value of parameter β_q is $\beta_q = 1.028$. This best value implies that the best fit value of the gluon condensate is $q \simeq (300 \text{ MeV})^4$. This best fit value is of the order of the values obtained in previous theoretical investigations. For example, in the original work in the framework of QCD spectral sum rules one obtains $q \simeq (440 \text{ MeV})^4$ [124, 149]. In addition Bell and Bertlmann, using an analysis of the non-relativistic version of heavy quark sum rules, obtained $q \simeq (514 \text{ MeV})^4$ [150]. Here, by using the q -theory and the large-scale observations, we can constrain a microscopic quantity i.e., the gluon condensate q . Constraining with recent data like Planck [151] and nine-year WMAP [152] could improve the bounds on parameter β_q . In addition, to improve the constraints further one can use the weakly or fully nonlinear scales [153, 154]. By using the most massive halos data inferred from SDSS and the galaxy-galaxy lensing signals [155], one can tighten constraints on β_q .

3.4 Chameleon behavior of the MG1 model

As has been discussed in section 2.1, $f(R)$ theories can survive as a viable theory of gravity if the related extra scalar degree of freedom behaves like a chameleon field on local scales. In the case of the large celestial objects like the Earth in the solar system, the chameleon field should be trapped inside the body. In other words, the celestial object should have a thin-shell. In this section, by applying the chameleon formalism [9, 10] (see section 2.2), we will try to investigate the validity of the suggested q -theory modified gravity models by considering their behavior on local scales. To do so, first in

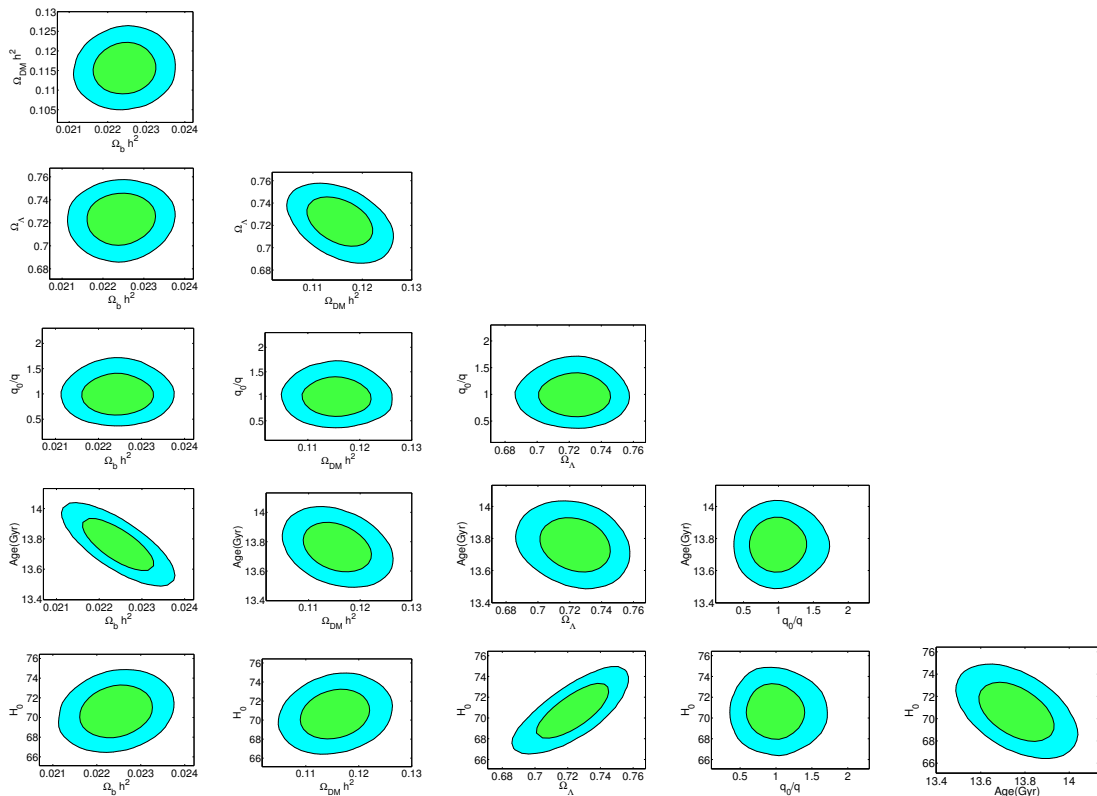


Figure 3.9: 2-D constraint contours of the cosmological parameters with 1σ and 2σ regions in the MG1 model. To obtain these plots, SNIa+CMB+BAO+X-ray gas mass fraction data with BBN constraints have been used. Furthermore $\beta_q = q_0/q$ where $q_0 = (300 \text{ Mev})^4$ is the gluon condensate.

section 3.4.1 we suggest some physical situations in which to consider the characteristics of the chameleon field in QCD-scale modified-gravity.

3.4.1 Local tests

In sections 3.4.2 and 3.4.3 we will consider the chameleon field of the square-root model and a local version of QCD-scale modified-gravity in the physical situations described in this section to see if these models can satisfy the local experiments. If the scalar degree of freedom exhibits a chameleon effect, deviations of the model from GR on the local scales are not detectable.

- **A. Ball in the atmosphere (BA):** In the first case, consider a small test copper ball of radius 1cm and density $\rho_c = 8.92\text{g/cm}^3$ such as those used in small scale

Parameter	MG1	Λ CDM
$\Omega_b h^2$	$0.0223^{+0.0016+0.0020}_{-0.0013-0.0017}$	0.02214 ± 0.00024
$\Omega_c h^2$	$0.1152^{+0.0122+0.0151}_{-0.0113-0.0141}$	0.1187 ± 0.0017
Ω_{DE}	$0.7245^{+0.0353+0.0446}_{-0.0445-0.0578}$	0.692 ± 0.010
β_q	$1.0288^{+0.9989+0.9989}_{-0.7411-0.7510}$...
$H_0(\text{kms}^{-1}\text{Mpc}^{-1})$	$70.6610^{+4.7186+6.0589}_{-4.4714-5.7971}$	67.80 ± 0.77
Age (Gyr)	$13.7741^{+0.2928+0.3716}_{-0.3013-0.3803}$	13.798 ± 0.45

Table 3.2: The best fit values of the model parameters with 1σ and 2σ regions from MCMC calculation using CMB, SNIa BAO and X-ray gas mass fraction data. $\beta_q = q_0/q$ where $q_0 = (300 \text{ Mev})^4$ is the gluon condensate. In the last column we have presented the results for Λ CDM (Planck+WMAP+BAO+highL) [127] for comparison.

gravity experiments [114]. We will investigate the effect of the chameleon field due to this ball in the atmosphere where $\rho_b \simeq 1.3 \times 10^{-3} \text{g/cm}^3$. The local gravity tests in this case can rule out those models that can not account for gravitational phenomena in laboratory tests.

- **B. Ball in the solar system (BSS):** in the second case we again consider the same ball as in case A, but this time, we assume that the ball is surrounded by a medium with the average density of the solar system system $\rho_b \simeq 10^{-24} \text{g/cm}^3$. It might be possible to detect the chameleon field footprint in this case if an experiment were done in a space-based environment such as the GG experiment [156].
- **C. Earth in the solar system (ESS):** in the third case we consider the Earth with $\rho_c \simeq 5.52 \text{g/cm}^3$ and $R_c \simeq 6 \times 10^6 \text{m}$ in the solar system where $\rho_b \simeq 10^{-24} \text{g/cm}^3$. For a modified gravity theory to describe gravity on solar system scales [94, 157], the chameleon field of celestial bodies like the Earth must be trapped inside the body. In other words, the celestial body should have thin-shell.

3.4.2 Large-scale model

As we have seen, Klinkhamer in [42, 126] suggested the following QCD-scale modified-gravity model as a description of the large-scale structure of the universe

$$f(R) = R - \frac{1}{L_0} |R|^{\frac{1}{2}}, \quad (3.28)$$

where $L_0 = M_{Pl}^2 / (2\eta q_0^{3/4})$, $\eta = 2.4 \times 10^{-4}$ and $q_0 = (300 \text{ MeV})^4$. The corresponding chameleon potential from eq. (2.9) in this case is

$$V(\phi) = \frac{M_{Pl}^2}{8L_0^2} \frac{1}{F^2(1-F)}, \quad (3.29)$$

where

$$F(\phi) \equiv f_R \equiv \exp(-2Q\phi/M_{Pl}), \quad (3.30)$$

and $Q = 1/\sqrt{6}$.

To investigate the local behavior of this $f(R)$ model we will test its chameleon field behavior in the three physical situations in section 3.4.1. The numerical results are presented in table 3.3. In addition, the behavior of the chameleon field is depicted in the left panel of figure 3.10. The right panel of figure 3.10 shows the acceleration due to the chameleon field of the ball a_ϕ on another test body in its vicinity

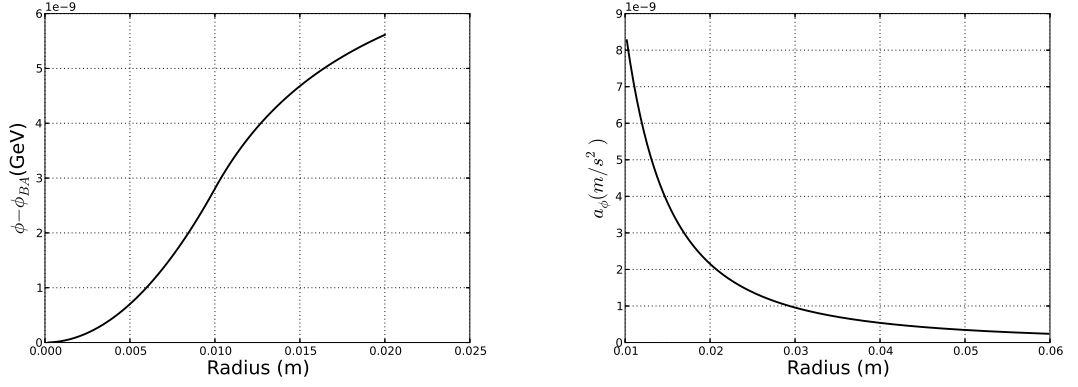
$$a_\phi = Q/M_{Pl} |\vec{\nabla}\phi|. \quad (3.31)$$

From table 3.3, we can see that in all cases we have the thick-shell effect. This is especially important for the case of the Earth in solar system (ESS) where the chameleon force should be trapped inside the celestial body (thin-shell effect) to avoid contradicting the results of the solar system tests [10]. In addition, the current experimental results for the fifth force searches give an upper bound $m_b \gtrsim 10^{-13}$ GeV (corresponding to an interaction distance $\lambda < 1$ mm) for the strong Yukawa force (i.e. $\alpha \sim \mathcal{O}(1)$) [8] (see section 2.2.2). However, for the ball in the atmosphere case we have $m_b = 0.34 \times 10^{-22} \ll 10^{-13}$ GeV and $\alpha = 0.33 \sim \mathcal{O}(1)$, therefore, this model contradicts the constraints of the fifth force searches on the local scales. From figure 3.10, we can see that the scalar field starts rolling down the potential very close to the center of all the bodies considered and the field value changes inside the bodies as are would expect for the thick-shell effect [10]. The chameleon accelerations are of order of the

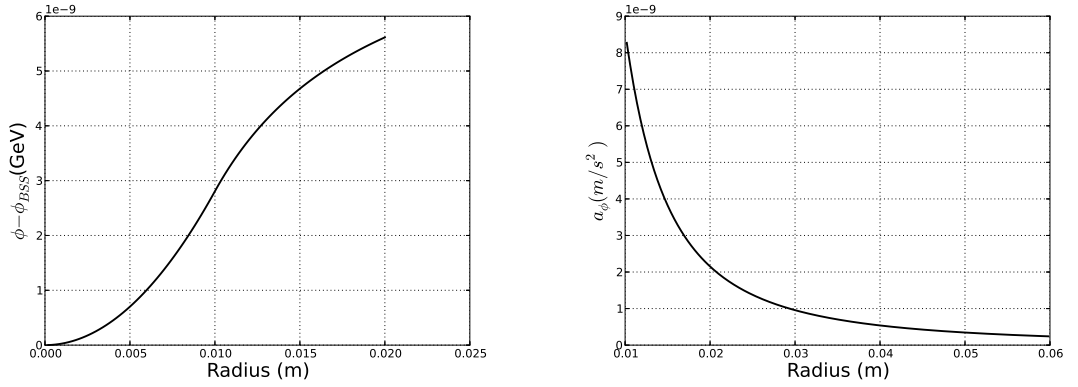
Experiment	BA	BSS	ESS
$\rho_c(\text{g/cm}^3)$	8.92	8.92	5.52
$\rho_b(\text{g/cm}^3)$	1.3×10^{-3}	10^{-24}	10^{-24}
$R_c(\text{m})$	0.01	0.01	6×10^6
$m_c(\text{GeV}/c^2)$	1.01×10^{-19}	1.01×10^{-19}	7.06×10^{-20}
$m_b(\text{GeV}/c^2)$	1.34×10^{-22}	1.95×10^{-38}	1.95×10^{-38}
ϵ_{th}	6.22×10^{12}	2.27×10^{23}	1.01×10^6
Shell Type	Thick	Thick	Thick
α	0.33	0.33	0.33
$\delta^2 = G_{\text{eff}}/G$	1.33	1.33	1.33
$\chi(\phi_b)$	1	0.99	0.99

Table 3.3: Chameleon behavior results for $f(R) = R - |R|^{\frac{1}{2}}/L_0$ (MG1). The second column (BA) corresponds to a small test body in the atmosphere (ground-based laboratory). The next column (BSS) is the results for the same test body but this time in a medium with density of the average density of the solar system (orbital-based laboratory). The fourth column is the results for the Earth inside the solar system (ESS) when the environment density is 10^{-24}g/cm^3 . The indices c and b indicate the test body and the background respectively.

Ball in Atmosphere (BA)



Ball in Solar System (BSS)



Earth in Solar System (ESS)

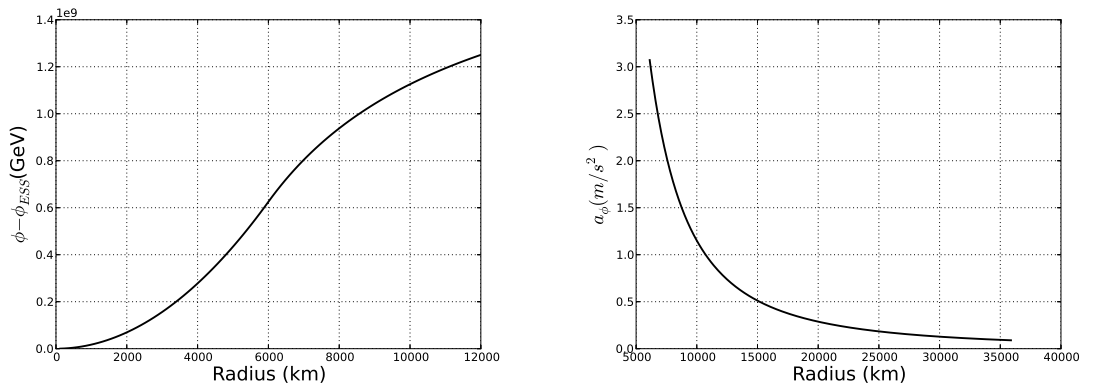


Figure 3.10: Left column: chameleon field for the $f(R) = R - \frac{1}{L_0}|R|^{\frac{1}{2}}$ (MG1) model. For visual clarity, y-axes are scaled with the value of the chameleon field in the center of the test bodies $\phi_{BA}, \phi_{BSS}, \phi_{ESS}$. Right column: acceleration a_ϕ caused by the chameleon field on the nearby bodies (3.31). The characteristics of the physical situations *BA*, *BSS* and *ESS* are explained in table 3.3.

gravitational acceleration as $\delta^2 = 1.33$ in these cases. In section 3.2.2 we considered the effective gravitational coupling constant in the perturbation theory and we obtained $G_{\text{eff}}/G \simeq 1.37$ which is close to the results of this section. But again we should assert that the G_{eff} of this section is directly measurable but the G_{eff} in section 3.2.2 is not directly measurable and they are different physical quantities.

If we consider this model in a background with the average density of the dark matter density $\rho_b = \rho_{DM} \simeq 0.25 \times 10^{-29} \text{ g/cm}^3$, we find the interesting result for the dark energy density ρ_{DE}

$$\rho_{DE} \equiv V(\phi_b) \simeq 2.47 \times 10^{-47} \text{ GeV} , \quad (3.32)$$

which is very close to the results of observations [144]. This result was expected as this model was proposed to explain the accelerating expansion of the Universe. In addition $\chi \equiv F(\phi_b)$, which is the value of scalar field in the Brans Dicke theory (see eq. (3.9)) at infinity, here is obtained as 0.68, which is close to the value which has been obtained in [42], $\chi \simeq 0.72$.

In summary we deduce that the squared-root modified gravity (i.e., $f(R) = R - |R|^{\frac{1}{2}}/L_0$) works very well for the large scale gravity, but on local scales this model does not satisfy the constraints from local experiments.

The following discussion may reveal the reason for the contradiction with local experiment constraints in this model. One can write the approximated form of the potential $V(\phi)$ in eq. (3.29) for $\phi \ll M_{Pl}$ (which is valid for the late-time universe) as

$$V(\phi) \approx \frac{M_{Pl}^2 M_{Pl}}{8L_0^2 2Q\phi} , \quad (3.33)$$

where $M_{Pl}^2/L_0^2 \simeq O(\rho_{DE}) \simeq 10^{-47} \text{ GeV}^4$. In fact, the potential (3.33) has the form of a power law potential, i.e,

$$V(\phi) = M^4 \left(\frac{M}{\phi} \right)^n , \quad (3.34)$$

with $n = 1$ and where M has dimension of mass. Power law potentials can explain the local tests or cosmological tests but not both [158]. If we were to make this potential appropriate for large scales we should choose $M = 10^3 \text{ eV}$, which contradicts the results of local experiments by a few orders of magnitude [158]. On the other hand if we want to have a power law potential that satisfies local experiments we should take $M = 10^{-3} \text{ eV}$. As the parameters in eq. (3.33) are chosen to satisfy large-scale constraints,

the potential can not simultaneously account for the behavior of gravity on local-scales. Therefore QCD-scale modified-gravity explains the gravity on the large scales very well but it fails as a gravitational theory on the local scales.

3.4.3 Local-scale model

In this section we consider an alternative form for the QCD-scale modified-gravity $f(R)$ theory which was suggested by Klinkhamer in [42]

$$f(R) = R - \frac{|R|^{1/2}/L_0}{1 + \zeta L_0 |R|^{1/2}}, \quad (3.35)$$

where ζ is a constant of order unity. The form of the chameleon potential is obtained as

$$V(\phi) = \frac{M_{Pl}^2}{2F^2} \left(R(F - 1) + \frac{1}{L_0 \zeta L_0 + |R|^{-1/2}} \right), \quad (3.36a)$$

$$F \equiv \exp(-2Q\phi/M_{Pl}), \quad (3.36b)$$

$$|R|^{1/2} = \frac{2}{3L_0\zeta} \left(\frac{A}{4} + \frac{1}{A} - 1 \right), \quad (3.36c)$$

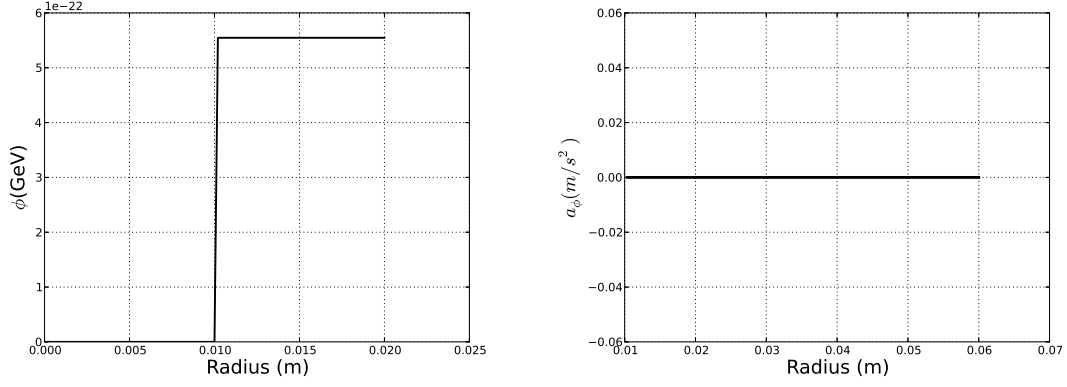
$$A = \frac{1}{(1 - F)^{1/3}} \left(8(1 - F) + 54\zeta + 6\sqrt{3\zeta(8(1 - F) + 27\zeta)} \right)^{\frac{1}{3}}. \quad (3.36d)$$

To investigate the chameleon behavior of this model we test it for the different cases described in section 3.4.1. Here again we take $\eta = 2.4 \times 10^{-4}$, $q_0 = (300 \text{ MeV})^4$ and consider two values of $\zeta = 1, 100$.

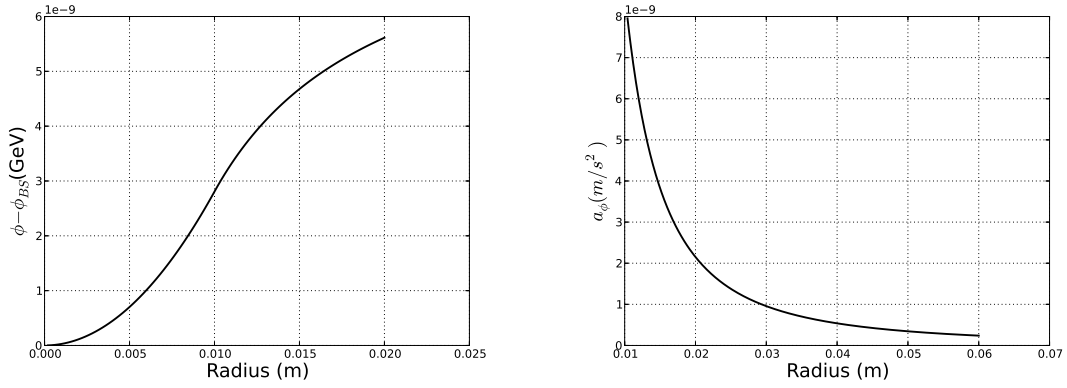
A. $\zeta = 1$: here we consider the experiments described in 3.4.1 for the local QCD-scale modified-gravity in eq. (3.35) for $\zeta = 1$. The numerical results are listed in table 3.4. In addition, the behavior of the chameleon field and the acceleration due to it, is depicted in figure (3.11).

From table 3.4, we can see that for $\zeta = 1$, we are always in the thick shell regime except for the case of a small test body in the atmosphere. However, we require that at least an astronomical object like the Earth, exhibits thin-shell behavior in the solar system as well. So, in the next case, we will test the model for a larger value of parameter ζ . In addition, this model is not suitable to explain the cosmological acceleration as the density of dark energy in this model is too small, $\rho_{DE} = V(\phi_b) \simeq 7.25 \times 10^{-48} \text{ GeV}^4$ for $\rho_b = \rho_{DM} \simeq 0.25 \times 10^{-29} \text{ g/cm}^3$.

Ball in the Atmosphere (BA)



Ball in the Solar System (BSS)



Earth in the Solar System (ESS)

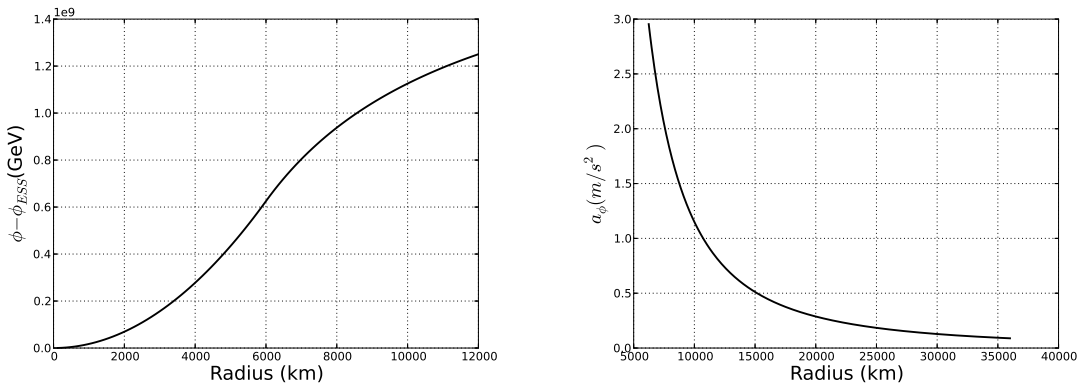


Figure 3.11: The chameleon field (right column) and the chameleon acceleration a_ϕ (3.31) (left column) in the $f(R) = R - \frac{|R|^{1/2}/L_0}{1+\zeta L_0|R|^{1/2}}$ model with $\zeta = 1$ for different physical situations. In the thick-shell cases (second and third rows), for the visual clarity, y-axes are scaled by the values of the field at the center of body ϕ_{BSS}, ϕ_{ESS} respectively.

Experiment	BA	BSS	ESS
$\rho_c(\text{g/cm}^3)$	8.92	8.92	5.52
$\rho_b(\text{g/cm}^3)$	1.3×10^{-3}	10^{-24}	10^{-24}
$R_c(\text{m})$	0.01	0.01	6×10^6
$m_c(\text{GeV}/c^2)$	6.69×10^{-5}	6.69×10^{-5}	3.67×10^{-5}
$m_b(\text{GeV}/c^2)$	1.07×10^{-9}	4.35×10^{-36}	4.35×10^{-36}
ϵ_{th}	3.29×10^{-14}	1.53×10^{18}	6.89
Shell Type	Thin	Thick	Thick
α	9.88×10^{-14}	0.33	0.33
$\delta^2 = G_{\text{eff}}/G$	1.00	1.33	1.33
$\chi(\phi_b)$	1.00	1.00	1.00

Table 3.4: Chameleon behavior results for $f(R) = R - \frac{|R|^{1/2}/L_0}{1+\zeta L_0|R|^{1/2}}$ for $\zeta = 1$. The second column (BA) corresponds to a small test body in the atmosphere (ground-based laboratory). The next column (BSS) shows the results for the same test body but this time in a medium with density of the average density of the solar system. The fourth column shows the results for the Earth inside the solar system (ESS) when the environment density is 10^{-24}g/cm^3 . The indices c and b indicate the test body and the background respectively.

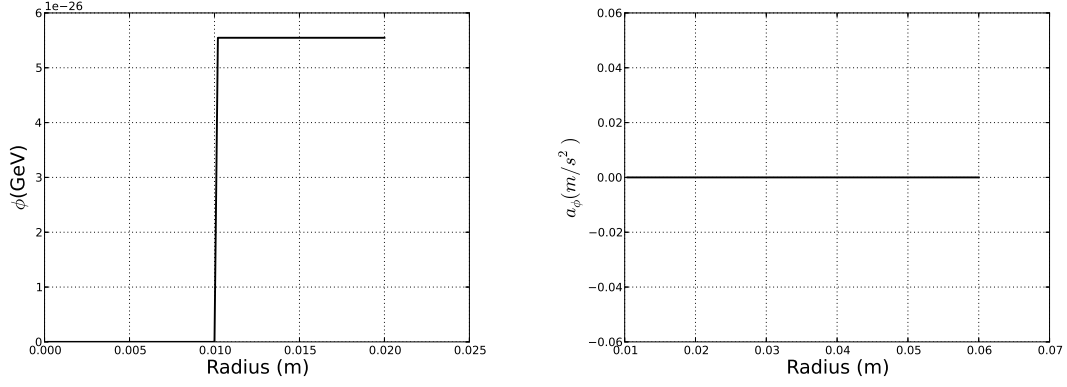
B. $\zeta = 100$: in this case, we consider the aforementioned experiments for the local QCD-scale modified-gravity model in eq. (3.35) for the $\zeta = 100$ case. The numerical results are listed in table 3.5. In addition, the behavior of the chameleon field and the acceleration due to it, is depicted in figure (3.12).

From table 3.5, we can see that for $\zeta = 100$, we are in thin shell regime for a small test body in atmosphere and for the Earth in the solar system, but for the the case of a small test body in the solar system, the object exhibits thick-shell behavior. This behavior is reported in [9, 10] as a test for detecting the chameleon field in orbital-based experiment. As before, this model is not suitable to explain the cosmological acceleration as the density of dark energy in this model is too small, $\rho_{DE} \simeq 1.23 \times 10^{-48}\text{GeV}^4$.

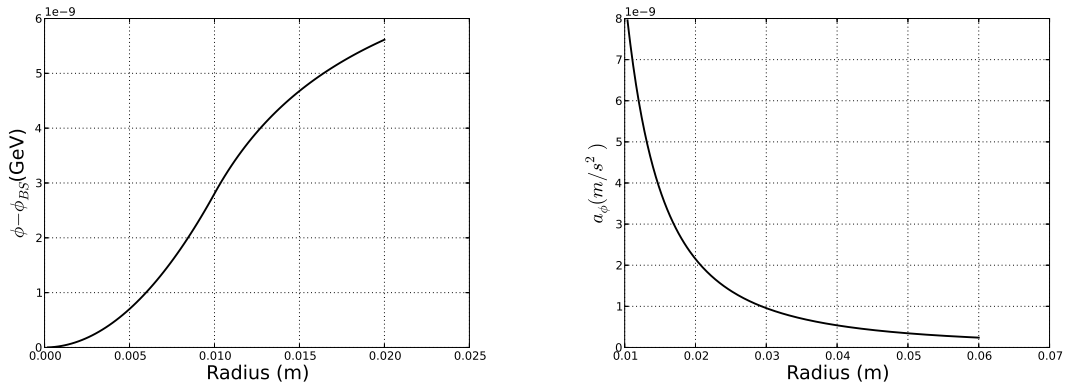
3.4.4 Discussion

To summarize, by using the chameleon formalism approach we investigated two proposed q -theory modified gravity models on local scales (scales which are very much

Ball in the Atmosphere (BA)



Ball in the Solar System (BSS)



Earth in the Solar System (ESS)

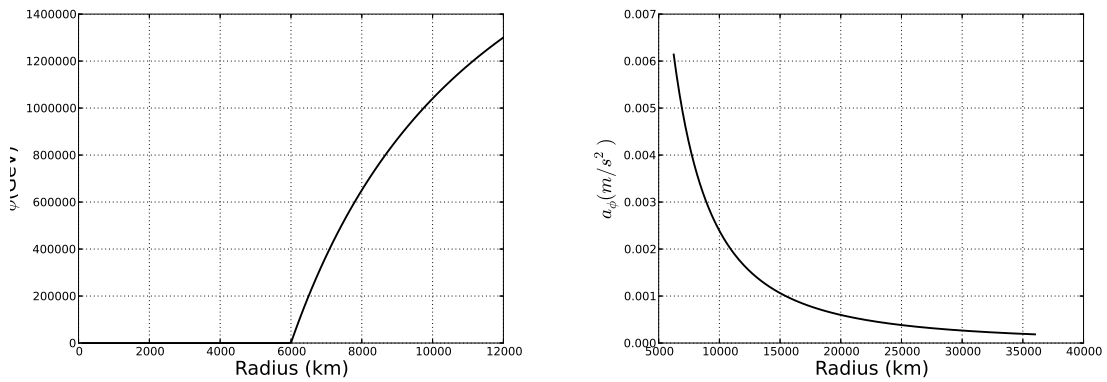


Figure 3.12: The chameleon field (right column) and the chameleon acceleration a_ϕ (3.31) (left column) in the $f(R) = R - \frac{|R|^{1/2}/L_0}{1+\zeta L_0|R|^{1/2}}$ with $\zeta = 100$ for different physical situations. In the thick-shell case (second row), for visual clarity, y-axis is scaled by the values of the field at the center of body ϕ_{BSS} .

Experiment	BA	BSS	ESS
$\rho_c(\text{g/cm}^3)$	8.92	8.92	5.52
$\rho_b(\text{g/cm}^3)$	1.3×10^{-3}	10^{-24}	10^{-24}
$R_c(\text{m})$	0.01	0.01	6×10^6
$m_c(\text{GeV}/c^2)$	6.69×10^{-3}	6.69×10^{-3}	3.67×10^{-3}
$m_b(\text{GeV}/c^2)$	1.07×10^{-7}	4.35×10^{-34}	4.34×10^{-34}
ϵ_{th}	3.29×10^{-18}	1.54×10^{14}	6.92×10^{-4}
Shell Type	Thin	Thick	Thin
α	9.88×10^{-18}	0.33	0.0020
$\delta^2 = G_{\text{eff}}/G$	1.00	1.33	1.00069
$\chi(\phi_b)$	1.00	1.00	1.00

Table 3.5: Chameleon behavior results for $f(R) = R - \frac{|R|^{1/2}/L_0}{1+\zeta L_0|R|^{1/2}}$ for $\zeta = 100$. The second column (BA) corresponds to a small test body in the atmosphere (ground-based laboratory). The next column (BSS) shows the results for the same test body but this time in a medium with density of the average density of the solar system. The fourth column shows the results for the Earth inside the solar system (ESS) when the environment density is 10^{-24}g/cm^3 . The indices c and b indicate the test body and the background respectively.

smaller than the size of the Hubble horizon.) By considering $f(R) = R - \frac{|R|^{1/2}}{L_0}$ (which is suggested in [126] to account for the accelerated expansion of the universe), we found that this model is not an appropriate model to describe the gravity on local scales. Regarding laboratory tests gravity, this model cannot satisfy the constraints from the local tests of gravity. In addition for larger bodies such as the Earth in the solar system, this model does not have a thin-shell, a necessary condition for any theory of gravity to survive as a viable theory on such scales. We have also considered a local version of the QCD-scale modified-gravity. By choosing an appropriate value for the parameter $\zeta \simeq \mathcal{O}(10^2)$ in $f(R) = R - \frac{|R|^{1/2}/L_0}{1+\zeta L_0|R|^{1/2}}$, we can make this model satisfy observational constraints on local scales. However, we could not use this model on large scales as this model does not reproduce the correct values of the observed dark energy density (ρ_{DE}) in this case.

3.5 Summary

In this chapter we have investigated the square-root QCD-scale modified-gravity model (MG1) on large and local scales using local tests of gravity and cosmological data. We investigated structure formation by solving the perturbation equations numerically in section 3.2, finding that the enhancement of the Newtonian potential Ψ causes the amplification of the growth of matter density perturbations. In order to discriminate between General Relativity and the MG1 model, we calculated the value of the gravity estimator E_G and showed that it is compatible with current observation limits.

Then in section 3.3 we performed a Markov chain Monte Carlo simulation to obtain detailed constraints on the cosmological parameters of the model. We found that the best fit values for the main cosmological parameters are comparable with the Λ CDM model. The best fit value for the gluon condensate q is found to be of the order of the values obtained in previous theoretical studies: $\beta_q = q_0/q = 1.0288$, where $q_0 = (300 \text{ MeV})^4$. To tighten the constraints on this fundamental parameter, an interesting direction for future work would be to make use of constraints arising from the most massive halos inferred from SDSS data and also the galaxy-galaxy lensing signals.

In section 3.4, we tested the MG1 model on local scales. We found that the model cannot satisfy laboratory tests of gravity as the effective gravitational coupling constant is too large ($G_{\text{eff}} \simeq 1.33G_N$). In addition, fifth force searches can detect a chameleon force because the scalar degree of freedom has a large interaction distance, detectable in laboratories. We also found that celestial bodies like the Sun and Earth in the framework of this model exhibit the thick-shell effect, leading to contradictions of solar system tests of gravity. To address these difficulties, we also considered a local version of the MG1 model that contains an extra degree of freedom ζ . We found that for appropriate choices of the model parameters, this local model can satisfy the laboratory and solar system tests easily. In addition, there is the possibility of detecting the chameleon field in future orbital experiments. However, this model cannot describe the large scale dynamics of the universe as it cannot predict the right value for the observed energy density of dark energy.

The source of the inconsistency of the MG1 model with the local experiments arises because it is considered as though it were exact. However, the motivation to introduce

the $f(R)$ theory in the first place was to generate new phenomenology at a specific scale. Many problems with modifications of this kind arise when they are tested on scales far removed from those for which they are designed.¹

In order to cure the problems associated with the local behavior of the MG1 model, a suggestion for future work would be to replace the constant ζ in the local model (3.35) by a function of Ricci scalar $\zeta(R)$ such that on cosmological scales ($R \ll 1$), the $\zeta L_0 |R|^{1/2}$ term in the denominator would be negligible compared to 1 and the model (3.35) would reduce to the large-scale model (3.5). With a reasonable choice of $\zeta(R)$, the extra term in the denominator could be considerable when $R \gg 1$, so as to give rise to the consistent behavior on local scales.

To summarize, the MG1 model has been shown to be a viable theory of gravity on large scales. An advantage of this phenomenological model is that it involves only parameters from known physics such as E_{PI} and E_{QCD} . However, this model cannot satisfy the constraints from local tests of gravity and, on local scales, must be replaced by a modified version that contains an extra degree of freedom.

¹ One technique to handle corrections to GR is to treat them as only next to leading order terms in a larger expansion. This technique is known as Gravity with Perturbative Constraints [159] (cf. section 4.3).

4

Modified gravity with logarithmic curvature corrections and the structure of relativistic stars

In this chapter, we will consider another QCD-scale modified gravity (the MG2 model). By considering the semiclassical approach to quantum gravity, we propose a phenomenological $f(R)$ model of the form $R + \alpha R^2 + \frac{\beta}{2} R^2 \ln(R^2/\mu^4)$ that is relevant for the strong field regime in the interior of relativistic stars. $f(R)$ theories with logarithmic terms have been previously considered as models of dark energy [160] and modified gravity models of this form have also been discussed in early works [161–163] in the context of the Starobinsky inflationary model. Cosmological evolution in a logarithmic model arising from a running gravitational coupling has also been studied in a recent work [164].

It is well known that in the absence of a viable theory of quantum gravity, semiclassical methods like quantum field theory in curved spacetime are useful tools to study the influence of gravitational fields on quantum phenomena [165]. The curvature of spacetime modifies the gluon propagator with terms proportional to the Ricci scalar in a constant-curvature spacetime locally around the gluons. As was first shown by Leen [166] and Calzetta et al. [167, 168] (see also [169]), one-loop renormalization of non-Abelian gauge theories in a general curved spacetime induces terms logarithmic in R that dominate at large curvature. Neutron stars probe the dense QCD phase diagram at low temperature and high baryon densities, where the baryon density in the

stellar interior can reach an order of magnitude beyond the nuclear saturation density $\rho_{ns} = 2.7 \times 10^{17} \text{kg m}^{-3}$. In such a dense medium, where the strong nuclear force plays a paramount role, we consider the effect of corrections to the EH action involving terms of the form $\alpha R^2 + \frac{\beta}{2} R^2 \ln(R^2/\mu^4)$ on the observational features of the neutron star.

We shall also consider the effect of the $f(R)$ model on a separate class of neutron stars: self-bound stars, consisting of strange quark matter with finite density but zero pressure at their surface [170–172]. The interior of the star is made up of deconfined quarks that form a colour superconductor, leading to a softer equation of state with possible observable effects on the minimum mass, radii, cooling behaviour and other observables [173–175].

The structure of this chapter is as follows. First in section 4.1 we motivate the $f(R)$ model by considering the calculation of the gauge invariant effective action for gauge fields in curved spacetime. Then in section 4.2, we investigate constraints imposed upon the model from the requirements of internal consistency and compatibility with observations, and discuss the potential observational signatures due to a change in the effective gravitational constant near the surface of the star. In section 4.3 the structure of relativistic stars is considered in the framework of the $f(R)$ theory, and we summarise our results in section 4.4. The work of this chapter is based on [176].

4.1 Motivations for the MG2 model

The behaviour of gauge theories in curved spacetime was studied in detail by several authors some thirty years ago, with the intention of seeing if quantitatively new effects appear in the high-curvature limit (cf. [177] for a textbook discussion and original references). In particular it was shown by Calzetta et al. [167, 168] that for a pure gauge theory in a general curved space-time, the effective value of the gauge coupling constant can become small in the high-curvature limit, due to the presence of $\ln(R/\mu^2)$ terms in the renormalised gauge-invariant effective action: a situation referred to as curvature-induced asymptotic freedom. Without going into details, in this section we sketch how this result comes about, and use the form of the full result to motivate the phenomenological $f(R)$ theory that will be investigated in more detail in the remainder of this chapter.

The classical action for a pure gauge field is $S_G[A] = \int d^d x \sqrt{-g} \mathcal{L}_G$, where \mathcal{L}_G is defined in (1.66a) and in curved spacetime

$$F_{\mu\nu}^a = \nabla_\mu A_\nu^a - \nabla_\nu A_\mu^a + e_g f_{abc} A_\mu^b A_\nu^c, \quad (4.1)$$

in terms of the metric covariant derivative ∇_μ . The generating function for disconnected graphs in the presence of a background gauge field \bar{A}_μ and a source J_μ (with only the gluon source) is¹

$$Z[J, \bar{A}] = \int \mathcal{D}[A] \mathcal{D}[\chi] \mathcal{D}[\bar{\chi}] \exp \left(i \left[S_G[\bar{A} + A] + S_{\text{GF}} + S_{\text{FP}} + S_{\text{grav}} + \int d^d x \sqrt{-g} J^a A^a \right] \right), \quad (4.2)$$

where in this chapter $S_{\text{gf}} = -\frac{1}{2\omega}(D \cdot a, D \cdot a)$ is the gauge fixing term and $S_{\text{ghost}} = -\int d^d x \sqrt{-g} \bar{\chi} D \cdot (D + a) \chi$ is the ghost field action. Here D refers to the (gauge) covariant derivative in curved spacetime $D_\mu = \nabla_\mu - ie_g \bar{A}_\mu$. Renormalizability in curved spacetime requires the inclusion of squared-curvature terms in addition to the Einstein-Hilbert action

$$S_{\text{grav}} = \int d^d x \sqrt{-g} \left(-M_{\text{Pl}}^2 \Lambda + \frac{M_{\text{Pl}}^2}{2} R + \alpha_1 R^{\mu\nu\rho\sigma} R_{\mu\nu\rho\sigma} + \alpha_2 R^{\mu\nu} R_{\mu\nu} + \alpha_3 R^2 \right), \quad (4.3)$$

where d is the number of spacetime dimensions, $M_{\text{Pl}}^2 = 1/8\pi G$ and the authors of [167, 168] use a metric with signature -2 and, relative to our convention, the opposite sign for $R^c{}_{\sigma\mu\nu}$. The gauge-invariant effective action $\Gamma[A]$ is obtained via a Legendre transformation from the functional $W = -i \ln(Z)$. To one-loop order, it is given by

$$\Gamma[\bar{A}] = S[\bar{A}] + S_{\text{grav}} + \frac{i}{2} \ln \det(K_{\mu\nu}) - i \ln \det(D^2), \quad (4.4)$$

where

$$K_{\mu\nu} = g_{\mu\nu} D^2 - (1 - 1/\omega) D_\mu D_\nu - 2ie_g F_{\mu\nu} + R_{\mu\nu}, \quad (4.5)$$

and $D^2 = D_\mu D^\mu$. Since $\Gamma[\bar{A}]$ is gauge invariant, the calculation may be simplified without affecting the final result by choosing the Feynman gauge $\omega = 1$. In general, one has a choice concerning the separation of the full action into a free part and an interacting part, which determines which terms provide propagators entering into Feynman

¹ In this section we use the shorthand $(f, g) = \int d^d x \sqrt{-g} f_a(x) g_a(x)$ for fields f, g with components f_a, g_a .

diagrams and which provide vertices. The above choice corresponds to taking the free part to consist of all terms quadratic in the quantum fields $A, \bar{\chi}, \chi$.¹ Regularising using dimensional regularisation gives

$$\begin{aligned} \Gamma[\bar{A}] &= S[\bar{A}_B] + S_{\text{grav},B} \\ &+ \frac{1}{(4\pi)^{d/2}} \int d^d x \sqrt{-g} \frac{1}{(-R/6)^{2-d/2}} \left\{ \left[1 + \frac{1}{12} \left(1 - \frac{d}{2} \right) \right] \Gamma\left(2 - \frac{d}{2}\right) C e_g^2 \mu^{(4-d)} F_{\mu\nu,a} F_a^{\mu\nu} + \right. \\ &\quad \left. + \Gamma\left(2 - \frac{d}{2}\right) N \left[-\frac{1}{9} \frac{(d+1)}{d(d-2)} R^2 + \frac{d-17}{360} R_{\mu\nu\rho\sigma} R^{\mu\nu\rho\sigma} + \frac{92-d}{360} R_{\mu\nu} R^{\mu\nu} \right] \right. \\ &\quad \left. + \sum_{j=3}^{\infty} \frac{\Gamma(j - \frac{d}{2})}{(-R/6)^{j-2}} \text{tr}[H_j] \right\}, \quad (4.6) \end{aligned}$$

where $\delta_{ab}C = \text{tr}(t_a, t_b)$, N is the dimension of the gauge group and H_j stands for curvature and field strength terms entering into the relevant Schwinger-DeWitt series. The subscript B indicates that these terms involve bare quantities. Adopting the minimal subtraction scheme, the renormalised gauge-invariant effective action $\Gamma[\bar{A}]$ is found to be

$$\begin{aligned} \Gamma[\bar{A}] &= S[\bar{A}] + S_{\text{grav}} \\ &- \frac{1}{16\pi^2} \int d^4 x \sqrt{-g} \left[\ln \left(\frac{-R/6}{4\pi\mu^2} \right) + \gamma_E \right] \\ &\times \left[\frac{11}{12} e_g^2 C F_a^{\mu\nu} F_{\mu\nu,a} \left(-\frac{13}{360} R_{\mu\nu\rho\sigma} R^{\mu\nu\rho\sigma} + \frac{11}{45} R_{\mu\nu} R^{\mu\nu} - \frac{5}{72} R^2 \right) N \right], \quad (4.7) \end{aligned}$$

where $S[\bar{A}] + S_{\text{grav}}$ contain finite renormalised coefficients and γ_E is the Euler-Mascheroni constant. Here, the minus sign is kept in the logarithm to emphasise that it is $-R/6$ that plays the role of ‘squared mass’ in the loop integrals, however, the integrals leading to this result are well-defined regardless of the sign of R [168]. From a phenomenological perspective the $\ln(-1) = i\pi$ is simply another finite contribution entering into the coefficients of the squared curvature and field strength terms in the gravitational and gauge field actions. It is noted in [167] that the appearance of a negative argument in the logarithm could possibly be interpreted as a vacuum instability. However, such imaginary terms could be cancelled by others arising from global topological effects or from further R -dependent corrections. It should also be noted that for effects such as curvature-induced asymptotic freedom, only the real part $\ln(|R|/|R_0|)$, where R_0 is a

¹ Another possibility is to treat terms involving the background field A as interaction terms, in which case the inverse propagator involves only the first and last terms in (4.5). As shown in [168], the final results for the two methods agree.

scalar curvature chosen so that e_g is small and so perturbation theory is valid, enters the expressions for the effective coupling constant e_g^{eff} [167].

Equation (4.7) takes account of the corrections to the quantum field theory due to the presence of non-negligible spacetime curvature. Ordinarily, QCD can be treated in Minkowski spacetime, which is maximally symmetric, however, in situations where the gravitational field is particularly strong it is desirable to generalise this. An obvious first step is to consider a spacetime that maintains maximal symmetry but allows for non-zero curvature, such as a de Sitter or anti-de Sitter spacetime (cf. [178, 179]). Hence in the interior of a neutron star, where the spacetime curvature is particularly large, one can consider a Lagrangian on local, microscopic scales with a maximally symmetric spacetime with constant curvature.

In a maximally symmetric spacetime with constant curvature, the Ricci and Riemann tensors are proportional to the Ricci scalar i.e. $R_{\mu\nu\rho\sigma}R^{\mu\nu\rho\sigma} \propto R^2$, $R_{\mu\nu}R^{\mu\nu} \propto R^2$. On the small scales relevant for QCD, the background spacetime is highly symmetric and one can consider the maximally symmetric case as an approximation: the gravitational part of the effective Lagrangian for a non-Abelian gauge field such as the gluon field would thus consist of R^2 and $R^2 \ln(R/\mu^2)$ terms. Here, the factors of R^2 arise as a combination of the $R_{\mu\nu\rho\sigma}R^{\mu\nu\rho\sigma}$, $R_{\mu\nu}R^{\mu\nu}$ and R^2 terms in (4.7).

On astrophysical scales, however, gluons are no longer the relevant degrees of freedom and the situation is quite different. On large scales, far removed from those relevant for subatomic particles, relaxing the constant curvature condition would lead to a non-standard dependence of the gravitational action on the curvature. The phenomenology of a neutron star is a window onto the strong-field limit of gravitational theories, and as such, it is of great theoretical interest to consider the observable effects of alternatives to General Relativity, the simplest being $f(R)$ theories. Modulo stability and consistency constraints, the form of the function $f(R)$ can be arbitrary. In this chapter we are interested in the effect of modifications to the EH action on the structure of relativistic stars, where QCD plays an important role. Motivated by the

results summarised in this section, we propose a phenomenological $f(R)$ model¹

$$S_{\text{tot}} = \frac{M_{Pl}^2}{2} \int d^4x \sqrt{-g} \left[R + \alpha R^2 + \frac{\beta}{2} R^2 \ln(R^2/\mu^4) \right] + S_{\text{matter}}, \quad (4.8)$$

where the constants α and β should be determined by observations. As we consider only astrophysical scales, we do not include the effect of the cosmological constant term. We note that modified gravity theories of this form have also been discussed in early works discussing the effective gravitational action of conformally covariant fields [161–163] in the context of the Starobinsky inflationary model.

As we are considering neutron stars, a natural choice of the parameter μ should contain the relevant mass scales. We will assume

$$\mu = m_n^2/M_{Pl}, \quad (4.9)$$

where m_n is the neutron mass and M_{Pl} is the reduced Planck mass. Taking account of factors of c and \hbar , the numerical value of μ^2 is $\mu^2 \simeq 1.3 \times 10^{-7} \text{m}^{-2}$. The characteristic value of the Ricci scalar for a neutron star can be estimated by (cf. [181]) $R_0 = 8\pi G\rho_* \sim 6M_*/c^2 r_*^3$ where M_* is the mass and r_* the radius of the star. For a typical neutron star with $M_* = 1.8M_\odot$ and $r_* = 10\text{km}$, we have $R_0 \simeq 1.6 \times 10^{-8} \text{m}^{-2}$, with larger values expected in the high-density region near the core. Thus, μ^2 is of the order of the curvature of a typical neutron star.

4.2 Constraints on the MG2 model

In section 4.3 we shall investigate the phenomenology of relativistic stars in the $f(R)$ theory described by the action (4.8), working in the metric formalism. Firstly, in sections 4.2.1 and 4.2.2 we consider consistency and observational constraints to check the viability of the model in such a medium. It is important to emphasise that we treat the model as an effective theory valid in the interior and vicinity of ultra-dense matter, and so do not consider cosmological or solar system tests.

¹ In principle one could extend this to include terms involving one (but making use of the Gauss-Bonnet invariant, not both, cf. [180]) of the other curvature invariants in (4.7). However, since on the small scales on which (4.7) is relevant we can treat the background spacetime as approximately maximally symmetric, we consider only a function of the Ricci scalar here.

4.2.1 Consistency constraints

An $f(R)$ model inevitably introduces a scalar degree of freedom, which is constrained by the requirement that the model must be free of instabilities [6]. Such consistency constraints are not always obvious at first sight; indeed, generalising the findings of Dolgov and Kawasaki [99], it was pointed out by Frolov [182] that many $f(R)$ models that deviate from General Relativity in the infrared possess a crippling nonlinear instability. In this section, we illustrate how these constraints can restrict the parameters of our model.

From (4.8) we have

$$f(R) = R + \alpha R^2 + \frac{\beta}{2} R^2 \ln \frac{R^2}{\mu^4}. \quad (4.10)$$

In this section and throughout this chapter, we shall restrict ourselves to the case in which the $R^2 \ln(R^2/\mu^4)$ term is subdominant to the R^2 term i.e. $|\gamma| \ll 1$, where

$$\gamma \equiv \beta/\alpha. \quad (4.11)$$

The system is best studied in the original frame (i.e without performing a conformal transformation to the Einstein frame). The equation of motion for the scalar degree of freedom is

$$\square f_R = \frac{2f - f_R R}{3} + \frac{8\pi G}{3} T, \quad (4.12)$$

where T is the trace of the stress-energy tensor and $f_R \equiv df(R)/dR$. Defining

$$\chi \equiv f_R - 1, \quad (4.13)$$

this can be recast in the form

$$\square \chi = \frac{dV}{d\chi} - \mathcal{F}, \quad (4.14)$$

where $\mathcal{F} = -(8\pi G/3)T$ appears as a force term and V is a potential satisfying

$$\frac{dV}{d\chi} = \frac{1}{3}(2f - f_R R). \quad (4.15)$$

In the model at hand, the form of $f(R)$ and its derivatives are given by

$$f(R) = R + \alpha R^2 + \frac{\beta}{2} R^2 \ln(R^2/\mu^4), \quad (4.16)$$

$$f_R(R) = 1 + (2\alpha + \beta)R + \beta R \ln(R^2/\mu^4), \quad (4.17)$$

$$f_{RR}(R) = 2\alpha + 3\beta + \beta \ln(R^2/\mu^4), \quad (4.18)$$

so that

$$\frac{dV}{d\chi} = \frac{1}{3}(R - \beta R^2). \quad (4.19)$$

As we shall see in section 4.3, the modified Einstein equations involve f_{RR} , which is not analytic at $R = 0$. Hence, we shall restrict our analysis to non-negative values of the curvature scalar. To obtain the form of the potential without inverting, one can multiply (4.19) by (4.18) and integrate with respect to R to yield the parametric equations¹

$$\chi(R) = R \left[2\alpha + \beta + \beta \ln \left(\frac{R^2}{\mu^4} \right) \right], \quad (4.20)$$

and

$$V(R) = -\frac{R^2}{9} \left\{ \beta R \left[2\alpha + \frac{7}{3}\beta + \beta \ln \left(\frac{R^2}{\mu^4} \right) \right] - 3\alpha - 3\beta - \frac{3}{2}\beta \ln \left(\frac{R^2}{\mu^4} \right) \right\}. \quad (4.21)$$

The potential is shown in figure 4.1. One can see immediately that in the limit of large curvature ($R \rightarrow \infty$) $V \rightarrow -\infty$ while $\chi \rightarrow \text{sgn}(\beta)\infty$ (for negative β the potential turns back on itself after an inflection point to reach negative χ .) This should be contrasted with the behavior of the basic $f(R) = R + \alpha R^2$ model, where the potential is a simple quadratic in the χ -field. Thus, Frolov's singularity — in which the curvature singularity is a finite distance in field and energy values away from the stable solution — will be avoided.

What is the nature of the stable solution in this model in the absence of matter? From (4.19) we note that there are two stationary points, at $R = 0$ and $R = 1/\beta$ respectively; to ensure perturbative stability, the scalar degree of freedom should satisfy the important requirement that its squared mass term is positive $m_\chi^2 \equiv d^2V/d\chi^2 > 0$. It follows from (4.18) that

$$m_\chi^2(R) = \frac{dR}{d\chi} \frac{d}{dR} \left(\frac{2f - f_{RR}R}{3} \right) = \frac{1 - 2\beta R}{3f_{RR}}, \quad (4.22)$$

however, one cannot substitute $R = 0$ into this expression due to the singularity in the logarithmic term in (4.18). For small ϵ we have from the form of the potential

$$V(R = \pm\epsilon) = \frac{\alpha}{3} \left[1 + \gamma + \frac{\gamma}{2} \ln(\epsilon^2/\mu^4) \right] \epsilon^2 + \mathcal{O}(\epsilon^3), \quad (4.23)$$

¹ Note that in order to show the full form of the potential obtained from (4.10) using the range $R \in (-\infty, \infty)$, we have adjusted the numerical factors here so that the arguments of the logs depend on R^2 . We shall only consider the part corresponding to $R \geq 0$.

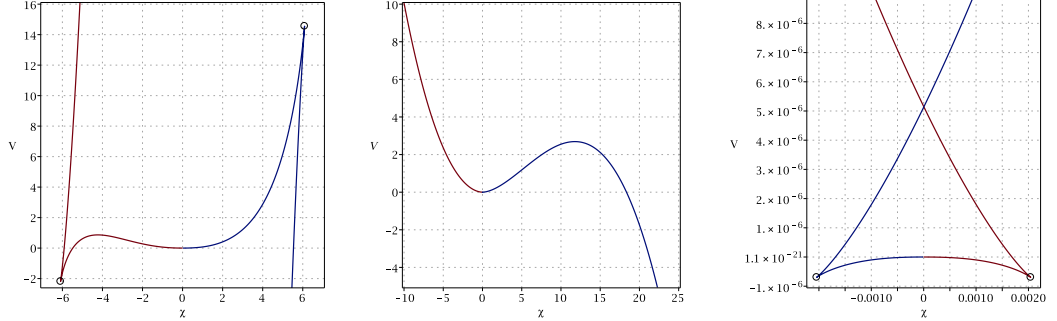


Figure 4.1: The potential $V(\chi)$ corresponding to positive (blue) and negative (red) R . The branch points at $\chi = \chi_*$ are indicated by the black circles. Large values, $\alpha = \mu = 1$, $|\beta| = 0.25$ have been chosen to illustrate the important features. Left panel: Negative β . Middle panel: Positive β . The apparent minimum at $\chi = 0$ in the middle panel is actually a maximum with branch points at $\chi = \chi_* \ll 1$, as can be seen in the right panel, which is a close-up of the region around $\chi = 0$ for $\beta > 0$.

which should be positive as $\epsilon \rightarrow 0$ if $R = 0$ is a minimum. Assuming $|\gamma| \ll 1$, this is true only when $\beta < 0$, regardless of the sign of α .

For $R = 1/\beta$ to be a minimum, one needs $f_{RR}(R = 1/\beta) < 0$. As we do not consider negative curvature, $\beta > 0$ and the condition is equivalent to

$$R_*\beta > 1, \quad (4.24)$$

where we have defined

$$R_* = \mu^2 \exp\left(-\frac{3}{2} - \gamma^{-1}\right). \quad (4.25)$$

When $|\gamma| \ll 1$, the dimensionless ratio R_*/μ^2 is exponentially large for negative γ and exponentially small for positive γ . We conclude that the stationary point at $R = 1/\beta$ is only stable for negative alpha.

Since maximally symmetric solutions lead to a constant Ricci scalar [and so the derivatives of χ vanish in (4.14)] one can conclude from this that the maximally symmetric solution is Minkowski spacetime ($R = 0$) when $\beta < 0$ and de Sitter spacetime when $\beta > 0$, $\alpha < 0$.

We can also analyse the sign of m_χ^2 away from the stationary points. For negative β we find

$$m_\chi^2 > 0 \quad \Rightarrow \quad R < R_* \quad (\beta < 0), \quad (4.26)$$

which in terms of χ is $\chi < \chi_* \equiv -2\beta R_*$. For positive β one must also take the numerator of (4.22) into account, giving

$$m_\chi^2 > 0 \quad \Rightarrow \quad \begin{cases} R_* < R < \frac{1}{2\beta}, & R_* < \frac{1}{2\beta} \\ R_* > R > \frac{1}{2\beta}, & R_* > \frac{1}{2\beta} \end{cases} \quad (\beta > 0). \quad (4.27)$$

The relevant interval depends on whether the condition $R_* < \frac{1}{2\beta}$ is satisfied. Since we are only interested in positive β here we can write this as

$$e^{\gamma^{-1} - \ln |\gamma|} > 2e^{-3/2} |\mu^2 \alpha|. \quad (4.28)$$

As discussed in section 4.3, in order to make use of the method of perturbative constraints we shall work with parameter values such that $|\alpha\mu^2| \ll 1$. Hence, when $|\gamma| \ll 1$, $R_* < \frac{1}{2\beta}$ is easily satisfied if $\alpha > 0$. Similarly, $R_* > \frac{1}{2\beta}$ when $\alpha < 0$.

The requirement that the graviton is not a ghost¹, or equivalently that the effective gravitational constant G_{eff} is positive, imposes the well-known condition $f_R(R) > 0$. Using the definition of χ this gives $\chi > -1$. We can write this condition in terms of R : for $\alpha > 0$, $\beta < 0$ the range of the scalar curvature is bounded

$$R < - \left[2\beta W_0 \left(- \frac{\exp(\frac{1}{2} + \gamma^{-1})}{2\mu^2\beta} \right) \right]^{-1},$$

where W_0 is the upper branch of the Lambert W function. If $|\gamma| \ll 1$, the exponential in the argument is small, so the upper limit is

$$f_R > 0 \quad \Rightarrow \quad R \lesssim \mu^2 e^{-\frac{2\alpha+\beta}{2\beta}} = e^1 R_* \quad (\alpha > 0, \beta < 0) \quad (4.29)$$

Thus, the condition ensuring the positivity of the scalar mass (4.26) is sufficient to ensure that $G_{\text{eff}} > 0$. If we were to consider positive β , we need only recognise that since the function $f_R(R)$ is decreasing as it crosses the axis at $f_R(R=0) = 1$ the smallest value it can reach is $f_R(R=R_*) = 1 - 2\beta R_*$. The condition can thus be expressed as

$$f_R > 0 \quad \Rightarrow \quad R_* < \frac{1}{2\beta} \quad (\alpha > 0, \beta > 0) \quad (4.30)$$

¹ As calculated by expanding the propagator about Minkowski spacetime.

Parameters		Unitarity	$m_\chi^2 > 0$
$\alpha > 0$	$\beta > 0$	$R_* < 1/2\beta$	$R_* < R < 1/2\beta$
	$\beta < 0$	$R < e^1 R_*$	$R < R_*$
$\alpha < 0$	$\beta > 0$	$R < -1/2\alpha, \quad R \gtrsim e^1 R_*$	$1/2\beta < R < R_*$
	$\beta < 0$	$R < -1/2\alpha$	$R < R_*$

Table 4.1: The unitarity and positive-squared-mass constraints on the allowed curvature range for different values of the parameters α and β , using $|\gamma| = |\beta/\alpha| \ll 1$ and $|\mu^2\alpha| \ll 1$. R_* is defined in (4.25).

which, as noted above, is easily satisfied with the choice $\gamma \ll 1$. For negative α we find¹

$$R < \begin{cases} - \left[2\beta W_0 \left(-\frac{\exp(\frac{1}{2} + \gamma^{-1})}{2\mu^2\beta} \right) \right]^{-1} & (\alpha < 0, \beta < 0) \\ - \left[2\beta W_{-1} \left(-\frac{\exp(\frac{1}{2} + \gamma^{-1})}{2\mu^2\beta} \right) \right]^{-1} & (\alpha < 0, \beta > 0) \end{cases}, \quad (4.31)$$

where W_0 and W_{-1} indicate the upper and lower branches of the Lambert W function respectively. Since for large x , $W_0(x) \sim \ln(x)$, and for small x , $W_{-1}(x) \sim \ln(-x)$, when $|\gamma| \ll 1$, we have

$$R \lesssim -\frac{1}{2\alpha}, \quad (4.32)$$

as in the $\beta = 0$ case i.e. $f(R) = R + \alpha R^2$. For $\beta > 0$ this is a stronger upper bound than that in (4.27). For $\beta < 0$, γ is positive and so (4.32) is weaker than (4.26), which already restricts R to exponentially small values. One difference between this and the $f(R) = R + \alpha R^2$ model is that the negative α case is not ruled out by the f_{RR} condition, so can be considered as a viable parameter choice, albeit for a restricted range of values of R . These constraints are summarised in table 4.1.

As with many $f(R)$ models in the literature, the potential $V(\chi)$ is multivalued, with branches at the points $\chi = \chi_*$ (see figure 4.1). As long as the conditions derived above are satisfied, the field will not reach these critical points. In the case of negative β (with $\alpha > 0$) this amounts to a (large) upper limit of the value of the spacetime curvature for which the model can be considered valid, which is far away from the stable solution

¹ Since the inverse function $R(\chi)$ is multivalued, for $\alpha < 0, \beta > 0$ there is a second valid region: $R > - \left[2\beta W_0 \left(-\exp(\frac{1}{2} + \gamma^{-1})/(2\mu^2\beta) \right) \right]^{-1} \simeq e^1 R_*$. However, this corresponds to an extremely large value of the scalar curvature.

at $R = 0$ and for the small values of $|\gamma|$ considered here, significantly larger than the curvature encountered in neutron stars. However, for positive β , the potential has no stable minimum when $\alpha > 0$ and the branch point occurs at the lower limit of the range of validity, corresponding to a value of R much smaller than the characteristic curvature of a neutron star. In a realistic scenario, this could be remedied by the presence of a matter term $T \neq 0$, which would give rise to a minimum in the effective potential. Since the model in this chapter is considered phenomenologically as an (ultraviolet) modification to General Relativity that is relevant in the presence of dense nuclear matter, and in reality neutron stars are not completely isolated but instead occur in astrophysical situations with a non-zero stress-tensor, the instability may be avoided in practice. This notwithstanding, in the remainder of this chapter we will consider only negative values of β .

The results of this subsection are presented in table 4.1. In particular we note that for $\beta > 0$, the condition ensuring unitarity — equivalent to $f_R > 0$ for $f(R)$ theories — is satisfied for a wide range of curvature values when α is positive, but is restricted to values less than $-1/2\alpha$ (as in the $f(R) = \alpha R^2$ case) when $\alpha < 0$. In the latter case, however, the condition for positive squared mass is significantly tighter, so this choice of parameters would lead to instabilities for all but a tiny range of curvature values in the absence of matter. Despite this, in the numerical work in section 4.2 we shall consider both positive and negative values of α , so as to compare with other works in the literature.

4.2.2 Observational constraints

We begin this subsection by considering the fifth force due to the extra scalar degree of freedom of the $f(R)$ theory. This fifth force can affect the effective gravitational constant G_{eff} and gravitational redshift at the surface of a neutron star z_s .

To investigate the effective gravitational coupling constant, consider the parameter δ^2 in equation (2.34). The parameter δ can be constrained with binary pulsar tests [183]. For example, observations of the famous Hulse-Taylor binary pulsar PSR B1913+16 [184] give $|\delta| < 0.04$. The binary pulsars PSR J141-6545 [185] and PSR1534+12 [186] give $|\delta| < 0.024$ and $|\delta| < 0.075$ respectively.

The parameter δ^2 for a neutron star of mass $M = 2M_\odot$ and radius $r_s = 11\text{km}$ for two values of parameter α and fixed $\gamma = \beta/\alpha$ is plotted in figure 4.2. In this figure

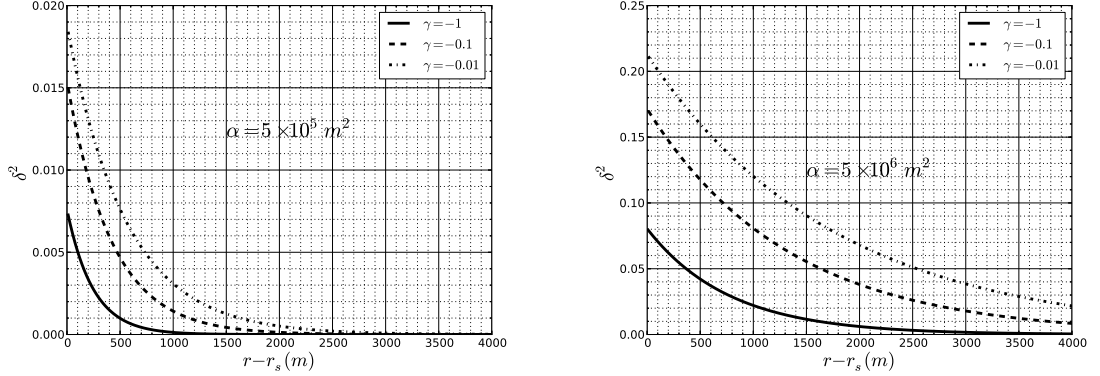


Figure 4.2: The parameter $\delta^2 \equiv G_{\text{eff}}/G - 1$ against the distance to the surface of a neutron star of radius $r_s = 11\text{km}$ and $M_s = 2M_\odot$ in the $f(R) = R + \alpha R^2 + \frac{\beta}{2} R^2 \ln(R/\mu^4)$ gravity for different values of α and $\gamma \equiv \beta/\alpha$.

one can see that for the case with $\alpha = 5 \times 10^5$, $\delta^2 \lesssim 0.001$ for $r \gtrsim 1.2r_s$, so the model easily satisfies the observational constraints quoted above. For the larger value, $\alpha = 5 \times 10^6$, δ^2 takes larger values further from the surface of the star, however, since binary pulsar tests are sensitive to the scale $r_{bs} \gg r_s$, corresponding of the order of the mean separation of the two stars, any effect on the orbital motion of a binary system is completely negligible.¹

However, near the surface of the star, the deviation from GR is larger: this deviation has observational effects on redshift of surface atomic lines that could in principle distinguish GR from modified theories of gravity [189, 190]. The thermal spectrum of a neutron star will be detected by an observer at infinity with a gravitational redshift z_s equal to

$$z_s \equiv \frac{\delta\lambda}{\lambda_0} = B(r)^{-1/2} - 1 \quad (4.33)$$

¹ One could also consider gravitational radiation from binary pulsars as a potential discriminant between GR and modified gravity [187]. It has been shown in [188] that an application of $f(R) = R + \alpha R^2$ to the gravitational radiation of a hypothetical binary pulsar system requires that $\alpha < 1.7 \times 10^{17} \text{m}^2$, under the assumption that the dipole power accounts for at most 1% of the quadrupole power. However, as we shall see in the following section, consistent application of the perturbative method means that we must restrict α to values $\alpha \lesssim 10^6 \text{m}^2$. Thus, as far as our assumption that the logarithmic term constitutes only a subdominant correction to the R^2 term holds true, the $f(R)$ model considered here is not significantly constrained by measurements of the orbital period decay of double neutron stars.

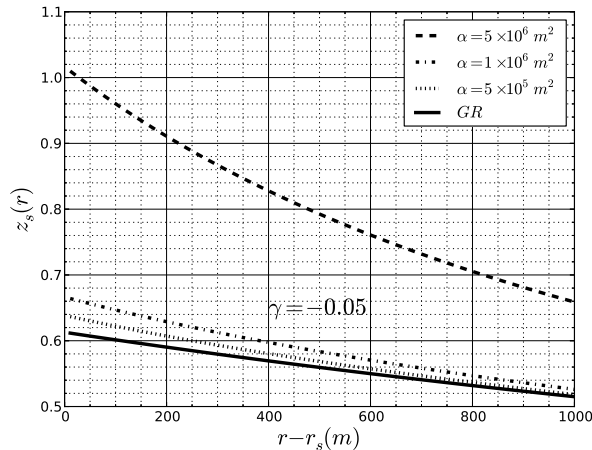


Figure 4.3: The gravitational redshift parameter z_s against the distance to the surface of a neutron star with radius $r_s = 11\text{km}$ and $M_s = 2M_\odot$ in the $f(R) = R + \alpha R^2 + \frac{\beta}{2} R^2 \ln(R/\mu^4)$ model for different values of α and $\gamma \equiv \beta/\alpha = -0.05$.

where $B(r) = 1 - 2GM/r$ and λ_0 is the wavelength in the laboratory. Buchdahl's theorem [191] limits the value of M/R for a spherical symmetric star in GR to $M/R < 4/9$, so the maximum possible value of the of the redshift from the surface is $z_s \leq 2$.

In figure 4.3 we have plotted z_s as a function of r in the immediate vicinity of the surface of a typical neutron star with mass $M_s = 2M_\odot$ and radius $r_s = 11\text{km}$ for $\gamma = \beta/\alpha = -0.05$. We can see that in the case of $\alpha = 5 \times 10^6\text{m}^2$, the deviation from GR is considerable, but for $\alpha = 10^6\text{m}^2$ and $\alpha = 5 \times 10^5\text{m}^2$, the gravitational redshift z_s is close to the GR value $z_s^{GR} \simeq 0.51$. A large number of neutron stars exhibiting thermal emission have been observed by X-ray satellites such as the Chandra X-ray Observatory, and XMM-Newton (see [192] for a recent review) and proposed missions such as ATHENA [193] promise an increase in the number and quality of the lines that can be used to analyse neutron star properties. In principle then, for large α this deviation could be observed in lines originating close to the surface of the neutron star; in practice this would be dogged by uncertainties relating to the composition of the outer envelope of the neutron star, and would require a careful treatment that is beyond the scope of this chapter.

4.3 Relativistic stars in the MG2 model

As mentioned in the Introduction of this chapter, neutron stars probe the dense QCD phase diagram at low temperature and high baryon densities, where the baryon density in the stellar interior can reach an order of magnitude beyond the nuclear saturation density $\rho_{ns} = 2.7 \times 10^{17} \text{kg m}^{-3}$. In such densities, matter can pass into a regime where the quark degrees of freedom are excited. In this section we consider the internal structure of relativistic stars within the framework of the phenomenological $f(R)$ model (4.8) and calculate the effect on the neutron star mass-radius (M-R) relation.

4.3.1 Field equations

To obtain the field equations, we will use the method of perturbation constraints adopted by Cooney et al. [194] for the study of neutron stars in $f(R)$ theory, and later used (in a slightly different form) by other authors [181, 195–197]. This method is useful for investigating corrections to GR that give rise to field equations that would otherwise be almost unmanageable. The correction terms are treated as next to leading order terms in a larger expansion. To this end, the modified theory in eq. (4.10) is rewritten as

$$S = \frac{M_{Pl}^2}{2} \int d^4x \sqrt{-g} (R + \alpha h(R)) + S^{\text{matter}}, \quad (4.34a)$$

$$h(R) = R^2 + \frac{\gamma}{2} R^2 \ln \frac{R^2}{\mu^4}, \quad (4.34b)$$

where $\gamma \equiv \beta/\alpha$. In order to avoid conflict with the consistency constraints discussed in Sec. 4.2.1, we can consider the regime in (α, β) parameter space where $\alpha > 0$ and $\beta < 0$ i.e. $\alpha > 0$ and $\gamma < 0$ with $|\gamma| \ll 1$. In this section, however, we elevate α to the status of a perturbative parameter and so focus on the (α, γ) parameter space. In addition, in order to compare with related works in the literature, we consider both negative and positive values of α .

The field equations arising from the action (4.34) are

$$R_{\mu\nu} - \frac{1}{2} g_{\mu\nu} R + \alpha \left[h_R R_{\mu\nu} - \frac{1}{2} g_{\mu\nu} h - (\nabla_\mu \nabla_\nu - g_{\mu\nu} \square) h_R \right] = 8\pi G T_{\mu\nu}^{\text{matter}}, \quad (4.35)$$

where $h_R \equiv \delta h / \delta R$ and $T_{\mu\nu}^{\text{matter}} \equiv -2 / \sqrt{-g} \partial S^{\text{matter}} / \partial g^{\mu\nu}$. Taking the trace of eq. (4.35)

$$R - \alpha [h_R R - 2h + 3\square h_R] = -8\pi G T^{\text{matter}}, \quad (4.36)$$

and substituting R from eq. (4.36) in to eq. (4.35) gives

$$\begin{aligned} R_{\mu\nu} + \alpha \left[h_R R_{\mu\nu} - \frac{1}{2} g_{\mu\nu} (h_R R - h) - \left(\nabla_\mu \nabla_\nu + \frac{1}{2} g_{\mu\nu} \square \right) h_R \right] \\ = 8\pi G \left(T_{\mu\nu}^{\text{matter}} - \frac{1}{2} g_{\mu\nu} T^{\text{matter}} \right). \end{aligned} \quad (4.37)$$

We shall consider the perturbative expansion in the dimensionless constant

$$c_R = \alpha \mu^2 \quad (4.38)$$

(recall from (4.9) that μ^2 is of the order of the curvature of a typical neutron star). At zeroth order in c_R , the equations are ordinary GR equations with $g_{\mu\nu}^{(0)}$ solutions; in the perturbative approach we expand the quantities in the metric and stress-energy tensor up to first order in c_R i.e.

$$g_{\mu\nu} = g_{\mu\nu}^{(0)} + c_R g_{\mu\nu}^{(1)}. \quad (4.39)$$

Considering the line element

$$ds^2 = -B(r)dt^2 + A(r)dr^2 + r^2 (d\theta^2 + \sin^2 \theta d\phi^2), \quad (4.40)$$

and assuming a perfect fluid inside the star ($T_{\nu}^{\text{matter}\mu} = \text{diag}[-\rho, P, P, P]$) the field equations (4.37) can be written

$$\frac{R_{00}}{B} + \alpha \left[h_R \frac{R_{00}}{B} + \frac{1}{2} (h_R R - h) + \frac{1}{2A} (h_R'' + \left(\frac{3B'}{2B} - \frac{A'}{2A} + \frac{2}{r} \right) h_R') \right] = 4\pi G(\rho + 3P), \quad (4.41a)$$

$$\frac{R_{11}}{A} + \alpha \left[h_R \frac{R_{11}}{B} - \frac{1}{2} (h_R R - h) - \frac{1}{2A} (3h_R'' + \left(\frac{B'}{2B} - \frac{3A'}{2A} + \frac{2}{r} \right) h_R') \right] = 4\pi G(\rho - P), \quad (4.41b)$$

$$\frac{R_{22}}{r^2} + \alpha \left[h_R \frac{R_{22}}{B} - \frac{1}{2} (h_R R - h) - \frac{1}{2A} (h_R'' + \left(\frac{B'}{2B} - \frac{A'}{2A} + \frac{4}{r} \right) h_R') \right] = 4\pi G(\rho - P), \quad (4.41c)$$

where a prime indicates differentiation with respect to r . To first order in c_R the pressure and the energy density are $P = P^{(0)} + c_R P^{(1)}$ and $\rho = \rho^{(0)} + c_R \rho^{(1)}$ respectively.

4.3.2 Modified Tolman-Oppenheimer-Volkov equations

In astrophysics, the Tolman-Oppenheimer-Volkoff (TOV) equations constrain the structure of a spherically symmetric body of isotropic material that is in static gravitational

equilibrium [198]. Before considering an ansatz for the solutions inside the star and obtaining the modified Tolman-Oppenheimer-Volkov equations (MTOV), something should be said about the exterior solutions. As the modified theory in eq. (4.34) is considered for high-curvature regimes in presence of matter, we assume that, outside of the star, the solutions can be approximately explained by the Schwarzschild solution

$$A_{\text{out}}(r) = B_{\text{out}}(r)^{-1} = \left(1 - \frac{2GM_{\text{tot}}}{r}\right)^{-1}, \quad (4.42)$$

where for a few radii far from the star, M_{tot} receives no corrections due to the modified theory. However for distances close to the surface of the star, a good approximation should include the α corrections.

The ansatz for the interior solutions is then

$$A(r) \equiv \left(1 - \frac{2GM(r)}{r}\right)^{-1}, \quad (4.43)$$

where $M(r)$ contains corrections to the first order in α arising from the form of $h(R)$. Using Eqs. (4.41) and the geometrical relation

$$\frac{R_{00}}{2B} + \frac{R_{11}}{2A} + \frac{R_{22}}{r^2} = \frac{2M'G}{r^2}, \quad (4.44)$$

the first MTOV equation is found to be

$$\frac{dM}{dr} = 4\pi\rho r^2 - \alpha r^2 \left(4\pi\rho h_R - \frac{1}{4G}(h_{RR}R - h) - \frac{1}{2AG} \left(\left(\frac{2}{r} - \frac{A'}{2A}\right)h'_R + h''_R\right)\right). \quad (4.45)$$

The second MTOV equation is derived by using eq. (4.41c), the conservation equation $\nabla_\mu T_\nu^{\text{matter}\mu} = 0$

$$\frac{B'}{B} = -\frac{2P'}{\rho + P}, \quad (4.46)$$

and the relation

$$\frac{R_{22}}{r^2} = \frac{G}{r^2} \left[\frac{dM}{dr} + \frac{M}{r} - \frac{r}{A} \left(\frac{B'}{B}\right) \right]. \quad (4.47)$$

This gives

$$\frac{dP}{dr} = -\frac{A}{r^2}(\rho + P) \left[MG + 4\pi G r^3 P - \alpha r^3 \left(\frac{1}{4}(h_{RR}R - h) + \frac{1}{2A} \left(\frac{2}{r} + \frac{B'}{2B}\right)h'_R + 4\pi G P h_R \right) \right]. \quad (4.48)$$

4.3.3 Neutron stars

The structure of neutron stars has been previously studied in $f(R)$ models of the form $f(R) \sim R + \alpha R^2$ [194–196] and the Starobinsky model [199] as well as in models incorporating $R^{\mu\nu} R_{\mu\nu}$ terms [181, 200] and the gravitational aether theory [201]. The modification to GR manifests itself in observable features such as the mass-radius (M-R) relation of neutron stars. To solve Eqs. (4.45) and (4.48) a third equation is needed to relate the matter density ρ and the pressure P i.e. the equation of state (EoS) of the neutron star. The EoS contains information about the behavior of the matter inside the star. As the properties of matter at high densities are not well known, there are different types of equation of state that give rise to different M-R relationships [174, 202]. Here, we consider two types of EoS: the simpler polytropic EoS and a more realistic SLy EoS [203].

4.3.3.1 Polytropic EoS

In this case we consider a simplified polytropic equation of state

$$\zeta = 2\xi + 5.0 , \quad (4.49)$$

where

$$\xi = \log(\rho/\text{g cm}^{-3}), \quad \zeta = \log(P/\text{dyn cm}^{-2}) . \quad (4.50)$$

The MTOV equations (4.45) and (4.48), together with (4.49), were then solved numerically, using a Fehlberg fourth-fifth order Runge-Kutta method to integrate from the center of star to the surface. We define the surface of the star as the point where the density drops to a value of order 10^9kg/m^3 . We use this value to define the surface (rather than $\rho = 0$) for numerical stability as the density and pressure drop precipitously near the surface of the neutron star. Moreover, this density corresponds to the boundary of the neutron star crust, and is thus the limit for the equations of states considered in the calculation, which describe nuclear matter at high densities (cf. [196]).

To obtain the M-R diagram for a given equation of state, one can solve the MTOV equations for stars with initial conditions (central densities) within a specified range. In the $f(R)$ model in hand, h_{RR} includes the $\ln(R^2/\mu^4)$ term, which is not well defined at $R = 0$. Thus, we restrict the calculation to the $R > 0$ domain i.e. we do not consider stars with a pressure high enough to give rise to negative curvature. The density at

i	$a_i(\text{SLy})$	i	$a_i(\text{SLy})$
1	6.22	10	11.4950
2	6.121	11	-22.775
3	0.005925	12	1.5707
4	6.48	14	14.08
6	11.4971	15	27.80
7	19.105	16	-1.653
8	0.8938	17	1.50
9	6.54	18	14.67

Table 4.2: Parameters of the SLy EoS model

the centre of the star is increased from ρ_{ns} ($\rho_{ns} = 2.7 \times 10^{17} \text{kg m}^{-3}$ is the nuclear saturation density) until the point where the Ricci scalar goes to zero. The numerical results for this case are shown in figure 4.4. In this case the deviation from GR can clearly be seen to increase for larger values of γ . For this type of equation of state it can also be seen that the deviation from GR becomes more asymmetric for negative and positive values of α as γ increases, and positive (negative) values of α give rise to lower (higher) mass stars for a given radius.

4.3.3.2 SLy EoS

The SLy equation of state models the behavior of nuclear matter at high densities . An explicit analytic representation is

$$\zeta = \frac{a_1 + a_2\xi + a_3\xi^3}{1 + a_4\xi} f_0(a_5(\xi - a_6)) + (a_7 + a_8\xi) f_0(a_9(a_{10} - \xi)) + (a_{11} + a_{12}\xi) f_0(a_{13}(a_{14} - \xi)) + (a_{15} + a_{16}\xi) f_0(a_{17}(a_{18} - \xi)) . \quad (4.51)$$

where ξ and ζ are defined as in (4.50) and

$$f_0(x) = \frac{1}{e^x + 1}. \quad (4.52)$$

The coefficients a_i are listed in table 4.2 [203].

The results are shown in Fig. 4.5. Here again the density at the center of star changes from ρ_{ns} to the point where the Ricci scalar goes to zero. As the SLy equation of state is stiff and $R \propto (\rho - 3P)$, when $\gamma \neq 0$ we do not obtain stars with a radius

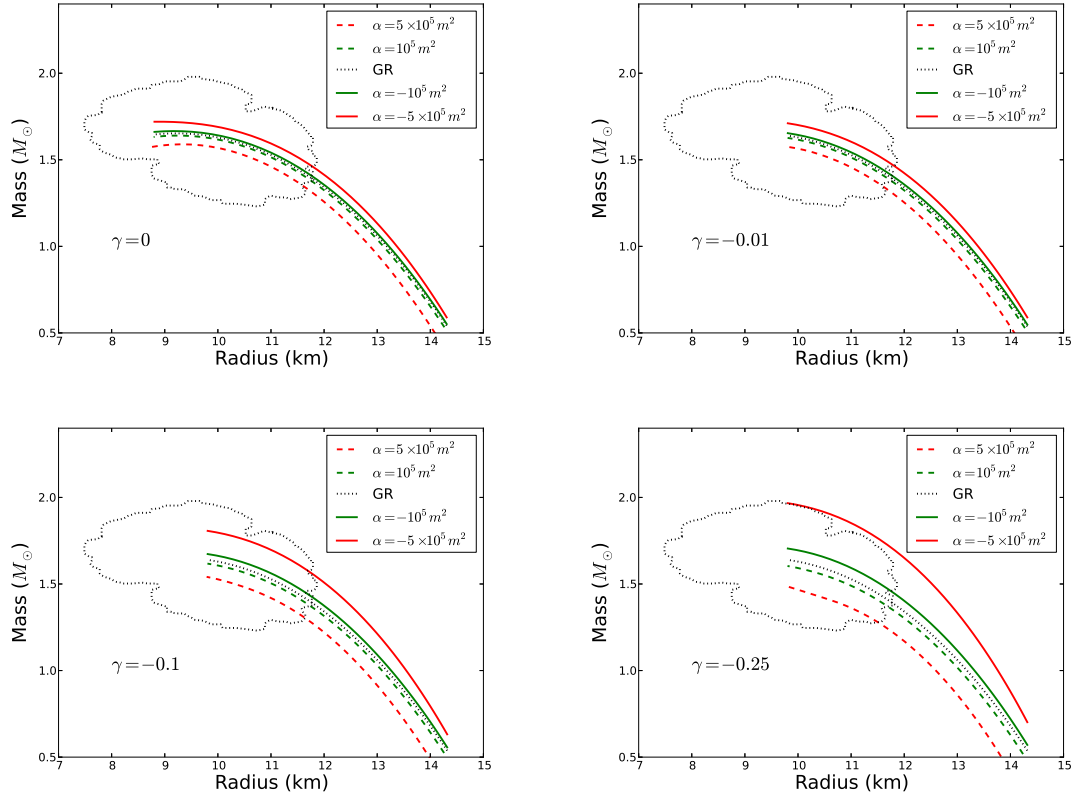


Figure 4.4: The mass-radius (M-R) diagram for neutron stars in GR ($\alpha = \beta = 0$) and $f(R) = R + \alpha R^2 + \frac{\beta}{2} R^2 \ln R^2 / \mu^4$ using a simplified polytropic equation of state (4.49). Here $\gamma \equiv \beta/\alpha$ and the range of the matter density at the center of the star is varied from ρ_{ns} to the point where the Ricci scalar goes to zero for the $\gamma \neq 0$ cases. $\rho_{ns} = 2.7 \times 10^{17} \text{kg m}^{-3}$ is the nuclear saturation density. The dotted contour gives the 2σ constraints derived from observations of three neutron stars reported in [204]. The presence of the logarithmic term ($\gamma \neq 0$) can be seen to cause larger deviations from the GR case compared to the R-squared model ($\gamma = 0$).

smaller than $r_s \sim 11\text{km}$, compared to $r_s < 10\text{km}$ for the R-squared model (left-top panel). The deviation from the GR case is most prominent where the central density (and thus the pressure) takes intermediate values such that R is large. At this point, which corresponds to extremely low-mass stars, an asymmetric deviation from GR that increases in magnitude with $|\gamma|$ can be seen, as with the polytropic equation of state. However, here it is the solutions corresponding to positive α that exhibit the greatest deviation from GR.

As in the $f(R) = R + \alpha R^2$ model [195, 196] there is an inversion of the modified gravity effect near the central density $\rho \simeq 5\rho_{ns}$ for the SLy equation of state. This point corresponds to stars with a mass $\sim 2M_\odot$; since this is close to the point where $R = 0$ (beyond which the logarithmic model is not valid) there is little deviation from the GR case for stars with astrophysical masses for this equation of state. If one were to use a softer equation of state (which permits a larger range of central densities) one would expect larger deviations from the GR case after this inversion point.

4.3.4 Binding energy

An important property of neutron stars that is often neglected in theoretical studies is the binding energy [205–207], which due to the extreme compactness of relativistic stars, can constitute a significant fraction of the mass of the star (as large as 25% [208]). This can be an important factor in models of binary evolution. The so-called baryonic mass¹ M_B necessarily exceeds the total mass of the star — the measurable quantity plotted in the M-R diagrams — as the latter includes both the rest-mass energy of its constituents and the negative binding energy. The baryonic mass is defined in terms of the volume element of the Schwarzschild metric (4.43) and the number density of particles $n(r)$ as [206]

$$M_B = 4\pi m_B \int_0^{r_s} n(r)[A(r)]^{1/2} r^2 dr, \quad (4.53)$$

where m_B is the mass of a baryon and r_s the surface radius of the star. In our case, since we do not consider mass transfer or accretion driven evolution, a more useful quantity is the proper mass

$$M_P = 4\pi \int_0^{r_s} \rho(r)[A(r)]^{1/2} r^2 dr, \quad (4.54)$$

¹ If the star were to be disassembled into its constituent baryons, M_B would be the total mass of the baryons.

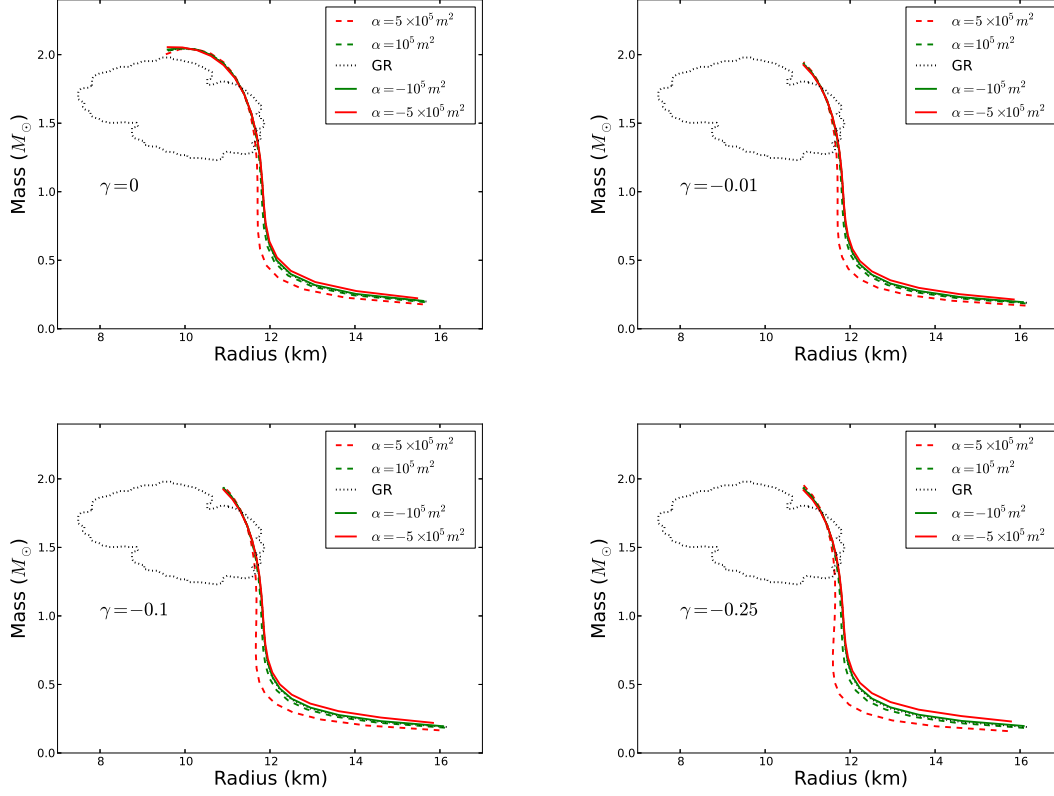


Figure 4.5: The mass-radius (M-R) diagram for neutron stars in GR ($\alpha = \beta = 0$) and $f(R) = R + \alpha R^2 + \frac{\beta}{2} R^2 \ln R^2 / \mu^4$ using the realistic SLy equation of state (4.51). Here $\gamma \equiv \beta/\alpha$ and the range of the matter density at the center of the star changes from ρ_{ns} to the point where the Ricci scalar goes to zero for the $\gamma \neq 0$ cases. $\rho_{ns} = 2.7 \times 10^{17} \text{kg m}^{-3}$ is the nuclear saturation density. The dotted contour gives the 2σ constraints derived from observations of three neutron stars reported in [204]. For larger values of γ , the presence of the logarithmic term can be seen to cause larger deviations from the GR case compared to the R-squared model ($\gamma = 0$). The deviation from the GR case is most prominent where the central density (and thus the pressure) takes intermediate values such that R is large.

given in terms of the mass density $\rho(r)$, which is related directly to the pressure by the equation of state [cf. (4.49) and (4.51)]. The mass density is related to the total mass M by

$$M = 4\pi \int_0^{r_s} \rho(r)r^2 dr. \quad (4.55)$$

In terms of this quantity we have the gravitational binding energy of the neutron star [207]

$$BE_G = (M_P - M)c^2, \quad (4.56)$$

which, following [207], we define as a positive quantity so that $M = M_P - BE_G/c^2$ (cf. [205]).

In figure 4.6 we calculate the gravitational binding energy using (4.56) in the framework of the $f(R)$ model for the polytropic and SLy equations of state. We find that the deviation of BE_G from the GR case follows the behaviour exhibited in the M-R diagrams in figures 4.4 and 4.5. In the polytropic case, where the simplified equation of state allows for significant deviations of the total mass M from the GR case, we see a decrease in the magnitude of BE_G for negative α and an increase for positive α corresponding to the increase and decrease respectively of the total mass. The size of the deviation increases with the magnitude of α , and very small values $< 0.8M_\odot$ (not relevant for astrophysical situations) can lead to a change in the sign of BE_G (i.e. positive gravitational binding energy) for large values of α . However, for realistic values of the total mass, this is not an issue. In the case of the more realistic SLy equation of state, the deviation from the GR case is almost negligible.

4.3.5 Quark stars

The concept of a star made of strange quark matter was first suggested by Itoh [170] and later expanded upon by Witten [171]. The unusual physical properties, such as the absence of a minimum mass and a finite density but zero pressure at their surface were later studied by Alcock et al. [172, 209]. In this model it is assumed that the star is made mostly of u, d, s quarks together with electrons, which give total charge neutrality. The interior of the star is made up of deconfined quarks that form a colour superconductor, leading to a softer equation of state with possible observable effects on the minimum mass, radii, cooling behaviour and other observables [173–175]. In this

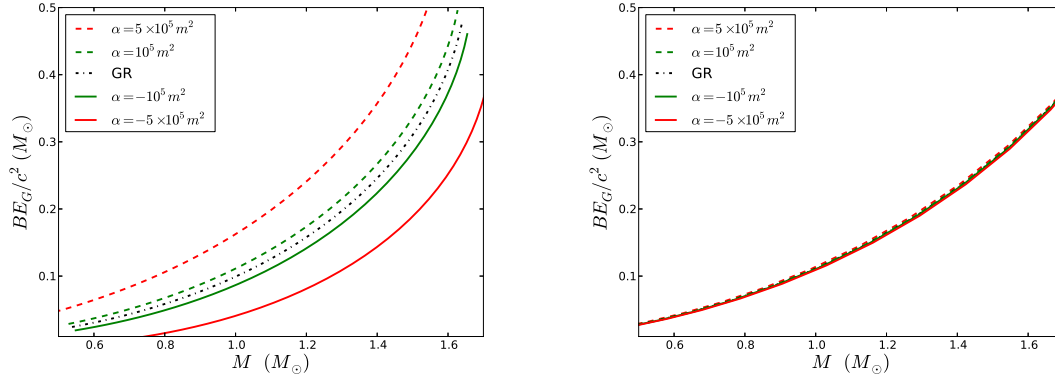


Figure 4.6: The gravitational binding energy BE_G [defined in (4.56)] as a function of the total mass M for the polytropic (left-panel) and SLy (right-panel) equations of state in the logarithmic $f(R)$ model. In each case, the value of γ is taken to be $\gamma = -0.1$.

subsection we investigate the effect of the modified gravity on the structure of this type of self-bound star.

The equation of state of strange matter made up of u,d, s quarks can be considered in the framework of the MIT bag model. In this model, a linear approximation is assumed as [210]

$$P \simeq a(\rho - \rho_0) , \quad (4.57)$$

where ρ_0 is the density of the strange matter at zero pressure. The MIT bag model describing the strange quark matter involves three parameters, viz. The bag constant $\mathcal{B} = \rho_0/4$, the strange quark mass m_s and the QCD coupling constant α_c . If we neglect the strange quark mass, then $a = 1/3$. For $m_s = 250$ MeV we have $a = 0.28$. In units of $\mathcal{B}_{60} = \mathcal{B}/(60\text{Mev fm}^{-3})$, the constant \mathcal{B} is restricted to $0.98 < \mathcal{B} < 1.52$ [210]. The M-R diagram for a quark star with $a = 0.28$ and $\mathcal{B} = 1$ is shown in Fig. 4.7. From this figure it is clear that the masses of quark stars with negative values of α are always enhanced with respect to GR and the masses of quark stars with positive values of α are diminished relative to GR, irrespective of the value of γ . Compared to the SLy and polytropic equations of state, larger values of α [i.e. $\alpha = \mathcal{O}(10^7 m^2)$] can give rise to stars with masses and radii in the ranges allowed by the observational constraints. As in the previous subsection, it can be seen that the deviation is larger for larger values of $|\gamma|$. In the case of the quark star, however, the equation of state is less stiff so there is more deviation in the mass-radius diagram with respect to GR.

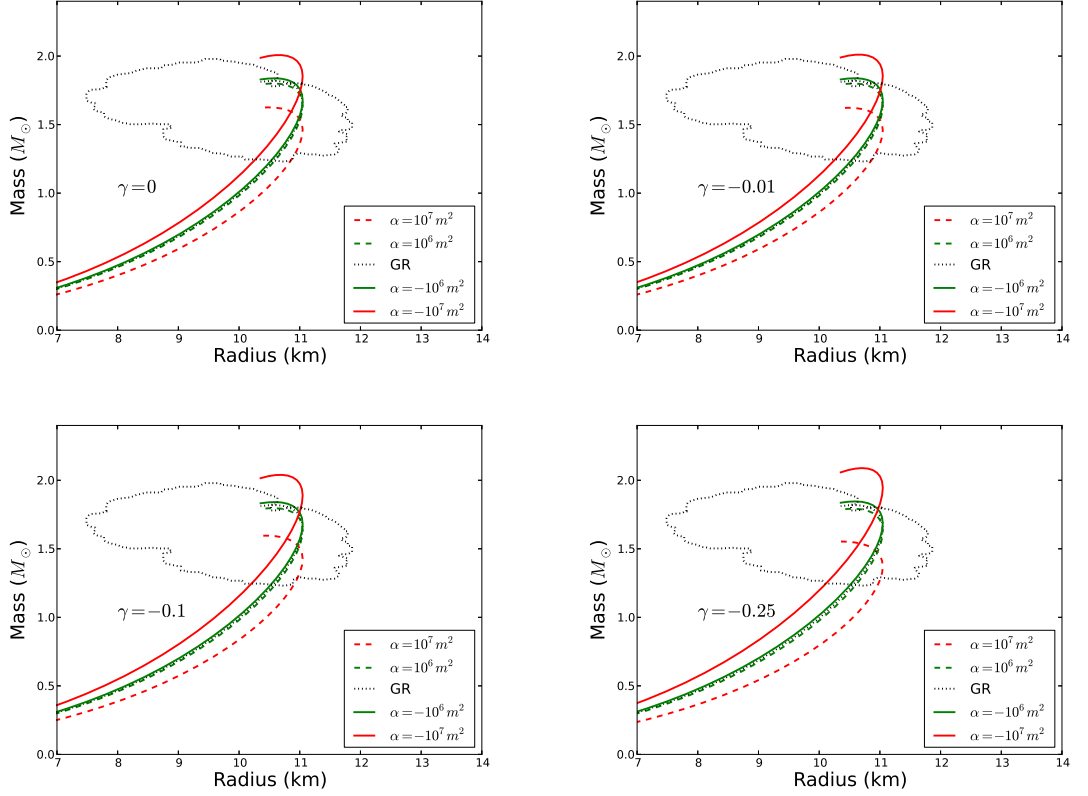


Figure 4.7: The mass-radius (M-R) diagram for the quark star case in GR and $f(R) = R + \alpha R^2 + \frac{\beta}{2} R^2 \ln R^2 / \mu^4$ using a linear equation of state (4.57) with $a = 0.28$ and $\mathcal{B} = 1$. Here $\gamma \equiv \beta/\alpha$ and the range of the matter density at the center of the star changes from $1.54\rho_{ns}$ to $9.3\rho_{ns}$, where $\rho_{ns} = 2.7 \times 10^{17} \text{kg m}^{-3}$ is the nuclear saturation density. The dotted contour gives the 2σ constraints derived from observations of three neutron stars reported in [204].

4.3.6 Perturbative regime

In all considered cases, it is important to stay in the perturbative regime, so that the first order corrections to the metric in (4.39) are small. This can be measured quantitatively with

$$|\Delta| = \left| \frac{A_{MG}(r)}{A_{GR}(r)} - 1 \right|, \quad (4.58)$$

where $A(r)$ is the rr component of the metric defined in eq. (4.43) and the subscripts MG and GR refer to the modified gravity and General Relativity cases respectively.

This quantity varies as a function of radius for each star, and also depends on the corresponding central density. In Fig. 4.8, we have plotted the quantity $|\Delta_{max}|$ as a function of $\alpha_5 = \alpha/10^5$ (where the subscript max refers to the maximum value for a given choice of parameters) for the SLy, polytropic and quark star equations of state.

A necessary condition for the validity of the perturbative approach is $|\Delta_{max}| < 1$. The plots for the SLy and polytropic equations of state (left and middle) show that the $f(R) = R + \alpha R^2 + \frac{\beta}{2} R^2 \ln R^2 / \mu^4$ model can be treated perturbatively for $|\alpha| \lesssim 10^6$. The dependence of $|\Delta_{max}|$ on α is linear, with the slope depending on the value of γ . Including a small logarithmic term ($\gamma = -0.01$) decreases $|\Delta_{max}|$, however, increasing γ further leads to larger deviations from GR and thus larger values of $|\Delta_{max}|$. As mentioned above, in the quark star case, we can reach larger values of α respect to neutron stars while remaining in the the perturbative regime.

4.4 Summary

In this chapter we have considered the effect of a logarithmic $f(R)$ theory, $f(R) = R + \alpha R^2 + \frac{\beta}{2} R^2 \ln R^2 / \mu^4$, motivated by the form of the one-loop effective action arising from gluons in curved spacetime, on the structure of relativistic stars. Unlike many $f(R)$ theories in the literature, the modifications to General Relativity are significant in the strong-field regime, which is less well constrained by observations. Considering the motivation, we treat the model as an effective theory, valid in the interior and near vicinity of neutron stars, where QCD effects play an important role.

An $f(R)$ theory inevitably introduces a scalar degree of freedom, and in section 4.2.1 we have derived the constraints imposed upon the parameters of the model due to stability and internal consistency requirements. Unlike the related $R + \alpha R^2$ model, we

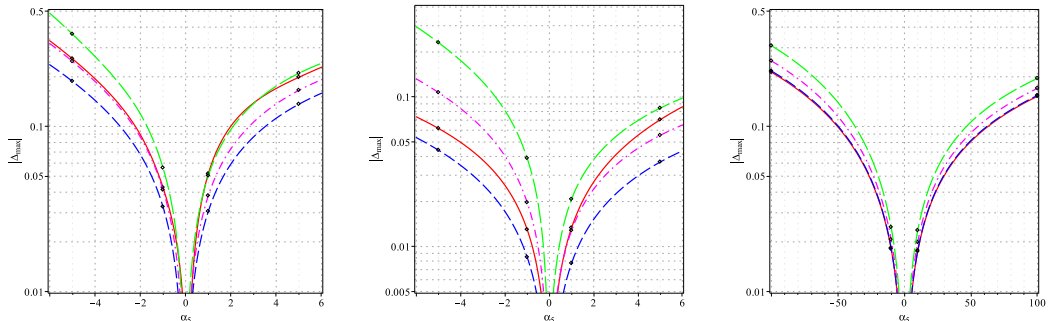


Figure 4.8: The parameter $|\Delta_{\max}| = |A_{MG}(r)/A_{GR}(r) - 1|_{\max}$ as a function of $\alpha_5 = \alpha/10^5$ for the SLy equation of state (left), polytropic equation of state (middle) and quark star (right) in the MG2 model. The red (solid), blue (short-dashed), magenta (dot-dashed), green (long-dashed) lines indicate the $\gamma = 0, -0.01, -0.1, -0.25$ cases respectively. A necessary condition for the validity of the perturbative approach is $|\Delta_{\max}| < 1$. The circles indicate the parameter values used in Figs. 4.4, 4.5 and 4.7.

find that, when the logarithmic term is a subdominant correction — i.e. $|\gamma| = |\beta/\alpha| \ll 1$, which we assume throughout this work — one can consider positive and negative values of α . In addition, in the absence of matter, the existence of a stable minimum at $R = 0$ forces us to work with negative values of the coefficient of the logarithmic term β .

In section 4.2.2, we have also considered the constraints imposed upon the model by observations; in particular relating to the possibility of a fifth force due to the scalar degree of freedom. Since we treat the model as an effective theory valid only in the vicinity of ultra-dense matter, we do not need to contend with cosmological or terrestrial constraints, however, it is important to consider the effect of the modification on binary pulsars and direct observations of neutron stars. Transforming the theory to the Einstein frame, we have shown that the model exhibits a chameleon effect, completely suppressing the effect of the modification on scales exceeding a few radii, so that any effect on the orbital motion of a binary system is completely negligible. We showed that this model satisfies the binary star observations of the effective gravitational constant for a wide range of parameters α and γ .

On smaller scales, near the surface of the neutron star, the deviation from General Relativity can be significant. Observations of bursting neutron stars depend strongly on the surface redshift z_s , which determines the shift in absorption (or emission) lines due

to elements in the atmosphere, as well as the Eddington critical luminosity. In figure 4.3 we have plotted the dependence of z_s on the radial coordinate in the immediate vicinity of the neutron star surface (which is directly related to the observable quantity $\delta\lambda/\lambda = z_s$) showing that there are strong α -dependent deviations from General Relativity, which could in principle be detected, utilising data from future X-ray missions.

In section 4.3, we have used the method of perturbative constraints to derive and solve the modified Tolman-Oppenheimer-Volkov equations for neutron and quark stars. The changes to the mass-radius diagram for neutron stars are shown in figure 4.4 for a toy polytropic equation of state and in figure 4.5 for a realistic SLy equation of state. As in the $f(R) = R + \alpha R^2$ model [195, 196] there is an inversion of the modified gravity effect near the central density $\rho \simeq 5\rho_{ns}$ for the SLy equation of state. For the SLy equation of state, the deviation from GR is more evident for smaller central densities (corresponding to the lower-right of the plots in figure 4.5). However, in the polytropic case, for higher central densities (top-left part of the plots in figure 4.4) one can observe a larger deviation from GR with respect to lower central densities (bottom-right on the plots). In addition, in the polytropic case, the deviation from GR is much larger than the SLy case for equal values of the parameter α . For the polytropic equation of state, the asymmetry in the M-R diagram for positive and negative values of parameter α is also reduced. In this section, we have also calculated the gravitational binding energy of the neutron stars for each equation of state.

As has been noted in the case of other $f(R)$ models, there is a degeneracy with the choice of equation of state that is largely unconstrained. To break this degeneracy, one could consider other observables, such as those relating to the cooling [211] or spin properties [212] of the neutron stars. In particular, it was suggested in [194] that since cooling by neutron emission — which is the dominant cooling mechanism for young ($\lesssim 10^4 - 10^6$ years) neutron stars — is particularly sensitive to the central density of the star, measurements of the surface temperature could offer a discriminant. However, in practice, the neutrino cooling rate is difficult to model due to the strong dependence on features such as condensates in the star's composition.

We find that the range of the parameter $\alpha \lesssim 10^6 \text{m}^2$ that is consistent with the perturbative treatment in our model for the SLy and polytropic equations of state is comparable with that in related works, where $\alpha < 10^9 \text{cm}^2$ [195, 197], $\alpha \lesssim 10^5 \text{m}^2$ [196].

In the quark star case, one can reach larger values of $\alpha \sim 10^7 \text{m}^2$ while remaining in the perturbative regime.

Finally, in section 4.3.5, we have considered the case of self-bound stars, consisting of strange quark matter. We found that the M - R diagram and internal density distribution were insensitive to the presence of the logarithmic term, and for positive α the mass is always enhanced relative to that calculated using General Relativity.

As the modified Tolman-Oppenheimer-Volkov equations for the $f(R)$ model considered here involve $\ln(R^2/\mu^4)$ terms that are not well defined at $R = 0$ we have restricted our analysis to the $R > 0$ domain. Since neutron star equations of state are stiff and $R \propto (\rho - 3P)$, when $\gamma \neq 0$ we cannot consider central densities above a maximum value. This is particularly evident in figure 4.5, as the largest deviations from GR occur for stars with low masses, corresponding to a medium central density. Using an equation of state that is less stiff for large densities would give rise to more significant deviations for larger mass stars. This can be seen in the quark star case.

To conclude, we have shown that considering the finite logarithmic terms arising in the calculation of the effective action for a gauge field in a phenomenological $f(R)$ framework leads to interesting observational consequences differing from the predictions of General Relativity. To make this connection more definite is beyond the scope of this Thesis, although as observational data improve, one can entertain the possibility that neutron star systems may in the future have a role to play in analysing the predictions of quantum field theory in curved spacetime.

5

Concluding remarks

In this Thesis we considered two QCD-scale $f(R)$ theories of gravity, one modifying General Relativity in the small curvature limit (MG1) and another in the high-curvature limit (MG2). The motivation for modifying such a successful physical theory on large-scales (small curvatures) stems from observations of the accelerating expansion of the universe, which forces physicists to address the cosmological constant problem. q -theory has been proposed as a solution to the main cosmological constant problem, one realization of which can utilize elements of known physics. QCD has a nontrivial vacuum structure that allows for the formation of condensates that can play the role of conserved charges in the q -theory framework. One advantage of this proposal is that the model provides a framework for the dynamics of dark energy without introducing new physics in an ad hoc manner.

The second model (MG2) we considered takes its motivation from the treatment of the gauge fields (gluons) in QCD in a curved spacetime background relevant for high-density environments. The resulting $f(R)$ theory induces corrections to General Relativity, not in recent cosmological situations, but instead in high-curvature environments such as neutron stars where GR has not been extensively tested. Although both of the models considered in the Thesis are phenomenological in nature, the motivation behind exploring both the high-energy and low-energy regimes is that testing the limits of the standard theory can reveal information relevant for a final theory of quantum gravity.

Following introductory material in chapters 1 and 2, we considered in chapter 3 a low-energy modified $f(R)$ model: the squared-root QCD-scale modified-gravity model

(MG1). We analyzed its phenomenology on large and local scales using cosmological data and local tests of gravity, finding that this model can explain the late time dynamics of the Universe very well. However, on local scales this model cannot satisfy local gravity tests and one needs to use a local version of the theory with additional degrees of freedom.

$f(R)$ theories, like all dark energy models, can give rise to differences in structure formation, compared to the standard Λ CDM model. We showed that the modifications to gravity enhance and diminish the Newtonian potential Ψ and the curvature potential Φ respectively compared to Λ CDM. The enhancement of the former causes the amplification of the growth of matter density perturbations. We calculated the evolution of the gravity estimator E_G (which acts as a discriminant between Λ CDM and modified gravity) and found its value to be constrained with current constraints.

In order to do a detailed comparison with the available cosmological data, in section 3.3 we performed a Markov chain Monte Carlo simulation to obtain the constraints on the cosmological parameters in the MG1 model. We found the best fit values for the main cosmological parameters to be comparable to those in Λ CDM, with dark energy density $\Omega_{\text{DE}} = 0.7245$, dark matter physical density $\Omega_c h^2 = 0.1152$, the baryon matter physical density $\Omega_b h^2 = 0.0223$ and the present value of the Hubble parameter $H_0 = 70.6610$. In addition we used the cosmological data to constrain the value of the gluon condensate q . The best fit value (2σ CL) for the parameter $\beta_q = q_0/q$ was found to be $1.0288^{+0.9989}_{-0.7510}$, where $q_0 = (300 \text{ MeV})^4$, which is of the order of the previous values obtained in theoretical works. To further improve the constraints on the value of this parameter, one could include weakly or fully nonlinear scales [153, 154] in the analysis. To tighten the constraints on this fundamental parameter, an interesting direction for future work would be to make use of constraints arising from the most massive halos inferred from SDSS data and also the galaxy-galaxy lensing signals. [155].

To test this model on local scales we used the chameleon mechanism. We found that this model cannot satisfy the laboratory tests of gravity as the measured effective gravitational coupling constant is too large on local scales i.e. $G_{\text{eff}} \simeq 1.33G_N$. This model cannot satisfy the constraints from fifth force searches as well as its scalar degree of freedom has a large interaction distance, which would be detectable in the laboratory. On the scales of order of the solar system, the celestial bodies in the framework of this model exhibit the thick-shell effect in contradictory to the solar system tests of gravity.

To attempt to address this problem, a local version of the MG1 model was considered, with an additional parameter. We showed that for appropriate choices of the model parameters, this model can satisfy the laboratory and solar system tests easily, however, as it cannot match the observed energy density of the dark energy, this model cannot describe the large scale dynamics of the universe.

In chapter 4 we considered another modified theory (MG2). We investigated the effect of a logarithmic $f(R)$ theory, $f(R) = R + \alpha R^2 + \frac{\beta}{2} R^2 \ln(R^2/\mu^4)$, motivated by the form of the one-loop effective action arising from gluons in curved spacetime, on the structure of relativistic stars. Unlike many $f(R)$ theories in the literature, the modifications to General Relativity are significant in the strong-field regime, which is less well constrained by observations. Considering the motivation, we treat the model as an effective theory, valid in the interior and near vicinity of neutron stars, where QCD effects play an important role.

We derived the constraints imposed upon the parameters of the model due to stability and internal consistency requirements, as well as those imposed upon the model by observations; in particular relating to the possibility of a fifth force due to the scalar degree of freedom. Transforming the theory to the Einstein frame, we showed that the model exhibits a chameleon effect, completely suppressing the effect of the modification on scales exceeding a few radii, so that any effect on the orbital motion of a binary system is completely negligible. We showed that this model satisfies the binary star observations of the effective gravitational constant for a wide range of parameters α and β .

On smaller scales, near the surface of the neutron star, the deviation from General Relativity can be significant. Observations of bursting neutron stars depend strongly on the surface redshift z_s , which determines the shift in absorption (or emission) lines due to elements in the atmosphere, as well as the Eddington critical luminosity. We found that there are strong α -dependent deviations from General Relativity, which could in principle be detected, utilising data from future X-ray missions. We also used the method of perturbative constraints to derive and solve the modified Tolman-Oppenheimer-Volkov equations for neutron and quark stars and calculated the range of validity of the perturbative treatment as a function of the parameters α and β . We showed that the model exhibits deviations from General Relativity in the mass-radius diagram for the relativistic stars, which are in principle measurable, although

the precise form is strongly dependent on the equation of state of the star. In the case of self-bound stars, consisting of strange quark matter, we found that the M - R diagram and internal density distribution were insensitive to the presence of the logarithmic term, and for positive α the mass is always enhanced relative to that calculated using General Relativity.

To break the degeneracy between the equation of state and the effect of modified gravity, one could consider other observables, such as those relating to the cooling or spin properties of the neutron stars. In particular, it was suggested in [194] that since cooling by neutron emission — which is the dominant cooling mechanism for young ($\lesssim 10^4 - 10^6$ years) neutron stars — is particularly sensitive to the central density of the star, measurements of the surface temperature could offer a discriminant. However, in practice, the neutrino cooling rate is difficult to model due to the strong dependence on features such as condensates in the star's composition.

In this Thesis we concentrated on phenomenological modifications to the General Theory of Relativity, motivated by the physics of the strong nuclear force. As we showed, a wide range of tests of the gravitational interaction exist in both the high and low curvature regimes that can be used to place strict constraints on the parameters of prospective models. Although gravity and QCD are normally studied in isolation, the possibility of a relationship between the two would open up an exciting new perspective on the physical world. In this Thesis we demonstrated that phenomenological QCD-scale $f(R)$ models can result in observable phenomena differing from the standard case.

Appendices

Appendix A

Data fitting method

In this appendix we discuss the data fitting method in the Markov Chain Monte Carlo (MCMC) simulation to estimate the parameters of the QCD-scale modified-gravity model in section 3.3 using cosmological data.

To get the best fit values of the relevant parameters, the maximum likelihood method is used. The total likelihood function $\mathcal{L}_{\text{total}} = e^{-\chi_{\text{tot}}^2/2}$ is defined as the product of the separate likelihood functions of uncorrelated observational data with

$$\chi_{\text{tot}}^2 = \chi_{\text{SNIa}}^2 + \chi_{\text{CMB}}^2 + \chi_{\text{BAO}}^2 + \chi_{\text{gas}}^2, \quad (\text{A.1})$$

where SNIa stands for type Ia supernovae, CMB for cosmic microwave background radiation, BAO for baryon acoustic oscillation and *gas* stands for X-ray gas mass fraction data. Best fit values of parameters are obtained by minimizing χ_{tot}^2 . In this thesis we use the cosmic microwave background radiation data from seven-year WMAP [144], type Ia supernovae data from 557 Union2 [145], baryon acoustic oscillation data from SDSS DR7 [146], and the cluster X-ray gas mass fraction data from the Chandra X-ray observations [147]. In following section we discuss each χ_i^2 in detail.

A.1 Cosmic microwave background

To obtain χ_{CMB}^2 , we use seven-year WMAP data [144] with the CMB data point (R, l_A, z_*) . The shift parameter R , which parametrizes the changes in the amplitude of the acoustic peaks is given by [213]

$$R = \sqrt{\frac{\Omega_{m0}}{c}} \int_0^{z_*} \frac{dz'}{E(z')}, \quad (\text{A.2})$$

where z_* is the redshift of recombination (see (A.7)), c is the speed of light in vacuum, $\Omega_{\text{m}0}$ is the present value of the matter density parameter, and $E(z) \equiv H(z)/H_0$. In addition, the acoustic scale l_{A} , which characterizes the changes of the peaks of CMB via the angular diameter distance out to recombination is defined as [213]

$$l_{\text{A}} = \frac{\pi r(z_*)}{r_{\text{s}}(z_*)}. \quad (\text{A.3})$$

The comoving distance $r(z)$ is defined

$$r(z) = \frac{c}{H_0} \int_0^z \frac{dz'}{E(z')}, \quad (\text{A.4})$$

and the comoving sound horizon distance at recombination $r_{\text{s}}(z_*)$ is given by

$$r_{\text{s}}(z_*) = \int_0^{a(z_*)} \frac{c_{\text{s}}(a)}{a^2 H(a)} da, \quad (\text{A.5})$$

in terms of the sound speed $c_{\text{s}}(a)$, defined by

$$c_{\text{s}}(a) = \left[3 \left(1 + \frac{3\Omega_{\text{b}0}}{4\Omega\gamma_0} a \right) \right]^{-1/2}. \quad (\text{A.6})$$

The seven-year WMAP observations gives $\Omega_{\gamma_0} = 2.469 \times 10^{-5} h^{-2}$ and $\Omega_{\text{b}0} = 0.02258_{-0.00056}^{+0.00057}$ [144].

The redshift of recombination z_* is obtained by using the fitting function proposed by Hu and Sugiyama [214]

$$z_* = 1048 [1 + 0.00124(\Omega_{\text{b}0} h^2)^{-0.738}] [1 + g_1(\Omega_{\text{m}0} h^2)^{g_2}], \quad (\text{A.7})$$

where

$$g_1 = \frac{0.0783(\Omega_{\text{b}0} h^2)^{-0.238}}{1 + 39.5(\Omega_{\text{b}0} h^2)^{0.763}}, \quad g_2 = \frac{0.560}{1 + 21.1(\Omega_{\text{b}0} h^2)^{1.81}}. \quad (\text{A.8})$$

Then one can define χ_{CMB}^2 as $\chi_{\text{CMB}}^2 = X^T C_{\text{CMB}}^{-1} X$, with [144]

$$X = \begin{pmatrix} l_{\text{A}} - 302.09 \\ R - 1.725 \\ z_* - 1091.3 \end{pmatrix}, \quad (\text{A.9a})$$

$$C_{\text{CMB}}^{-1} = \begin{pmatrix} 2.305 & 29.698 & -1.333 \\ 293689 & 6825.270 & -113.180 \\ -1.333 & -113.180 & 3.414 \end{pmatrix}, \quad (\text{A.9b})$$

where C_{CMB}^{-1} is the inverse covariant matrix.

A.2 Type Ia supernovae data

To obtain χ_{SNIa}^2 , the SNIa Union2 data [145] is used which includes 577 type Ia supernovae. The expansion history of the universe $H(z)$ can be given by a specific cosmological model. To test this model, we can use the observational data for some predictable cosmological parameter such as luminosity distance d_L . Assume that the Hubble parameter $H(z; \alpha_1, \dots, \alpha_n)$ is used to describe the Universe, where parameters $(\alpha_1, \dots, \alpha_n)$ are predicted by a theoretical cosmological model. For such a theoretical model we can predict the theoretical 'Hubble-constant free' luminosity distance as

$$\begin{aligned} D_L^{\text{th}} = H_0 \frac{d_L}{c} &= (1+z) \int_0^z \frac{dz'}{E(z'; \alpha_z, \dots, \alpha_n)} \\ &= H_0 \frac{1+z}{\sqrt{|\Omega_k|}} \text{sinn} \left[\sqrt{|\Omega_k|} \int_0^z \frac{dz'}{H(z'; \alpha_z, \dots, \alpha_n)} \right], \end{aligned} \quad (\text{A.10})$$

where $E \equiv H/H_0$, z is the redshift parameter, and

$$\text{sinn}(\sqrt{|\Omega_k|}x) = \begin{cases} \sin(\sqrt{|\Omega_k|}x) & \text{for } \Omega_k < 0 \\ \sqrt{|\Omega_k|}x & \text{for } \Omega_k = 0 \\ \sinh(\sqrt{|\Omega_k|}x) & \text{for } \Omega_k > 0. \end{cases}$$

Then one can write the theoretical modulus distance

$$\mu_{\text{th}}(z) = 5 \log_{10}[D_L^{\text{th}}(z)] + \mu_0, \quad (\text{A.11})$$

where $\mu_0 = 5 \log_{10}(cH_0^{-1}/Mpc) + 25$. On the other hand, the observational modulus distance of SNIa, $\mu_{\text{obs}}(z_i)$, at redshift z_i is given by

$$\mu_{\text{obs}}(z_i) = m_{\text{obs}}(z_i) - M, \quad (\text{A.12})$$

where m and M are apparent and absolute magnitudes of SNIa respectively. Then the parameters of the theoretical model, α_i s, can be determined by a likelihood analysis by defining $\bar{\chi}_{\text{SNIa}}^2(\alpha_i, M')$ in Eq. (A.1) as

$$\begin{aligned} \bar{\chi}_{\text{SNIa}}^2(\alpha_i, M') &\equiv \sum_j \frac{(\mu_{\text{obs}}(z_j) - \mu_{\text{th}}(\alpha_i, z_j))^2}{\sigma_j^2} \\ &= \sum_j \frac{(5 \log_{10}[D_L(\alpha_i, z_j)] - m_{\text{obs}}(z_j) + M')^2}{\sigma_j^2}, \end{aligned} \quad (\text{A.13})$$

where the nuisance parameter, $M' = \mu_0 + M$, can be marginalized over as

$$\chi_{\text{SNIa}}^2(\alpha_i) = -2 \ln \int_{-\infty}^{+\infty} dM' \exp[-\frac{1}{2} \bar{\chi}_{\text{SNIa}}^2(\alpha_i, M')]. \quad (\text{A.14})$$

A.3 Baryon acoustic oscillation

The baryon acoustic oscillation data from the Sloan Digital Sky Survey (SDSS) Data Release 7 (DR7) [146] is used here for constraining model parameters. The data constrain parameter $d_z \equiv r_s(z_d)/D_V(z)$, where $r_s(z_d)$ is the comoving sound horizon distance (see (A.5)) at the drag epoch (where baryons were released from photons) and D_V is given by [215]

$$D_V(z) \equiv \left[c \left(\int_0^z \frac{dz'}{H(z')} \right)^2 \frac{z}{H(z)} \right]^{1/3}. \quad (\text{A.15})$$

The drag redshift is given by the fitting formula [216]

$$z_d = \frac{1291(\Omega_{m0}h^2)^{0.251}}{1 + 0.659(\Omega_{m0}h^2)^{0.828}} \left[1 + b_1(\Omega_{b0}h^2)^{b_2} \right], \quad (\text{A.16})$$

where

$$\begin{aligned} b_1 &= 0.313(\Omega_{m0}h^2)^{-0.419} [1 + 0.607(\Omega_{m0}h^2)^{0.607}], \\ b_2 &= 0.238(\Omega_{m0}h^2)^{0.223}. \end{aligned} \quad (\text{A.17})$$

Then we can obtain χ_{BAO}^2 by $\chi_{\text{BAO}}^2 = Y^T C_{\text{BAO}}^{-1} Y$, where

$$Y = \begin{pmatrix} d_{0.2} - 0.1905 \\ d_{0.35} - 0.1097 \end{pmatrix}, \quad (\text{A.18})$$

and its covariance matrix is given by [146]

$$C_{\text{BAO}}^{-1} = \begin{pmatrix} 30124 & -17227 \\ -17227 & 86977 \end{pmatrix}. \quad (\text{A.19})$$

A.4 X-Ray gas mass fraction

The ratio of X-ray gas mass to the total mass of a cluster is defined as the X-ray gas mass fraction [147]. The model fitted to the Λ CDM model is [147]

$$f_{\text{gas}}^{\Lambda\text{CDM}}(z) = \frac{KA\gamma b(z)}{1 + s(z)} \left(\frac{\Omega_b}{\Omega_{m0}} \right) \left(\frac{D_A^{\Lambda\text{CDM}}(z)}{D_A(z)} \right)^{1.5}. \quad (\text{A.20})$$

The elements in Eq. (A.20) are defined as follows: $D_A^{\Lambda\text{CDM}}(z)$ and $D_A(z)$ are the proper angular diameter distance in Λ CDM and the alternative theoretical model respectively, where

$$D_A(z) = \frac{c}{(1+z)\sqrt{|\Omega_k|}} \text{sinn} \left[\sqrt{|\Omega_k|} \int_0^z \frac{dz'}{H(z')} \right]. \quad (\text{A.21})$$

The angular correction factor A

$$A = \left(\frac{\theta_{2500}^{\Lambda CDM}}{\theta_{2500}} \right)^\eta \approx \left(\frac{H(z)D_A(z)}{[H(z)D_A(z)]^{\Lambda CDM}} \right)^\eta, \quad (\text{A.22})$$

is caused by changes in angle for the alternative theoretical model θ_{2500} compared to $\theta_{2500}^{\Lambda CDM}$, where $\eta = 0.214 \pm 0.022$ [147] is the slope of the $f_{\text{gas}}(r/r_{2500})$ data within the radius r_{2500} (r_{2500} is the radius of the gas core in Mpc/h units).

The bias factor $b(z)$ in Eq. (A.20) contains information about the uncertainties in the cluster depletion factor $b(z) = b_0(1 + \alpha_b z)$ and the parameter γ accounts for departures from the hydrostatic equilibrium. The function $s(z) = s_0(1 + \alpha_s z)$ denotes the uncertainties of the baryonic mass fraction in stars with a Gaussian prior for s_0 , with $s_0 = (0.16 \pm 0.05)h_{70}^{0.5}$ [147]. The factor K describes the combined effects of the residual uncertainties, such as the instrumental calibration. A Gaussian prior for the 'calibration' factor is considered as $K = 1.0 \pm 0.1$ [147].

Then χ_{gas}^2 is defined as [147]

$$\chi_{\text{gas}}^2 = \sum_i^N \frac{[f_{\text{gas}}^{\Lambda CDM}(z_i) - f_{\text{gas}}(z_i)]^2}{\sigma_{f_{\text{gas}}}^2(z_i)} + \frac{(s_0 - 0.16)^2}{0.0016^2} + \frac{(K - 1.0)^2}{0.01^2} + \frac{(\eta - 0.214)^2}{0.022^2}, \quad (\text{A.23})$$

with the statistical uncertainties $\sigma_{f_{\text{gas}}}(z_i)$.

Appendix B

Chameleon-field solutions

In this appendix we will present the chameleon-field solutions in the case of a spherically symmetric object. We follow the treatment in [112].

For a spherically symmetric test body eq. (2.15) yields

$$\frac{d^2\phi}{dr^2} + \frac{2}{r} \frac{d\phi}{dr} = \frac{dV_{\text{eff}}}{d\phi} = V_{,\phi} + \frac{Q}{M_{\text{Pl}}} \rho e^{Q\phi/M_{\text{Pl}}} . \quad (\text{B.1})$$

We consider the following boundary conditions to solve field equation (B.1) [10]

$$\frac{d\phi}{dr}(r=0) = 0 , \quad (\text{B.2a})$$

$$\phi(r \rightarrow \infty) = \phi_b . \quad (\text{B.2b})$$

Eq. (B.2a) guarantees that the chameleon-field is non-singular at $r = 0$ and the second condition (B.2b) asserts that the fifth force vanishes at infinity.

Consider a sphere with matter density ρ_c with mass $M_c = (4\pi/3)\rho_c R_c^3$, where R_c is the radius of the body. We assume that this sphere is immersed in an environment with density ρ_b . We define the following quantities for later use

$$\begin{aligned} \phi_c &\equiv \phi_{\text{min}} \Big|_{\rho=\rho_c} , & \phi_b &\equiv \phi_{\text{min}} \Big|_{\rho=\rho_b} , \\ m_c &\equiv m_{\text{min}}(\phi_c) , & m_b &\equiv m_{\text{min}}(\phi_b) , \end{aligned} \quad (\text{B.3})$$

where ϕ_{min} and $m(\phi)$ are defined in equations (2.17) and (2.18). In the following, we discuss the solution of the field equation (B.1).

As a first approximation, we assume that $V_{\text{eff},\phi}$ can be approximated with a harmonic oscillator in $r > R_c$ (where $\phi \simeq \phi_b$) so that

$$\frac{d^2\phi}{dr^2} + \frac{2}{r} \frac{d\phi}{dr} = m_b^2(\phi - \phi_b) . \quad (\text{B.4})$$

The solution of the field equation (B.4) can be written

$$\phi(r) = A \frac{e^{-m_b(r-R_c)}}{r} + B \frac{e^{m_b(r-R_c)}}{r} + \phi_b, \quad (\text{B.5})$$

with two dimensionless constants A and B . By imposing the boundary condition (B.2b) we get $B = 0$. Therefore, the solution for the external regions of the test body have the form

$$\phi(r) = A \frac{e^{-m_b(r-R_c)}}{r} + \phi_b. \quad (\text{B.6})$$

To investigate the interior solutions $r < R_c$, we divide the interior region into two different regions: from $r = 0$ to R_1 (where $\phi \simeq \phi_c$), and from $r = R_1$ to $r = R_c$ (where $\phi \gg \phi_c$). When $\phi \gg \phi_c$, the second term in the effective potential dominates and so

$$V_{\text{eff},\phi} \approx \frac{Q}{M_{\text{Pl}}} \rho_c. \quad (\text{B.7})$$

We can then rewrite equation (B.1) as

$$\frac{d^2\phi}{dr^2} + \frac{2}{r} \frac{d\phi}{dr} \approx \frac{Q}{M_{\text{Pl}}} \rho_c. \quad (\text{B.8})$$

The solution of eq. (B.8) is

$$\phi(r) = \frac{Q}{6M_{\text{Pl}}} \rho_c r^2 + \frac{C}{r} + D\phi_c \quad R_1 < r < R_c, \quad (\text{B.9})$$

where D and C are dimensionless constants. When $\phi \simeq \phi_c$, then again we can use the harmonic oscillator approximation

$$V_{\text{eff},\phi} = m_c^2(\phi - \phi_c), \quad (\text{B.10})$$

with solution

$$\phi(r) = E \frac{e^{-m_c r}}{r} + F \frac{e^{m_c(r-R_c)}}{r} + \phi_c, \quad 0 < r < R_1, \quad (\text{B.11})$$

where E and F are dimensionless constants (and $E = -F e^{-m_c R_c}$ to prevent a singularity at $r = 0$).

Using the boundary conditions (B.2) and the continuity of solutions (B.6), (B.9) and (B.11) and their first derivatives $d\phi/dr$ at the boundaries $r = R_1$ and $r = R_c$ we can obtain the dimensionless constants A , C , D , and F .

There are three types of solution for the chameleon-field depending on the value of R_1 .

Type 1. No-Shell solutions. In this type $R_1 = R_c$ so we can use eq. (B.6) for the external region and eq. (B.11) for the interior i.e.

$$\phi(r) = \begin{cases} F (e^{m_c(r-R_c)} - e^{-m_c(r+R_c)}) \frac{1}{r} + \phi_c & r < R_c \\ A (e^{-m_b(r-R_c)}) \frac{1}{r} + \phi_b & r > R_c . \end{cases} \quad (\text{B.12})$$

The constants A and F are obtained by matching the interior and external solutions in equation (B.12) and their first derivatives at $R = R_c$ as

$$\begin{aligned} A &= \frac{\phi_b - \phi_c}{m_c + m_b + m_c e^{-2m_c R_c} - m_b e^{-2m_c R_c}} \\ &\quad \times (1 - m_c R_c - e^{2m_c R_c} - m_c R_c e^{-2m_c R_c}) , \\ F &= \frac{\phi_b - \phi_c}{m_c + m_b + m_c e^{-2m_c R_c} - m_b e^{-2m_c R_c}} (1 + m_b R_c) . \end{aligned} \quad (\text{B.13})$$

Type 2. Thick-Shell solutions ($R_1 = 0$). In this case eq. (2.24) is again applicable for the external region and eq. (2.27) is applicable inside. Therefore, we can write

$$\phi(r) = \begin{cases} \frac{Q}{6M_{\text{Pl}}} \rho_c r^2 + D \phi_c & r < R_c \\ A \frac{e^{-m_b(r-R_c)}}{r} + \phi_b & r > R_c . \end{cases} \quad (\text{B.14})$$

The coefficients A and D are obtained by matching the interior and external solutions and their first derivative at $R = R_c$. In this case one obtains

$$A = -\frac{Q}{3M_{\text{Pl}}} \rho_c \frac{R_c^3}{1 + m_b R_c} , \quad (\text{B.15a})$$

$$D = \frac{\phi_b}{\phi_c} - \left(\frac{1}{1 + m_b R_c} + \frac{1}{2} \right) \frac{Q \rho_c R_c^2}{3\phi_c M_{\text{Pl}}} . \quad (\text{B.15b})$$

Type 3. Thin-Shell solution ($0 < R_1 < R_c$). In this case using the solutions (B.6), (B.9) and (B.11) we can write for the scalar field $\phi(r)$

$$\phi(r) = \begin{cases} F (e^{m_c(r-R_1)} - e^{-m_c(r+R_1)}) \frac{1}{r} + \phi_c & 0 < r < R_1 \\ \frac{Q}{6M_{\text{Pl}}} \rho_c r^2 + C \frac{1}{r} + D \phi_c & R_1 < r < R_c \\ A (e^{-m_b(r-R_c)}) \frac{1}{r} + \phi_b & r > R_c \end{cases} \quad (\text{B.16})$$

In this case by matching the solutions and their first derivatives at the boundaries we will get four equations for five unknowns A , C , D , F and R_1 . First we find R_1 as a function of other unknowns.

We saw above that whenever $\phi \approx \phi_c$ in the interval $[0, R_1]$, we used the harmonic approximation $V_{\text{eff},\phi} \approx m_\phi^2 (\phi - \phi_c)$ and where $\phi \gg \phi_c$ we used the linear approximation $V_{\text{eff},\phi} \approx \frac{Q \rho_c}{M_{\text{Pl}}}$. So to obtain R_1 , where the harmonic oscillator approximation changes to

the linear one, we use the following procedure [158]: at $R = R_1$, ϕ starts to increase from $\phi = \phi_c$ and so $m_c^2(\phi - \phi_c)$ increases as well until $m_c^2(\phi - \phi_c) = \frac{Q\rho_c}{M_{\text{Pl}}}$. But as always $V_{\text{eff},\phi} \approx V_{,\phi} + \frac{Q\rho_c}{M_{\text{Pl}}} < \frac{Q\rho_c}{M_{\text{Pl}}}$ (as $V_{,\phi} < 0$), so the harmonic approximation is a suitable approximation for $m_c^2(\phi - \phi_c) < \frac{Q\rho_c}{M_{\text{Pl}}}$ and the linear approximation is suitable for the $m_c^2(\phi - \phi_c) > \frac{Q\rho_c}{M_{\text{Pl}}}$.

1. If $R_1 = R_c$ (No-shell), then we should have

$$m_c^2(\phi(R_c) - \phi_c) < \frac{Q\rho_c}{M_{\text{Pl}}}, \quad (\text{B.17})$$

where $\phi(R_c)$ is obtained by replacing $r = R_c$ in (B.12). If the above condition is satisfied then $R_1 = R_c$ is a good approximation.

2. If $R_1 = 0$ (Thick-shell), then we should have

$$m_c^2(\phi(0) - \phi_c) > \frac{Q\rho_c}{M_{\text{Pl}}}, \quad (\text{B.18})$$

where $\phi(0)$ is the interior solution in (B.14) at $r = 0$. If the above condition is satisfied then $R_1 = 0$ is a good approximation.

3. Otherwise we will obtain R_1 by the condition

$$m_c^2(\phi(R_1) - \phi_c) = \frac{Q\rho_c}{M_{\text{Pl}}}, \quad (\text{B.19})$$

where $\phi(R_1) = \phi(r = R_1)$ in (B.16). In this case we can find R_1 by solving equation (B.19)

$$F = \frac{Q\rho_c R_1}{m_c^2 M_{\text{Pl}} (1 - e^{-2m_c R_1})}. \quad (\text{B.20})$$

The unknowns A , C , D and F in (B.16) can be obtained numerically by matching the solutions and their first derivatives at the boundaries $R = R_1$ and $R = R_c$. For the thin-shell case, when $R_1 \ll R_c$, one can approximate $F \simeq 0$ and write [158]

$$A \approx -\frac{\beta}{4\pi M_{\text{Pl}}} \left(\frac{4}{3} \pi R^3 \rho_c \right) \frac{3M_{\text{Pl}} (\phi_b - \phi_c)}{\beta \rho_c R^2}, \quad (\text{B.21a})$$

$$C = \frac{Q}{3M_{\text{Pl}}} \rho_c R_c^3, \quad (\text{B.21b})$$

$$D = 1 - \frac{Q\rho_c R_c^2}{2M_{\text{Pl}}} \frac{1}{\phi_c}. \quad (\text{B.21c})$$

Bibliography

- [1] A. S. Eddington, *The Mathematical Theory of Relativity*. Cambridge University Press, Cambridge, 1923.
- [2] H. Weyl, “Eine neue Erweiterung der Relativitätstheorie,” *Annalen der Physik* **364** no. 10, (1919) 101–133.
- [3] A. Starobinsky, “A new type of isotropic cosmological models without singularity,” *Physics Letters B* **91** no. 1, (1980) 99 – 102.
- [4] **Supernova Search Team** Collaboration, A. G. Riess *et al.*, “Observational evidence from supernovae for an accelerating universe and a cosmological constant,” *Astron.J.* **116** (1998) 1009–1038, [arXiv:astro-ph/9805201](#) [astro-ph].
- [5] **Supernova Cosmology Project** Collaboration, S. Perlmutter *et al.*, “Measurements of Omega and Lambda from 42 high redshift supernovae,” *Astrophys. J.* **517** (1999) 565–586, [arXiv:astro-ph/9812133](#) [astro-ph].
- [6] T. P. Sotiriou and V. Faraoni, “f(R) Theories Of Gravity,” *Rev.Mod.Phys.* **82** (2010) 451–497, [arXiv:0805.1726](#) [gr-qc].
- [7] A. De Felice and S. Tsujikawa, “f(R) theories,” *Living Reviews in Relativity* **13** (2010) 3, [arXiv:1002.4928](#) [gr-qc].
- [8] C. M. Will, *Theory and Experiment in Gravitational physics, 2nd ed.* Basic Books/Perseus Group, New York, 1993.
- [9] J. Khoury and A. Weltman, “Chameleon fields: Awaiting surprises for tests of gravity in space,” *Phys. Rev. Lett.* **93** (2004) 171104, [arXiv:astro-ph/0309300](#) [astro-ph].

- [10] J. Khoury and A. Weltman, “Chameleon cosmology,” *Phys. Rev.* **D69** (2004) 044026, [arXiv:astro-ph/0309411](#) [astro-ph].
- [11] P. Brax, C. van de Bruck, A.-C. Davis, and D. J. Shaw, “ $f(R)$ Gravity and Chameleon Theories,” *Phys. Rev.* **D78** (2008) 104021, [arXiv:0806.3415](#) [astro-ph].
- [12] D. Psaltis, “Probes and Tests of Strong-Field Gravity with Observations in the Electromagnetic Spectrum,” *Living Reviews in Relativity* **11** no. 9, (2008) , [arXiv:0806.1531](#) [astro-ph].
- [13] L.-F. L. Ta-Pei Cheng, *Gauge Theory of Elementary Particle Physics*. Oxford, 1988.
- [14] D. Gross and F. Wilczek, “Ultraviolet Behavior of Non-Abelian Gauge Theories,” *Phys.Rev.Lett.* **30** (1973) 1343–1346.
- [15] H. D. Politzer, “Reliable Perturbative Results for Strong Interactions?,” *Phys.Rev.Lett.* **30** (1973) 1346–1349.
- [16] M. A. Shifman, A. Vainshtein, and V. I. Zakharov, “QCD and Resonance Physics. Sum Rules,” *Nucl.Phys.* **B147** (1979) 385–447.
- [17] S. Weinberg, *Gravitation and Cosmology*. John Wiley & Sons, 1972.
- [18] E. Fischbach and C. Talmadge, *The Search for Non-Newtonian Gravity*. Springer-Verlag, New York,, 1999.
- [19] S. Schlamminger, K.-Y. Choi, T. Wagner, J. Gundlach, and E. Adelberger, “Test of the equivalence principle using a rotating torsion balance,” *Phys.Rev.Lett.* **100** (2008) 041101, [arXiv:0712.0607](#) [gr-qc].
- [20] S. Baessler, B. R. Heckel, E. Adelberger, J. Gundlach, U. Schmidt, *et al.*, “Improved Test of the Equivalence Principle for Gravitational Self-Energy,” *Phys.Rev.Lett.* **83** (1999) 3585.
- [21] P. Touboul, G. Metris, V. Lebat, and A. Robert, “The MICROSCOPE experiment, ready for the in-orbit test of the equivalence principle,” *Class.Quant.Grav.* **29** (2012) 184010.

- [22] R. D. Reasenber, B. R. Patla, J. D. Phillips, and R. Thapa, “Design and characteristics of a WEP test in a sounding-rocket payload,” *Class.Quant.Grav.* **29** (2012) 184013, [arXiv:1206.0028 \[gr-qc\]](#).
- [23] S. Weinberg, “The cosmological constant problem,” *Rev. Mod. Phys.* **61** (1989) 1–23.
- [24] F. R. Klinkhamer, “Revisiting the cosmological constant problem,” presented at Department of Applied Mathematics and Theoretical Physics, Cambridge, UK, September 18, 2012.
- [25] B. Zumino, “Supersymmetry and the Vacuum,” *Nucl.Phys.* **B89** (1975) 535.
- [26] E. Cremmer, S. Ferrara, C. Kounnas, and D. V. Nanopoulos, “Naturally Vanishing Cosmological Constant in N=1 Supergravity,” *Phys.Lett.* **B133** (1983) 61.
- [27] K. R. Dienes, “New string partition functions with vanishing cosmological constant,” *Phys.Rev.Lett.* **65** (1990) 1979–1982.
- [28] K. R. Dienes, “Generalized Atkin-Lehner Symmetry,” *Phys.Rev.* **D42** (1990) 2004–2021.
- [29] T. Banks, “SUSY breaking, cosmology, vacuum selection and the cosmological constant in string theory,” [arXiv:hep-th/9601151 \[hep-th\]](#).
- [30] C. Schmidhuber, “AdS(5) and the 4-D cosmological constant,” *Nucl.Phys.* **B580** (2000) 140–146, [arXiv:hep-th/9912156 \[hep-th\]](#).
- [31] S. Weinberg, “Anthropic Bound on the Cosmological Constant,” *Phys.Rev.Lett.* **59** (1987) 2607.
- [32] G. Efstathiou, “An anthropic argument for a cosmological constant,” *Monthly Notices of the Royal Astronomical Society* **274** (1995) L73–L76.
- [33] F. R. Klinkhamer and G. E. Volovik, “Self-tuning vacuum variable and cosmological constant,” *Phys.Rev.* **D77** (2008) 085015, [arXiv:0711.3170 \[gr-qc\]](#).

- [34] F. R. Klinkhamer and G. E. Volovik, “Towards a solution of the cosmological constant problem,” *JETP Lett.* **91** (2010) 259–265, [arXiv:0907.4887](#) [hep-th].
- [35] F. R. Klinkhamer, “Equilibrium boundary conditions, dynamic vacuum energy, and the Big Bang,” *Phys.Rev.* **D78** (2008) 083533, [arXiv:0803.0281](#) [gr-qc].
- [36] F. R. Klinkhamer, “Lorentz Invariance, Vacuum Energy, and Cosmology,” [arXiv:0810.1684](#) [gr-qc].
- [37] F. R. Klinkhamer and G. E. Volovik, “Gluonic vacuum, q-theory, and the cosmological constant,” *Phys.Rev.* **D79** (2009) 063527, [arXiv:0811.4347](#) [gr-qc].
- [38] F. R. Klinkhamer and G. E. Volovik, “Vacuum energy density triggered by the electroweak crossover,” *Phys.Rev.* **D80** (2009) 083001, [arXiv:0905.1919](#) [astro-ph.CO].
- [39] F. R. Klinkhamer, “Effective cosmological constant from TeV-scale physics: Simple field-theoretic model,” *Phys.Rev.* **D84** (2011) 023011, [arXiv:1101.1281](#) [hep-th].
- [40] F. R. Klinkhamer, “Effective cosmological constant from TeV-scale physics,” *Phys.Rev.* **D82** (2010) 083006, [arXiv:1001.1939](#) [hep-ph].
- [41] F. R. Klinkhamer and G. E. Volovik, “Dynamic vacuum variable and equilibrium approach in cosmology,” *Phys.Rev.* **D78** (2008) 063528, [arXiv:0806.2805](#) [gr-qc].
- [42] F. R. Klinkhamer and G. E. Volovik, “ $f(R)$ cosmology from q-theory,” *JETP Lett.* **88** (2008) 289–294, [arXiv:0807.3896](#) [gr-qc].
- [43] F. R. Klinkhamer, “QCD-Scale Modified-Gravity Universe,” *Adv.Space Res.* **49** (2012) 213, [arXiv:1005.2885](#) [astro-ph.CO].
- [44] V. Rubakov and P. Tinyakov, “Ruling out a higher spin field solution to the cosmological constant problem,” *Phys.Rev.* **D61** (2000) 087503, [arXiv:hep-ph/9906239](#) [hep-ph].

- [45] V. Emelyanov and F. R. Klinkhamer, “Reconsidering a higher-spin-field solution to the main cosmological constant problem,” *Phys.Rev.* **D85** (2012) 063522, [arXiv:1107.0961 \[hep-th\]](#).
- [46] V. Emelyanov and F. R. Klinkhamer, “Possible solution to the main cosmological constant problem,” *Phys.Rev.* **D85** (2012) 103508, [arXiv:1109.4915 \[hep-th\]](#).
- [47] V. Emelyanov and F. R. Klinkhamer, “Vector-field model with compensated cosmological constant and radiation-dominated FRW phase,” *Int.J.Mod.Phys.* **D21** (2012) 1250025, [arXiv:1108.1995 \[gr-qc\]](#).
- [48] F. R. Klinkhamer, “Inflation and the cosmological constant,” *Phys.Rev.* **D85** (2012) 023509, [arXiv:1107.4063 \[gr-qc\]](#).
- [49] V. Emelyanov and F. R. Klinkhamer, “De Sitter-spacetime instability from a nonstandard vector field,” *Phys.Rev.* **D86** (2012) 027302, [arXiv:1204.5085 \[gr-qc\]](#).
- [50] A. Dolgov and M. Kawasaki, “Realistic cosmological model with dynamical cancellation of vacuum energy,” [arXiv:astro-ph/0307442 \[astro-ph\]](#).
- [51] L. Ford, “Cosmological constant damping by unstable scalar fields,” *Phys.Rev.* **D35** (1987) 2339.
- [52] E. Tomboulis, “Dynamically adjusted cosmological constant and conformal anomalies,” *Nucl.Phys.* **B329** (1990) 410.
- [53] I. Antoniadis and E. Mottola, “4-D quantum gravity in the conformal sector,” *Phys.Rev.* **D45** (1992) 2013–2025.
- [54] I. Antoniadis, P. O. Mazur, and E. Mottola, “Fractal geometry of quantum space-time at large scales,” *Phys.Lett.* **B444** (1998) 284–292, [arXiv:hep-th/9808070 \[hep-th\]](#).
- [55] N. Tsamis and R. Woodard, “Relaxing the cosmological constant,” *Phys.Lett.* **B301** (1993) 351–357.

- [56] N. Tsamis and R. Woodard, “Quantum gravity slows inflation,” *Nucl.Phys.* **B474** (1996) 235–248, [arXiv:hep-ph/9602315](#) [hep-ph].
- [57] L. R. W. Abramo, R. H. Brandenberger, and V. F. Mukhanov, “The Energy - momentum tensor for cosmological perturbations,” *Phys.Rev.* **D56** (1997) 3248–3257, [arXiv:gr-qc/9704037](#) [gr-qc].
- [58] F. R. Klinkhamer and G. E. Volovik, “Dynamics of the quantum vacuum: Cosmology as relaxation to the equilibrium state,” *J.Phys.Conf.Ser.* **314** (2011) 012004, [arXiv:1102.3152](#) [gr-qc].
- [59] F. R. Klinkhamer, “On vacuum-energy decay from particle production,” *Mod.Phys.Lett.* **A27** (2012) 1250150, [arXiv:1205.7072](#) [hep-th].
- [60] W. Fang, W. Hu, and A. Lewis, “Crossing the Phantom Divide with Parameterized Post-Friedmann Dark Energy,” *Phys.Rev.* **D78** (2008) 087303, [arXiv:0808.3125](#) [astro-ph].
- [61] L. Lombriser, A. Slosar, U. Seljak, and W. Hu, “Constraints on f(R) gravity from probing the large-scale structure,” *Phys.Rev.* **D85** (2012) 124038, [arXiv:1003.3009](#) [astro-ph.CO].
- [62] V. F. Mukhanov, H. Feldman, and R. H. Brandenberger, “Theory of cosmological perturbations. Part 1. Classical perturbations. Part 2. Quantum theory of perturbations. Part 3. Extensions,” *Phys.Rept.* **215** (1992) 203–333.
- [63] E. Lifshitz and I. Khalatnikov, “Investigations in relativistic cosmology,” *Adv.Phys.* **12** (1963) 185–249.
- [64] E. Bertschinger, “Cosmological dynamics: Course 1,” [arXiv:astro-ph/9503125](#) [astro-ph].
- [65] S. Dodelson, *Modern Cosmology*. Academic Press, 2003.
- [66] A. D. Linde, “A New Inflationary Universe Scenario: A Possible Solution of the Horizon, Flatness, Homogeneity, Isotropy and Primordial Monopole Problems,” *Phys.Lett.* **B108** (1982) 389–393.

- [67] A. H. Guth, “The Inflationary Universe: A Possible Solution to the Horizon and Flatness Problems,” *Phys.Rev.* **D23** (1981) 347–356.
- [68] Y. Zeldovich, “A Hypothesis, unifying the structure and the entropy of the universe,” *Mon.Not.Roy.Astron.Soc.* **160** (1972) 1P–3P.
- [69] E. R. Harrison, “Fluctuations at the threshold of classical cosmology,” *Phys. Rev. D* **1** (1970) 2726–2730.
- [70] C. Ma and E. Bertschinger, “A Cosmological kinetic theory for the evolution of cold dark matter halos with substructure: Quasilinear theory,” *Astrophys.J.* **612** (2004) 28–49, arXiv:astro-ph/0311049 [astro-ph].
- [71] C. N. Yang and R. L. Mills, “Conservation of isotopic spin and isotopic gauge invariance,” *Phys. Rev.* **96** (1954) 191–195.
- [72] S. L. Glashow, “Partial-symmetries of weak interactions,” *Nuclear Physics* **22** no. 4, (1961) 579 – 588.
- [73] J. Goldstone, A. Salam, and S. Weinberg, “Broken Symmetries,” *Phys.Rev.* **127** (1962) 965–970.
- [74] D. J. Gross and F. Wilczek, “Asymptotically free gauge theories. II,” *Phys. Rev. D* **9** (Feb, 1974) 980–993.
- [75] T. Muta, *Foundations Of Quantum Chromodynamics*. World Scientific, 2009. Third Edition.
- [76] H. Goldstein, *Classical Mechanics*. Addison-Wesley, 1980.
- [77] L. Faddeev and V. Popov, “Feynman diagrams for the Yang-Mills field,” *Physics Letters B* **25** no. 1, (1967) 29 – 30.
- [78] R. Feynman, “Space-time approach to nonrelativistic quantum mechanics,” *Rev.Mod.Phys.* **20** (1948) 367–387.
- [79] G. F. Smoot, C. Bennett, A. Kogut, E. Wright, J. Aymon, *et al.*, “Structure in the COBE differential microwave radiometer first year maps,” *Astrophys.J.* **396** (1992) L1–L5.

- [80] V. Sahni and A. A. Starobinsky, “The Case for a positive cosmological Lambda term,” *Int.J.Mod.Phys.* **D9** (2000) 373–444, [arXiv:astro-ph/9904398](#) [astro-ph].
- [81] P. Peebles and B. Ratra, “The Cosmological constant and dark energy,” *Rev.Mod.Phys.* **75** (2003) 559–606, [arXiv:astro-ph/0207347](#) [astro-ph].
- [82] C. Wetterich, “Cosmology and the Fate of Dilatation Symmetry,” *Nucl.Phys.* **B302** (1988) 668.
- [83] B. Ratra and P. Peebles, “Cosmological Consequences of a Rolling Homogeneous Scalar Field,” *Phys.Rev.* **D37** (1988) 3406.
- [84] R. Caldwell, “A Phantom menace?,” *Phys.Lett.* **B545** (2002) 23–29, [arXiv:astro-ph/9908168](#) [astro-ph].
- [85] S. Nojiri and S. D. Odintsov, “Quantum de Sitter cosmology and phantom matter,” *Phys.Lett.* **B562** (2003) 147–152, [arXiv:hep-th/0303117](#) [hep-th].
- [86] S. Nojiri and S. D. Odintsov, “De-Sitter brane universe induced by phantom and quantum effects,” *Phys.Lett.* **B565** (2003) 1–9, [arXiv:hep-th/0304131](#) [hep-th].
- [87] E. Elizalde, S. Nojiri, and S. D. Odintsov, “Late-time cosmology in (phantom) scalar-tensor theory: Dark energy and the cosmic speed-up,” *Phys.Rev.* **D70** (2004) 043539, [arXiv:hep-th/0405034](#) [hep-th].
- [88] S. Nojiri, S. D. Odintsov, and S. Tsujikawa, “Properties of singularities in (phantom) dark energy universe,” *Phys.Rev.* **D71** (2005) 063004, [arXiv:hep-th/0501025](#) [hep-th].
- [89] A. Anisimov, E. Babichev, and A. Vikman, “B-inflation,” *JCAP* **0506** (2005) 006, [arXiv:astro-ph/0504560](#) [astro-ph].
- [90] C. Armendariz-Picon, V. F. Mukhanov, and P. J. Steinhardt, “A Dynamical solution to the problem of a small cosmological constant and late time cosmic acceleration,” *Phys.Rev.Lett.* **85** (2000) 4438–4441, [arXiv:astro-ph/0004134](#) [astro-ph].

- [91] C. Armendariz-Picon, V. F. Mukhanov, and P. J. Steinhardt, “Essentials of k essence,” *Phys.Rev.* **D63** (2001) 103510, [arXiv:astro-ph/0006373](#) [astro-ph].
- [92] N. Arkani-Hamed, H.-C. Cheng, M. A. Luty, and S. Mukohyama, “Ghost condensation and a consistent infrared modification of gravity,” *JHEP* **0405** (2004) 074, [arXiv:hep-th/0312099](#) [hep-th].
- [93] F. Piazza and S. Tsujikawa, “Dilatonic ghost condensate as dark energy,” *JCAP* **0407** (2004) 004, [arXiv:hep-th/0405054](#) [hep-th].
- [94] C. M. Will, “The Confrontation between general relativity and experiment,” *Living Rev.Rel.* **9** (2006) 3, [arXiv:gr-qc/0510072](#) [gr-qc].
- [95] A. A. Starobinsky, “A New Type of Isotropic Cosmological Models Without Singularity,” *Phys.Lett.* **B91** (1980) 99–102.
- [96] S. Capozziello, “Curvature quintessence,” *Int.J.Mod.Phys.* **D11** (2002) 483–492, [arXiv:gr-qc/0201033](#) [gr-qc].
- [97] S. Capozziello, S. Carloni, and A. Troisi, “Quintessence without scalar fields,” *Recent Res.Dev.Astron.Astrophys.* **1** (2003) 625, [arXiv:astro-ph/0303041](#) [astro-ph].
- [98] S. M. Carroll, V. Duvvuri, M. Trodden, and M. S. Turner, “Is cosmic speed - up due to new gravitational physics?,” *Phys.Rev.* **D70** (2004) 043528, [arXiv:astro-ph/0306438](#) [astro-ph].
- [99] A. Dolgov and M. Kawasaki, “Can modified gravity explain accelerated cosmic expansion?,” *Phys. Lett.* **B573** (2003) 1–4, [arXiv:astro-ph/0307285](#) [astro-ph].
- [100] V. Faraoni, “Matter instability in modified gravity,” *Phys.Rev.* **D74** (2006) 104017, [arXiv:astro-ph/0610734](#) [astro-ph].
- [101] G. J. Olmo, “The Gravity Lagrangian according to solar system experiments,” *Phys.Rev.Lett.* **95** (2005) 261102, [arXiv:gr-qc/0505101](#) [gr-qc].

- [102] G. J. Olmo, “Post-Newtonian constraints on $f(R)$ cosmologies in metric and Palatini formalism,” *Phys.Rev.* **D72** (2005) 083505, [arXiv:gr-qc/0505135](#) [gr-qc].
- [103] V. Faraoni, “Solar System experiments do not yet veto modified gravity models,” *Phys.Rev.* **D74** (2006) 023529, [arXiv:gr-qc/0607016](#) [gr-qc].
- [104] L. Amendola, R. Gannouji, D. Polarski, and S. Tsujikawa, “Conditions for the cosmological viability of $f(R)$ dark energy models,” *Phys.Rev.* **D75** (2007) 083504, [arXiv:gr-qc/0612180](#) [gr-qc].
- [105] B. Li and J. D. Barrow, “The Cosmology of $f(R)$ gravity in metric variational approach,” *Phys.Rev.* **D75** (2007) 084010, [arXiv:gr-qc/0701111](#) [gr-qc].
- [106] A. A. Starobinsky, “Disappearing cosmological constant in $f(R)$ gravity,” *JETP Lett.* **86** (2007) 157–163, [arXiv:0706.2041](#) [astro-ph].
- [107] G. Cognola, E. Elizalde, S. Nojiri, S. Odintsov, L. Sebastiani, *et al.*, “A Class of viable modified $f(R)$ gravities describing inflation and the onset of accelerated expansion,” *Phys.Rev.* **D77** (2008) 046009, [arXiv:0712.4017](#) [hep-th].
- [108] W. Hu and I. Sawicki, “Models of $f(R)$ Cosmic Acceleration that Evade Solar-System Tests,” *Phys.Rev.* **D76** (2007) 064004, [arXiv:0705.1158](#) [astro-ph].
- [109] Y.-S. Song, W. Hu, and I. Sawicki, “The Large Scale Structure of $f(R)$ Gravity,” *Phys.Rev.* **D75** (2007) 044004, [arXiv:astro-ph/0610532](#) [astro-ph].
- [110] L. Pogosian and A. Silvestri, “The pattern of growth in viable $f(R)$ cosmologies,” *Phys.Rev.* **D77** (2008) 023503, [arXiv:0709.0296](#) [astro-ph].
- [111] R. Caldwell, R. Dave, and P. J. Steinhardt, “Cosmological imprint of an energy component with general equation of state,” *Phys.Rev.Lett.* **80** (1998) 1582–1585, [arXiv:astro-ph/9708069](#) [astro-ph].
- [112] D. F. Mota and D. J. Shaw, “Evading Equivalence Principle Violations, Cosmological and other Experimental Constraints in Scalar Field Theories with a Strong Coupling to Matter,” *Phys.Rev.* **D75** (2007) 063501, [arXiv:hep-ph/0608078](#) [hep-ph].

- [113] E. Fischbach, D. Sudarsky, A. Szafer, C. Talmadge, and S. Aronson, “Reanalysis of the Eotvos Experiment,” *Phys.Rev.Lett.* **56** (1986) 3.
- [114] J. K. Hoskins, R. D. Newman, R. Spero, and J. Schultz, “Experimental tests of the gravitational inverse-square law for mass separations from 2 to 105 cm,” *Phys. Rev. D* **32** (1985) 3084–3095.
- [115] P. Zhang, M. Liguori, R. Bean, and S. Dodelson, “Probing Gravity at Cosmological Scales by Measurements which Test the Relationship between Gravitational Lensing and Matter Overdensity,” *Phys.Rev.Lett.* **99** (2007) 141302, [arXiv:0704.1932](#) [astro-ph].
- [116] W. Hu and N. Sugiyama, “The Small scale integrated Sachs-Wolfe effect,” *Phys.Rev.* **D50** (1994) 627–631, [arXiv:astro-ph/9310046](#) [astro-ph].
- [117] M. Hutter, “Instantons in QCD: Theory and application of the instanton liquid model,” [arXiv:hep-ph/0107098](#) [hep-ph].
- [118] T. Schäfer and E. V. Shuryak, “Instantons in QCD,” *Rev.Mod.Phys.* **70** (1998) 323–426, [arXiv:hep-ph/9610451](#) [hep-ph].
- [119] R. Crewther, “Nonperturbative evaluation of the anomalies in low-energy theorems,” *Phys.Rev.Lett.* **28** (1972) 1421.
- [120] M. S. Chanowitz and J. R. Ellis, “Canonical Anomalies and Broken Scale Invariance,” *Phys.Lett.* **B40** (1972) 397.
- [121] M. S. Chanowitz and J. R. Ellis, “Canonical Trace Anomalies,” *Phys.Rev.* **D7** (1973) 2490–2506.
- [122] E. V. Shuryak, “Theory and phenomenology of the QCD vacuum,” *Phys.Rep.* **115** (1984) 151–314.
- [123] V. Gogohia and H. Toki, “Topological structure of chiral QCD vacuum,” *Phys.Rev.* **D61** (2000) 036006, [arXiv:hep-ph/9908301](#) [hep-ph].
- [124] M. Shifman, A. Vainshtein, and V. Zakharov, “QCD and resonance physics. theoretical foundations,” *Nuclear Physics B* **147** no. 5, (1979) 385 – 447.

- [125] C. Brans and R. Dicke, “Mach’s principle and a relativistic theory of gravitation,” *Phys.Rev.* **124** (1961) 925–935.
- [126] F. R. Klinkhamer, “Gluon condensate, modified gravity, and the accelerating Universe,” *Phys.Rev.* **D81** (2010) 043006, [arXiv:0904.3276 \[gr-qc\]](#).
- [127] **Planck Collaboration** Collaboration, P. Ade *et al.*, “Planck 2013 results. XVI. Cosmological parameters,” [arXiv:1303.5076 \[astro-ph.CO\]](#).
- [128] R. Giotri, M. V. d. Santos, I. Waga, R. Reis, M. Calvao, *et al.*, “From cosmic deceleration to acceleration: new constraints from SN Ia and BAO/CMB,” *JCAP* **1203** (2012) 027, [arXiv:1203.3213 \[astro-ph.CO\]](#).
- [129] Y.-S. Song, W. Hu, and I. Sawicki, “Large scale structure of $f(R)$ gravity,” *Phys. Rev. D* **75** (2007) 044004.
- [130] A. Hojjati, L. Pogosian, and G.-B. Zhao, “Testing gravity with CAMB and CosmoMC,” *JCAP* **1108** (2011) 005, [arXiv:1106.4543 \[astro-ph.CO\]](#).
- [131] E. Bertschinger and P. Zukin, “Distinguishing Modified Gravity from Dark Energy,” *Phys.Rev.* **D78** (2008) 024015, [arXiv:0801.2431 \[astro-ph\]](#).
- [132] T. Giannantonio, M. Martinelli, A. Silvestri, and A. Melchiorri, “New constraints on parametrised modified gravity from correlations of the CMB with large scale structure,” *JCAP* **1004** (2010) 030, [arXiv:0909.2045 \[astro-ph.CO\]](#).
- [133] Y.-S. Song, G.-B. Zhao, D. Bacon, K. Koyama, R. C. Nichol, *et al.*, “Complementarity of Weak Lensing and Peculiar Velocity Measurements in Testing General Relativity,” *Phys.Rev.* **D84** (2011) 083523, [arXiv:1011.2106 \[astro-ph.CO\]](#).
- [134] R. Bean and M. Tangmatitham, “Current constraints on the cosmic growth history,” *Phys.Rev.* **D81** (2010) 083534, [arXiv:1002.4197 \[astro-ph.CO\]](#).
- [135] A. Lewis and S. Bridle, “Cosmological parameters from CMB and other data: A Monte Carlo approach,” *Phys.Rev.* **D66** (2002) 103511, [arXiv:astro-ph/0205436 \[astro-ph\]](#).

- [136] S. Tsujikawa, “Matter density perturbations and effective gravitational constant in modified gravity models of dark energy,” *Phys.Rev.* **D76** (2007) 023514, arXiv:0705.1032 [astro-ph].
- [137] **SDSS Collaboration** Collaboration, D. J. Eisenstein *et al.*, “Spectroscopic target selection for the Sloan Digital Sky Survey: The Luminous red galaxy sample,” *Astron.J.* **122** (2001) 2267, arXiv:astro-ph/0108153 [astro-ph].
- [138] **SDSS Collaboration** Collaboration, D. G. York *et al.*, “The Sloan Digital Sky Survey: Technical Summary,” *Astron.J.* **120** (2000) 1579–1587, arXiv:astro-ph/0006396 [astro-ph].
- [139] R. Reyes *et al.*, “Confirmation of general relativity on large scales from weak lensing and galaxy velocities,” *Nature* **464** (2010) 256.
- [140] S. Nesseris and L. Perivolaropoulos, “Testing Lambda CDM with the Growth Function $\delta(a)$: Current Constraints,” *Phys.Rev.* **D77** (2008) 023504, arXiv:0710.1092 [astro-ph].
- [141] R. Sachs and A. Wolfe, “Perturbations of a cosmological model and angular variations of the microwave background,” *Astrophys.J.* **147** (1967) 73–90.
- [142] M. Rees and D. Sciama, “Large scale Density Inhomogeneities in the Universe,” *Nature* **217** (1968) 511–516.
- [143] R. S. Somerville, K. Lee, H. C. Ferguson, J. P. Gardner, L. A. Moustakas, *et al.*, “Cosmic variance in the great observatories origins deep survey,” *Astrophys.J.* **600** (2004) L171, arXiv:astro-ph/0309071 [astro-ph].
- [144] **WMAP Collaboration** Collaboration, E. Komatsu *et al.*, “Seven-Year Wilkinson Microwave Anisotropy Probe (WMAP) Observations: Cosmological Interpretation,” *Astrophys.J.Suppl.* **192** (2011) 18, arXiv:1001.4538 [astro-ph.CO].
- [145] R. Amanullah, C. Lidman, D. Rubin, G. Aldering, P. Astier, *et al.*, “Spectra and Light Curves of Six Type Ia Supernovae at $0.511 < z < 1.12$ and the Union2 Compilation,” *Astrophys.J.* **716** (2010) 712–738, arXiv:1004.1711 [astro-ph.CO].

- [146] **SDSS Collaboration** Collaboration, W. J. Percival *et al.*, “Baryon Acoustic Oscillations in the Sloan Digital Sky Survey Data Release 7 Galaxy Sample,” *Mon.Not.Roy.Astron.Soc.* **401** (2010) 2148–2168, [arXiv:0907.1660](#) [[astro-ph.CO](#)].
- [147] S. Allen, D. Rapetti, R. Schmidt, H. Ebeling, G. Morris, *et al.*, “Improved constraints on dark energy from Chandra X-ray observations of the largest relaxed galaxy clusters,” *Mon.Not.Roy.Astron.Soc.* **383** (2008) 879–896, [arXiv:0706.0033](#) [[astro-ph](#)].
- [148] B. Hu, M. Liguori, N. Bartolo, and S. Matarrese, “Parametrized modified gravity constraints after Planck,” [arXiv:1307.5276](#) [[astro-ph.CO](#)].
- [149] V. I. Zakharov, “Gluon condensate and beyond,” *Int.J.Mod.Phys.* **A14** (1999) 4865–4880, [arXiv:hep-ph/9906264](#) [[hep-ph](#)].
- [150] R. Bertlmann and J. Bell, “Gluon condensate potentials,” *Nucl.Phys.* **B227** (1983) 435.
- [151] **Planck Collaboration** Collaboration, P. Ade *et al.*, “Planck 2013 results. I. Overview of products and scientific results,” [arXiv:1303.5062](#) [[astro-ph.CO](#)].
- [152] **WMAP Collaboration** Collaboration, C. Bennett *et al.*, “Nine-Year Wilkinson Microwave Anisotropy Probe (WMAP) Observations: Final Maps and Results,” [arXiv:1212.5225](#) [[astro-ph.CO](#)].
- [153] S. F. Daniel, E. V. Linder, T. L. Smith, R. R. Caldwell, A. Cooray, *et al.*, “Testing General Relativity with Current Cosmological Data,” *Phys.Rev.* **D81** (2010) 123508, [arXiv:1002.1962](#) [[astro-ph.CO](#)].
- [154] D. Rapetti, S. W. Allen, A. Mantz, and H. Ebeling, “The Observed Growth of Massive Galaxy Clusters III: Testing General Relativity on Cosmological Scales,” *Mon.Not.Roy.Astron.Soc.* **406** (2010) 1796–1804, [arXiv:0911.1787](#) [[astro-ph.CO](#)].
- [155] R. Mandelbaum, A. Slosar, T. Baldauf, U. Seljak, C. M. Hirata, *et al.*, “Cosmological parameter constraints from galaxy-galaxy lensing and galaxy clustering with the SDSS DR7,” [arXiv:1207.1120](#) [[astro-ph.CO](#)].

- [156] A. Nobili, M. Shao, R. Pegna, G. Zavattini, S. Turyshev, *et al.*, “Galileo Galilei’ (GG): Space test of the weak equivalence principle to 10⁽⁻¹⁷⁾ and laboratory demonstrations,” *Class.Quant.Grav.* **29** (2012) 184011.
- [157] S. Shapiro, J. Davis, D. Lebach, and J. Gregory, “Measurement of the Solar Gravitational Deflection of Radio Waves using Geodetic Very-Long-Baseline Interferometry Data, 1979-1999,” *Phys.Rev.Lett.* **92** (2004) 121101.
- [158] T. P. Waterhouse, “An Introduction to Chameleon Gravity,” [arXiv:astro-ph/0611816](https://arxiv.org/abs/astro-ph/0611816) [astro-ph].
- [159] A. Cooney, S. DeDeo, and D. Psaltis, “Gravity with Perturbative Constraints: Dark Energy Without New Degrees of Freedom,” *Phys.Rev.* **D79** (2009) 044033, [arXiv:0811.3635](https://arxiv.org/abs/0811.3635) [astro-ph].
- [160] S. Nojiri and S. D. Odintsov, “Modified gravity with $\ln R$ terms and cosmic acceleration,” *Gen. Rel. Grav.* **36** (2004) 1765–1780, [arXiv:hep-th/0308176](https://arxiv.org/abs/hep-th/0308176) [hep-th].
- [161] M. B. Baibosunov, V. T. Gurovich, and U. M. Imanaliev, “Model of the early universe in $f(R)$ theory,” *Soviet Journal of Experimental and Theoretical Physics* **71** (Oct., 1990) 636–642.
- [162] A. Vilenkin, “Classical and quantum cosmology of the starobinsky inflationary model,” *Phys. Rev. D* **32** (Nov, 1985) 2511–2521.
- [163] G. M. Shore, “Radiatively induced spontaneous symmetry breaking and phase transitions in curved spacetime,” *Annals of Physics* **128** no. 2, (1980) 376 – 424. <http://www.sciencedirect.com/science/article/pii/0003491680903267>.
- [164] J.-Q. Guo and A. V. Frolov, “Cosmological evolution in $f(R)$ gravity and a logarithmic model,” [arXiv:1305.7290](https://arxiv.org/abs/1305.7290) [astro-ph.CO].
- [165] N. Birrell and P. Davies, *Quantum Fields in Curved Space*. Cambridge Monographs on Mathematical Physics. Cambridge University Press, 1982.
- [166] T. Leen, “Renormalization and scaling behavior of non-abelian gauge fields in curved spacetime,” *Annals of Physics* **147** no. 2, (1983) 417 – 444.

- [167] E. Calzetta, I. Jack, and L. Parker, “Curvature-induced asymptotic freedom,” *Phys. Rev. Lett.* **55** (Sep, 1985) 1241–1243.
<http://link.aps.org/doi/10.1103/PhysRevLett.55.1241>.
- [168] E. Calzetta, I. Jack, and L. Parker, “Quantum gauge fields at high curvature,” *Phys. Rev. D* **33** (Feb, 1986) 953–977.
- [169] N. K. Nielsen and B. S. Skagerstam, “Curvature influence on asymptotic freedom and finite-temperature effects in a Bianchi type-II space-time,” *Phys. Rev. D* **34** (Nov, 1986) 3025–3030.
- [170] N. Itoh, “Hydrostatic Equilibrium of Hypothetical Quark Stars,” *Progress of Theoretical Physics* **44** (July, 1970) 291–292.
- [171] E. Witten, “Cosmic separation of phases,” *Phys. Rev. D* **30** (Jul, 1984) 272–285. <http://link.aps.org/doi/10.1103/PhysRevD.30.272>.
- [172] C. Alcock and A. Olinto, “Exotic Phases of Hadronic Matter and their Astrophysical Application,” *Ann. Rev. Nucl. Part. Sci.* **38** (1988) 161–184.
- [173] F. Weber, A. Torres i Cuadrat, A. Ho, and P. Rosenfield, “Strangeness in compact stars,” *PoS JHW2005* (2006) 018, [arXiv:astro-ph/0602047](https://arxiv.org/abs/astro-ph/0602047) [astro-ph].
- [174] J. Lattimer and M. Prakash, “Neutron star structure and the equation of state,” *Astrophys. J.* **550** (2001) 426, [arXiv:astro-ph/0002232](https://arxiv.org/abs/astro-ph/0002232) [astro-ph].
- [175] F. Ozel, “Soft equations of state for neutron-star matter ruled out by EXO 0748-676,” *Nature* **441** (2006) 1115–1117.
- [176] H. Alavirad and J. M. Weller, “Modified gravity with logarithmic curvature corrections and the structure of relativistic stars,” *Phys.Rev.* **D88** (2013) 124034, [arXiv:1307.7977](https://arxiv.org/abs/1307.7977) [gr-qc].
- [177] L. Parker and D. Toms, *Quantum field theory in curved spacetime. Quantized fields and gravity*. Cambridge Monographs on Mathematical Physics. Cambridge University Press, 2009.

- [178] S. Davis, “Scalar field theory in curved space and the definition of momentum,” [arXiv:hep-th/9702070](#) [hep-th].
- [179] C. FRONSDAL, “Elementary Particles in a Curved Space,” *Rev.Mod.Phys.* **37** (1965) 221–224.
- [180] E. Santos, “Quantum vacuum effects as generalized $f(R)$ gravity. Application to stars,” *Phys.Rev.* **D81** (2010) 064030, [arXiv:0909.0120](#) [gr-qc].
- [181] C. Deliduman, K. Eksi, and V. Keles, “Neutron star solutions in perturbative quadratic gravity,” *JCAP* **1205** (2012) 036, [arXiv:1112.4154](#) [gr-qc].
- [182] A. V. Frolov, “A Singularity Problem with $f(R)$ Dark Energy,” *Phys.Rev.Lett.* **101** (2008) 061103, [arXiv:0803.2500](#) [astro-ph].
- [183] G. Esposito-Farese, “Binary pulsar tests of strong field gravity and gravitational radiation damping,” [arXiv:gr-qc/0402007](#) [gr-qc].
- [184] J. M. Weisberg and J. H. Taylor, “The Relativistic binary pulsar B1913+16,” *ASP Conf.Ser.* (2002) , [arXiv:astro-ph/0211217](#) [astro-ph].
- [185] M. Bailes, S. Ord, H. Knight, and A. Hotan, “Self-consistency of relativistic observables with general relativity in the white dwarf - neutron star binary pulsar PSR J1141-6545,” *Astrophys. J.* **595** (2003) L49–L52, [arXiv:astro-ph/0307468](#) [astro-ph].
- [186] A. Wolszczan, “A nearby 37.9 ms radio pulsar in a relativistic binary system,” *Nature* **350** (1991) 688–690.
- [187] T. Damour and G. Esposito-Farese, “Gravitational wave versus binary - pulsar tests of strong field gravity,” *Phys. Rev.* **D58** (1998) 042001, [arXiv:gr-qc/9803031](#) [gr-qc].
- [188] J. Naf and P. Jetzer, “On Gravitational Radiation in Quadratic $f(R)$ Gravity,” *Phys.Rev.* **D84** (2011) 024027, [arXiv:1104.2200](#) [gr-qc].
- [189] S. DeDeo and D. Psaltis, “Towards New Tests of Strong-field Gravity with Measurements of Surface Atomic Line Redshifts from Neutron Stars,” *Phys. Rev. Lett.* **90** (2003) 141101, [arXiv:astro-ph/0302095](#) [astro-ph].

- [190] D. Psaltis, “Testing General Metric Theories of Gravity with Bursting Neutron Stars,” *Phys. Rev.* **D77** (2008) 064006, [arXiv:0704.2426](#) [astro-ph].
- [191] H. A. Buchdahl, “General relativistic fluid spheres,” *Phys. Rev.* **116** (Nov, 1959) 1027–1034.
- [192] F. Özel, “Surface Emission from Neutron Stars and Implications for the Physics of their Interiors,” *Rept. Prog. Phys.* **76** (2013) 016901, [arXiv:1210.0916](#) [astro-ph.HE].
- [193] X. Barcons, D. Barret, A. Decourchelle, J.-W. Herder, T. Dotani, *et al.*, “Athena (Advanced Telescope for High ENergy Astrophysics) Assessment Study Report for ESA Cosmic Vision 2015-2025,” [arXiv:1207.2745](#) [astro-ph.HE].
- [194] A. Cooney, S. DeDeo, and D. Psaltis, “Neutron Stars in $f(R)$ Gravity with Perturbative Constraints,” *Phys.Rev.* **D82** (2010) 064033, [arXiv:0910.5480](#) [astro-ph.HE].
- [195] A. S. Arapoglu, C. Deliduman, and K. Y. Eksi, “Constraints on Perturbative $f(R)$ Gravity via Neutron Stars,” *JCAP* **1107** (2011) 020, [arXiv:1003.3179](#) [gr-qc].
- [196] M. Orellana, F. Garcia, F. A. T. Pannia, and G. E. Romero, “Structure of neutron stars in R-squared gravity,” [arXiv:1301.5189](#) [astro-ph.CO].
- [197] M.-K. Cheoun, C. Deliduman, C. Güngör, V. Keleş, C. Ryu, *et al.*, “Neutron stars in a perturbative $f(R)$ gravity model with strong magnetic fields,” [arXiv:1304.1871](#) [astro-ph.HE].
- [198] J. R. Oppenheimer and G. M. Volkoff, “On massive neutron cores,” *Phys. Rev.* **55** (Feb, 1939) 374–381.
- [199] E. Babichev and D. Langlois, “Relativistic stars in $f(R)$ and scalar-tensor theories,” *Phys.Rev.* **D81** (2010) 124051, [arXiv:0911.1297](#) [gr-qc].
- [200] E. Santos, “Neutron stars in generalized $f(R)$ gravity,” *Astrophys. Space Sci.* **341** (2012) 411–416, [arXiv:1104.2140](#) [gr-qc].

- [201] F. Kamiab and N. Afshordi, “Neutron Stars and the Cosmological Constant Problem,” *Phys. Rev.* **D84** (2011) 063011, [arXiv:1104.5704](#) [astro-ph.CO].
- [202] A. W. Steiner, J. M. Lattimer, and E. F. Brown, “The Equation of State from Observed Masses and Radii of Neutron Stars,” *Astrophys.J.* **722** (2010) 33–54, [arXiv:1005.0811](#) [astro-ph.HE].
- [203] P. Haensel and A. Y. Potekhin, “Analytical representations of unified equations of state of neutron-star matter,” *Astron. Astrophys.* **428** (2004) 191–197, [arXiv:astro-ph/0408324](#) [astro-ph].
- [204] F. Ozel, G. Baym, and T. Guver, “Astrophysical Measurement of the Equation of State of Neutron Star Matter,” *Phys.Rev.* **D82** (2010) 101301, [arXiv:1002.3153](#) [astro-ph.HE].
- [205] C. W. Misner, K. S. Thorne, J. A. Wheeler, *Gravitation*. Freeman, San Francisco, 1973.
- [206] E. Alecian and S. M. Morsink, “The effect of neutron star gravitational binding energy on gravitational radiation-driven mass-transfer binaries,” *Astrophys.J.* **614** (2004) 914–921, [arXiv:astro-ph/0302219](#) [astro-ph].
- [207] M. Bagchi, “The role of binding energies of neutron stars on the accretion driven evolution,” *Mon.Not.Roy.Astron.Soc.* **413** (2011) L47, [arXiv:1102.2912](#) [astro-ph.SR].
- [208] G. B. Cook, S. L. Shapiro, and S. A. Teukolsky, “Rapidly rotating neutron stars in general relativity: Realistic equations of state,” *Astrophys.J.* **424** (1994) 823.
- [209] C. Alcock, E. Farhi, and A. Olinto, “Strange stars,” *Astrophys. J.* **310** (1986) 261–272.
- [210] N. Stergioulas, “Rotating stars in relativity,” *Living Reviews in Relativity* **6** no. 3, (2003) . <http://www.livingreviews.org/lrr-2003-3>.
- [211] D. Page, U. Geppert, and F. Weber, “The Cooling of compact stars,” *Nucl.Phys.* **A777** (2006) 497–530, [arXiv:astro-ph/0508056](#) [astro-ph].

- [212] M. Baubock, E. Berti, D. Psaltis, and F. Özel, “Relations Between Neutron-Star Parameters in the Hartle-Thorne Approximation,” [arXiv:1306.0569](#) [astro-ph.HE].
- [213] J. R. Bond, G. Efstathiou, and M. Tegmark, “Forecasting cosmic parameter errors from microwave background anisotropy experiments,” *Mon. Not. Roy. Ast. Soc* **291** (November, 1997) L33–L41, [arXiv:astro-ph/9702100](#).
- [214] W. Hu and N. Sugiyama, “Small-scale cosmological perturbations: An analytic approach,” *The Astrophysical Journal* **471** no. 2, (1996) 542.
<http://stacks.iop.org/0004-637X/471/i=2/a=542>.
- [215] **SDSS Collaboration** Collaboration, D. J. Eisenstein *et al.*, “Detection of the baryon acoustic peak in the large-scale correlation function of SDSS luminous red galaxies,” *Astrophys.J.* **633** (2005) 560–574, [arXiv:astro-ph/0501171](#) [astro-ph].
- [216] D. J. Eisenstein and W. Hu, “Baryonic features in the matter transfer function,” *Astrophys.J.* **496** (1998) 605, [arXiv:astro-ph/9709112](#) [astro-ph].